CIVIL AVIATION AUTHORITY OF VIETNAM

****

FINAL REPORT[1]

INVESTIGATION RESULT OF SERIOUS INCIDENT

VIETNAM AIRLINES UNCONTAINED ENGINE FAILURE

AIRBUS A321 MSN 5306 (VN-A392)

FLIGHT VN920 ON MARCH 18th 2020

[1] This report was implemented based on the Annex 13 of International Civil Aviation Organization and decree 75/2007/ND-CP in aircraft incident and accident investigation. The reported results are consulting from the State of Manufacture - Engine (USA), State of Manufacture - Aircraft (France) based on the requirements of ICAO in serious incident.

The final report was conducted by Civil Aviation Authority of Vietnam (CAAV) according to Decision number 1370/QĐ-BGTVT of Minitry of Transport dated on 21 May 2009 about authorized to CAAV to conduct investigation of incident and accident.

According to Annex 13 of the ICAO and Article 5, Chapter III of Decree No. 75/2007/ND-CP of the Government on investigation of civil aircraft incidents and accidents, the purpose of the investigation of aircraft accidents and incidents is not to seek responsibility or liability, but to study and determine the causes of aircraft incidents and accidents and to make recommendations for aviation safety.

TABLE OF CONTENTS

I. FACTUAL INFORMATION

1.1 History of the flight

- Aircraft Registration: VN-A392;
- Aircraft Type: Airbus A321
- Flight number: VN920;
- Number of Passenger: 152;
- Number of Crew member: 02 pilots and 05 flight attendants;
- Luggage and cargo information: 146 pieces and 2480kg;
- Time of event: 16:04 (LCT) dated 18/03/2020;
- Place of occurrence: Runway 25L, Tan Son Nhat In'l Airport (Ho Chi Minh City, Vietnam).
- Operator: Vietnam Airlines JSC (VNA);
- Type of operation: Commercial air transport;
- Departure at Tan Son Nhat In't airport (Ho Chi Minh City – Vietnam);
- Planned Arrival at Phnom Penh airport (Pnompenh– Cambodia).

- The history of the flight is based on the results of analysis of flight data recorder's parameter (Appendix I), cockpit voice recorder, voice communications between air traffic controller and flight crew and flight crew interview results, using UTC (UTC - international time, Vietnam time is UTC + 7) as follows:

- At 09:02:49 (UTC): aircraft heading 248.2 deg, aircraft A321, VN-A392 line up runway 25L, Tan Son Nhat In'l Airport (SGN) and prepare for take off.

- At 09:03:23, flight crew was received take off clearence from ATC, first officer was the person who directly controlled the aircraft (pilot flying) and the captain was in charge of monitoring (pilot monitoring). Engine parameters were normal.

- At 09:03:32, aircraft heading 248.02 deg, engine thrust lever angles increased from 0 deg (IDLE) to 10 deg, and then 25 deg (CLIMB) and then to 35 deg (FLEX/MCT). Engine parameters were normal.

- At 09:04:07, aircraft heading 248.02 deg, aircraft ground speed 132 knots (244km/h), thrust lever at FLX-MCT position, the Engine #2 parameters began to change, the aircraft tended to drift to the right, at this time the crew heard a loud explosion on the right side of the aircraft.

- At 09:04:08, aircraft heading 250.5 deg aircraft ground speed 132 knots (244km/h) the flight crew performed the procedure to Reject Take Off according to the operation manual.

- At 09:04:23, aircraft heading 249.26 degrees, aircraft completed stop safely on the runway. The flight crew immediately informed the air traffic control and performed the procedure according to the instructions on the Electronic Centralized Aircraft Monitoring (ECAM), shutdown the Engine #2, discharged the fire extinguisher number 1 of engine #2.

- Upon receiving the information, the Southern Airport Authority and Tan Son Nhat International Airport immediately carried out emergency procedure, collected and marked location of the fragments, sealed the aircraft for investigation.

- At 09:33, all passengers disembarked from the aircraft by ladder car and were brought back to the terminal safely, no passengers or crew members were injured.

1.2 Injuries to persons

No person was injured.

1.3 Damage to aircraft

Some damages were found during on-site aircraft inspection as follow:

- Engine #2 was major damaged:
    + HPT 1st disc was broken and thrown out (Picture 01 and 02);
    + Thrust Reverser was torn (Picture 04),
    + Fan cowling was thrown out of engine (Picture 05);
    + The liberated portion of the HPT 1st disk, to include the disk bore and hub cone, was separated circumferentially from the inner portion of the disk which remained connected to the HPC shaft and in the engine;
- Main wheel #3, 4 was blown-out (picture 06), main wheel #2 was worn out of limit (picture 07);
- 01 hole on right hand side of Engine #1 (Picture 03);
- Some evidence of scratches and gouges were observed on the primary structure of the wings and fuselage.

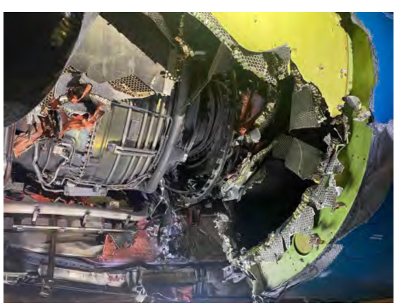

Picture 01

Picture 02

Picture 03


Picture 04


Picture 05


Picture 06


Picture 07

1.4 Other Damages

- Some of small fragment hit to the runway 25L/07R causing 07 small holes on the runway and burning grass on the north side of the runway (Picture 08, 09 and 10).
- 01 fragment of HPT 1st disc was thrown into the weather radar station area, breaking the window of the office in this area (Picture 11).


Picture 08


Picture 09


Picture 10


Picture 11

1.5 Personnel information

1.5.1 Pilot - In - Command (PIC)

- Date of Birth: 12/4/1965; Nationality: Russia;
- Flight Time / On A321: 16509h/ 7345h (Until 02/2020);
- Licenses and certificates:
  + License type: ATPL;
  + Expiration date: 31/8/2024;
  + Expiration date of A321 type certificate: 31/7/2020;
  + Expiration date of medical certificate: 30/4/2020.

1.5.2 First officer

- Date of Birth: 18/4/1991; Nationality: Vietnam;
- Flight Time / On A321: 1194h/ 961h (Until 02/2020);
- Licenses and certificates:
  + License type: CPL;
  + Expiration date: 30/6/2022;
  + Expiration date of A321 type certificate: 31/5/2020;
  + Expiration date of medical certificate: 30/4/2020.

1.5.3 Maintenance staff

- Date of Birth: 23/8/1984
- License and certificate number: 41381
- Company Identification number: VAECO 1754 AC

- Aircraft Rating: A320/321 (CFM56/V2500/PW1100G) CAT B2

1.6 Aircraft information

1.6.1 General information

- Aircraft model: A321-231
- Manufacture Serial Number (MSN): 5306
- Production Delivery: 10/2012
- Aircraft registration: VN-A392
- Expiration date of Airworthiness certificate: 28/02/2021;

The aircraft VN-A392 was in good technical condition without any damage relating to Engine #2 before the flight VN920 on 18/3/2020, total 04 ADD type B under control follow by procedure and aircraft manufacture manual (Sratch on skin plates at frame, Radome radar difference color with aircraft, Delamination on top of left-hand sliding windows, Delamination on left hand fix window dimension measure).

1.6.2 Engine information

1.6.2.1 Engine N#01:

- MSN: V15928, manufactured date on 12/07/2011.
- Engine Model: IAE AG V2533-A5 manufactured by International Aero Engines, a global partnership of aerospace leaders including Pratt & Whitney, Japanese Aero Engine Corporation and MTU Aero Engines.
- Engine flight time and flight cycels:

+ FH: 35254.34 from date of manufacture.

+ FC: 23487 from date of manufacture.

1.6.2.2 Engine No#2:

- MSN: V16580, manufactured date on 19/09/2012.
- Engine Model: IAE AG V2533-A5 manufactured by International Aero Engines, a global partnership of aerospace leaders including Pratt & Whitney, Japanese Aero Engine Corporation and MTU Aero Engines.
- 20/11/2018, Engine V16850 was sent to Christchurch Engine Center, New Zeland - AMO validated by CAAV (Certificate number: VN-079NN/CAAV), after release to service, Engine V16850 was installed on VN-A392 from 18/03/2019;
- Engine flight time and flight cycle (until occurence):

  + 17911.18h / 12634 cycles from date of manufacture

  + 2631.6h/1926 cycles from last engine shop visit
- During Engine shop visit, the HPT #1 stage disk was replaced.

1.7 Meteorological Information

1.7.1 TAF at Tan Son Nhat Airprot (VVTS)

As the forecast conditions in TAF for VVTS issued on 05:00 UTC of 18 March

2020, from 06:00 UTC of 18 March to 06:00 UTC of 19 March 2020, the weather forecast was in the operational standard to take off.

+ Wind: 100/10kt
+ Visibility: 10km or more
+ Clouds: SCT 1700ft

TAF VVTS 180500Z 1806/1906 10010KT 9999 SCT017=

1.7.2 METAR at VVTS

Based on the Meteorological Aerodrome Report (METAR) issued on 09:00 UTC dated 18 March 2020, meteorological condition was in the operational standard to take off at VVTS:

+ Wind: 150/10kt and variable 130 to 190 Degree.
+ Visibility: 10km or more
+ Clouds: FEW 2000ft
+ Temperature: 33°C
+ Dew pt: 17°C
+ QNH: 1007
+ Trend: NOSIG

METAR VVTS 180900Z 15010KT 130V190 9999 FEW020 33/19 Q1007 NOSIG=

1.7.3 Actual weather at VVTS (passed to the Aircraft by ATC)

Runway dry, wind component: 190/10 kts, Visibility: 10 km or more, Temperature: 34°C.

1.8 Aerodrome Information

1.8.1 General Information

Tan Son Nhat International Airport is the busiest and largest airport in Vietnam. It is located 4 mi (6 km) North West from the city center (District 1) of Ho Chi Minh City (Saigon). The airport's IATA code, SGN and ICAO code is VVTS.

VVTS has two runways with information as following:

Runway 07L/25R	**10000ft x 148ft (3048m x 45m)**	
	07L	**25R**
Elevation	24	32
Latitude	10.815	10.8249

Longtitude	106.637	106.663
True magnetic hdg	69.1	249.1
Runway 07R/25L		**12468ft x 148ft (3800m x 45m)**
	07R	**25L**
Elevation	24	32
Latitude	10.815	10.8237
Longtitude	106.637	106.67
True magnetic hdg	69	249

1.9 Flight recorder

The Aircraft VN-A392 was equipped with Flight Data Recorder and Cockpit Voice Recorder in accordance with Vietnam Aviation Regulations (VARs) Part 6. The detailed Flight Recorders installed on the aircraft are as below:

Flight Recorders	Make	Part Number	Serial Number
DFDR	L3 Communications Corporation	2100-4045-00	000916280
CVR	Honeywell	980-6022-001	CVR120-12108

Both devices were under good technical condition and after the incident, it was removed from the aircraft and sent to CAAV to decode and analyze.

1.10 Wreckage Information

The incident investigation team coordinated with relevant organizations (Sounthern Airport Authority, Tan Son Nhat Airport, Vietnam Airlines) to collect fragments from the aircraft engine immediately after the incident. In which, 02 fragments have been collected from the HPT 1st disc, which plays an important role in determining the cause of the incident. In addition, the investigation team preliminarily analyzed data from the flight data recorder (FDR) to determine the time of the incident. Based on the above data, the investigation team carried out the recovery the incident site, the location of the incident and the location of the fragments from the HPT 1st disc.

Fragment #1 of the HPT 1st disc (2/3 discs) was thrown out of the engine, 734m to the right of the runway from the event location.

Fragment #2 of the HPT 1st disc (approximate about 1/3 discs) is determined about 80m to the left of the runway from the event location, specifically according to the following figure:

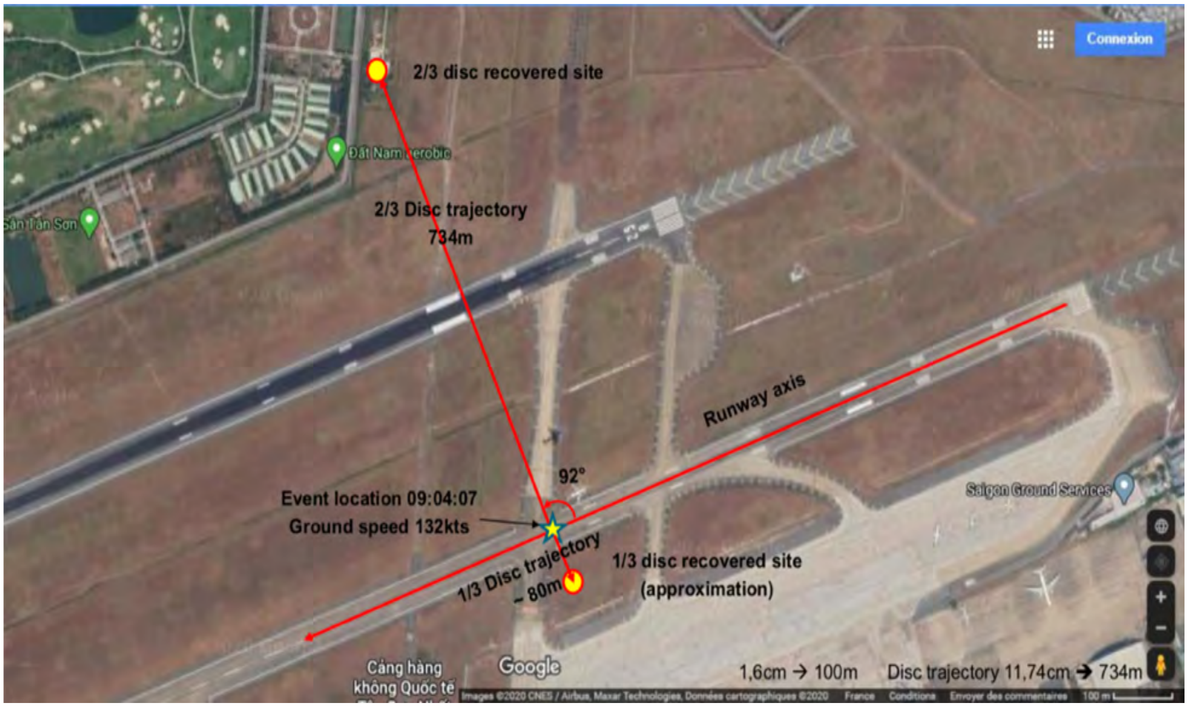

Picture 12: Incident Mapping

Picture 13: Engine No#2 (Right side)

Picture 14: Engine No#2 (Left side)

Picture 15: 2/3 Disc

Picture 16: 1/3 Disc

Picture 17: Full disc

1.11 Medical and pathological information

Flight crews, cabin crews and maintenance staff were in the good health conditions and complied with requirements of HVN and VARs.

1.12 Fire

There was not a fire on aircraft, but there was a fire of grass on right side of runway 25L because of debris from engine.

Picture 18: Right side of runway

Picture 19: One of the engine parts on right side of runway

1.13 Test and research

- CAAV interviewed the flight crews for operation procedures and maintenance staff, AMO for maintenance procedures.

- The CAAV downloaded, analysed the flight recorder data and shared it to The National Transportation Safety Board (NTSB) and The Bureau of Enquiry and Analysis (BEA).

- The CAAV had sent 02 fragments of the HPT 1st stage disc to the engine manufacturer P&W for metallurgical examination and investigation to determine the root cause of the incident.

- The BEA performed an initial assessment of the incident and analyzed the data from FDR and CVR;

- NTSB and Pratt & Whitney suspected that there was a manufacturing anomaly in the HPT 1st stage disc and on March 21, 2020 (3 days after the incident).

- Immediately after receiving 02 fragments of the HPT 1st stage disc from the CAAV (April 2020), the manufacturer Pratt & Whitney carried out metallurgical examination 02 fragments and continuously worked with the CAAV, NTSB, BEA to update progress, assessment results and analysis. On May 11, 2021, the engine manufacturer Pratt & Whitney finished the process of evaluating, analyzing and completing the Metallurgical Investigation Final Report for 02 fragments of the HPT 1st stage disc of VN-A392 (Report is attached).

- The P&W used the following in-depth assessment and analysis methods to exam the fragments:

a) Visual Review As-Received;

b) Visual and Binocular review;

c) SEM examination;

d) White Light Scanning;

e) Micro-CT/UT Scans;

g) Metallographic Examination;

h) Serial Polish;

i) Electron Microprobe Analysis;

k) Electron Backscatter Diffraction.

II. ANALYSIS

2.1 Implemented investigation

Based on the occurrence, CAAV has classified this event as serious incident (class B). Moreover, CAAV's General Director established an incident investigation team according to decision number 501/QĐ-CHK on 19/03/2020. The investigation team has carried out the investigation according to the regulations and procedures for investigating aircraft incidents as prescribed in Decree 75/2007/ND-CP and Annex 13 of the ICAO, specifically as follows:

- On-site investigated and analysed the incidents;
- Collected and analyzed related information including: flight documents, training documents of flight crews, aircraft documents, communication between flight crews and ATC, maintenance records, maintenance procedures;
- Analyzed the data downloaded from CVR and FDR;
- Initially notified of the serious incident to International Civil Aviation Organization (ICAO), NTSB as state of engine manufacture, BEA as state of aircraft manufacture and Pratt&Whitney - Engine manufacturer in according to Annex 13 of Chicago Convention;
- The CAAV has shared the initial informations, data from CVR and FDR to NTSB, BEA in according to Annex 13 of Chicago Convention;
- The BEA and NTSB have appointed authorized representatives to participate in the incident investigation process in according to Annex 13 of Chicago Convention;
- The investigation team has established a common database and shared it with related parties;
- The BEA performed an initial assessment of the incident and analyzed the data from FDR and CVR;
- NTSB and Pratt & Whitney determined that there was a manufacturing anomaly in the HPT 1st stage disc and on March 21, 2020 (3 days after the incident), the engine manufacturer – IAE AG had issued a Newsflash (NF-064 Issue 2 on 20 Mar 2020) for immediate recall of all discs of the same heat lot as the disc in the event engine (Total 16 HPT 1st stage) being installed on A321 aircraft family and the Federal Aviation Administration (FAA - Stage of manufacture) had issued the Emergency Airworthiness Directive (No. 2020-07-51) which required actions: For affected IAE AG model turbofan engines with an engine serial number and HPT 1st-stage disk serial number listed in Table 1 to paragraph (g) of this AD, within 5 flight cycles after the effective date of this AD, remove the HPT 1st-stage disk from service, For all other affected IAE AG model turbofan engines, review the engine records within 3 calendar days after the effective date of this AD to determine if an HPT 1st-stage disk with serial number PKLBR37442, PKLBR38661, or PKLBR40207 is installed in the engine. If an affected HPT 1st-stage disk is installed, within 05 flight cycles after this determination remove the affected HPT 1st-stage disk from service.
- Immediately after the FAA had issued the Emergency AD, the CAAV deployed this AD to all Vietnammese Operators who opetate the A320/1 aircraft installed Engine V2500 and identified Vietnam Airlines as opeating 01 aircraft

Airbus A321 with registration mark VN-A605 using the HPT 1st stage disc with the same heat lot as the disc in the event engine and CAAV requested to grounded this aircraft to remove engine.

- The CAAV had sent 02 fragments of the HPT 1st stage disc to the engine manufacturer P&W for metallurgical examination and investigation to determine the root cause of the incident.

- Economic Security Department - Ministry of Public Security coordinated with CAAV to evaluate to consider whether there is a criminal element to the incident.

- Immediately after receiving 02 fragments of the HPT 1st stage disc from the CAAV (April 2020), the manufacturer Pratt & Whitney carried out metallurgical examination 02 fragments and continuously worked with the CAAV, NTSB, BEA to update progress, assessment results and analysis. On May 11, 2021, the engine manufacturer Pratt & Whitney finished the process of evaluating, analyzing and completing the Metallurgical Investigation Final Report for 02 fragments of the HPT 1st stage disc of VN-A392 (Report is attached).

- On December 28, 2020, the FAA issued AD No. 2021-01-03, effective from January 21, 2021, which required actions: remove the V2500 HPT 1st and 2nd stage disc listed of this AD for improve safety.

- On February 9, 2022, the FAA issued AD No. 2022-02-09, effective from March 15, 2022, which required the implementation of Ultrasonic Inspection method for Engine V2500 (specified in AD) for improve safety.

2.2 HPT 1st stage disc Metallurgical investigation report

Two fragments of HPT 1st stage disc had been analyzed by the Engine manufacturer - Pratt&Whitney at the East Hartford, Connecticut, USA under the supervision of NTSB, as follows:

2.2.1 Informations of HPT 1st stage disc fragments

- Part number: 2A5001
- Serial number: PKLBR40204
- Heat Code: PIIGE2011
- Fragment 1: The fragment and remnant blades weighed a total of 32.89kg (72.5 Lbs) consisted of approximately two-thirds of the hub, detail pictures as below:

Picture 20: Forward side

Picture 21: Aft side

Picture 22: Facture A

Picture 23: Facture B

Picture 24

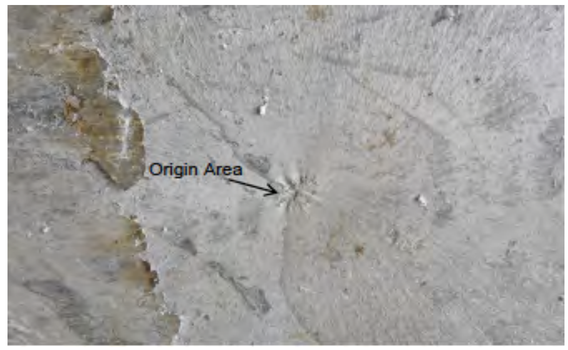

Picture 25

- Fragment 2: The fragment and remnant blades weighed a total of 14.29kg (31.5 Lbs) consisted of the remaining one-thirds of the hub, detail pictures as below:

Picture 26: Forward side

Picture 27: Aft side

Picture 28: Facture A

Picture 29: Facture B

2.2.2 Analysis results

a) Fragment 1

When using in-depth assessment and analysis methods to exam fragment 1, manufacturing defects were detected when carried out the following analysis methods:

- Visual and Binocular review:

The Fracture A surface on Fragment 1 was sectioned from the remainder of the hub via wire electrical discharge machining (EDM).

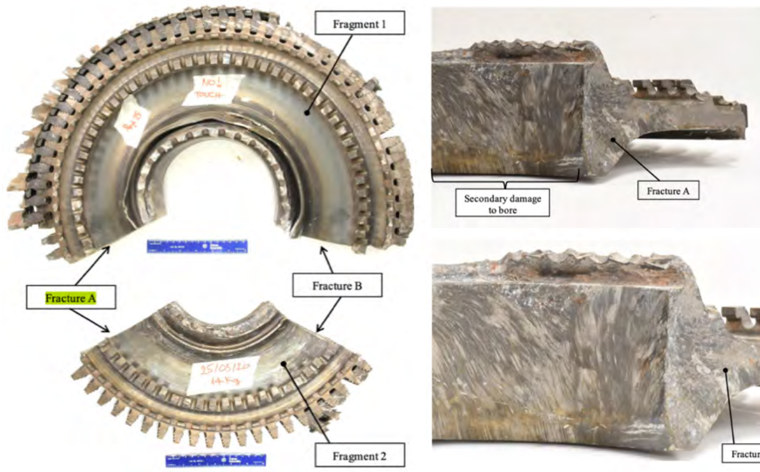

Picture 30: Fracture A

The origin was located approximately 1.5" from the aft surface of the bore, 1.1" from the ID surface of the bore, and approximately 5.25" from the blade slot bottom

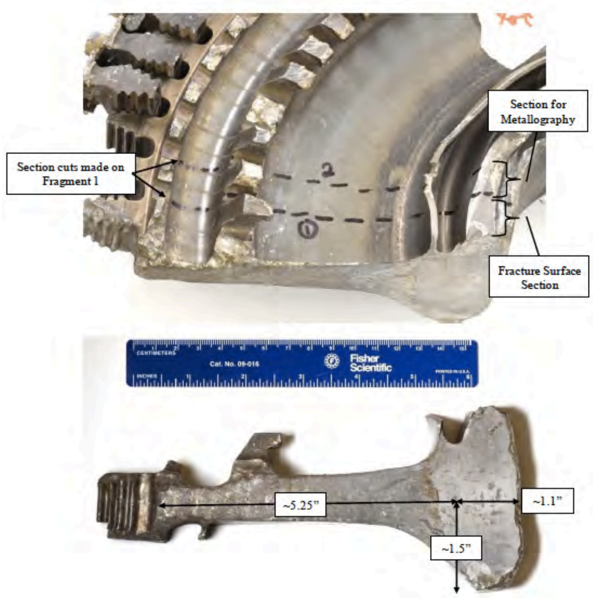

Picture 31

Further visual and binocular review of the fracture surface identified cyclic markers throughout the crack progression surrounding the oval shaped origin area. The oval shaped origin region appeared rougher textured compared to the surrounding area. This region measured approximately 0.120” x 0.075”

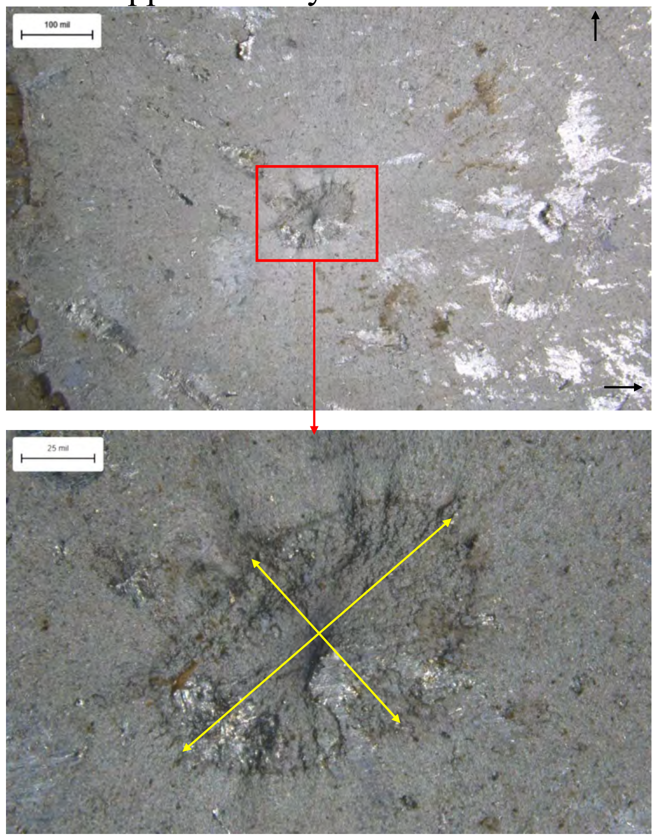

Picture 32

- Scanning Electron Microscope (SEM) examination:

+ SEM examination of the oval-shaped origin area identified an inclusion roughly centered in this region. The main inclusion area consisted of a concentrated area of voids and foreign particles. This area measured 0.4064 x 0.0635 mm (0.016 inch x 0.0025 inch).

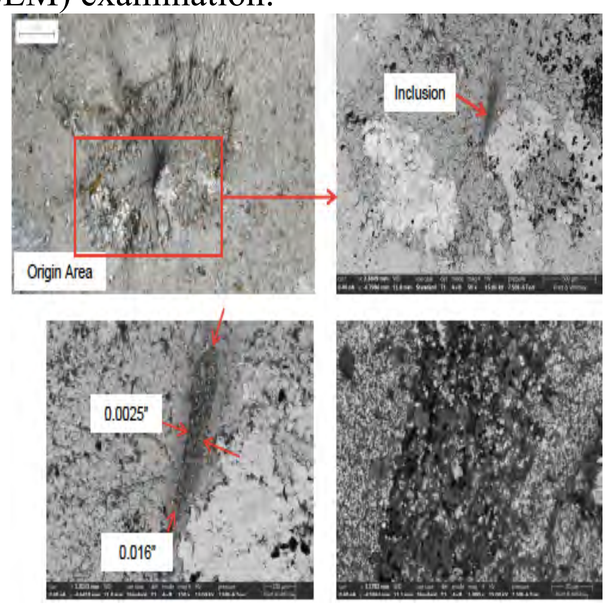

Picture 33

+ the oval-shaped origin area measured overall 3.048 mm x 1.905 mm (0.120 inch x 0.075 inch)

+ The inclusion region identified an increased concentration of oxygen, magnesium, aluminum, phosphorous, and titanium (O, Mg, Al, P, and Ti).

+ Fracture surface features within the oval shaped region were intergranular. Immediately surrounding the oval shaped region was a ring of ductile dimples, and the remainder of the fracture surface outside this area had transgranular features.

+ Micro computed tomography (CT) scan images after sectioning the Fragment 1 origin area to a 0.1” thick section. The focus scan at the origin area identified a region extending approximately 0.005” – 0.007” into the sample at the location of the inclusion that exhibited a difference in density when compared with the surrounding base metal. No other indications were found within the rest of the scan.

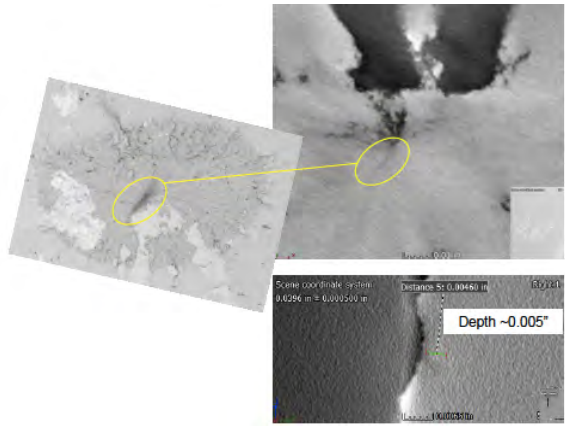

Picture 34

- Serial Polish:

The inclusion was found through the serial polish, at each of these locations, the inclusion was roughly centered within the intergranular region of the fracture.

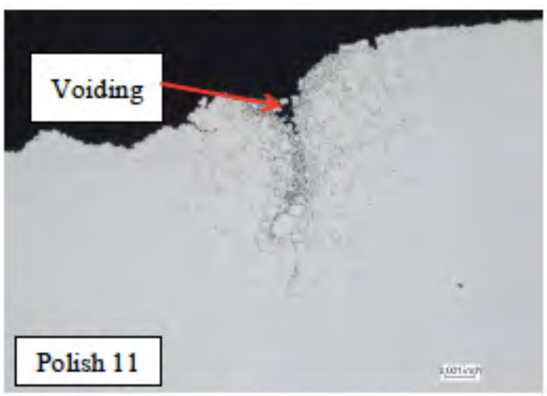

Picture 35.

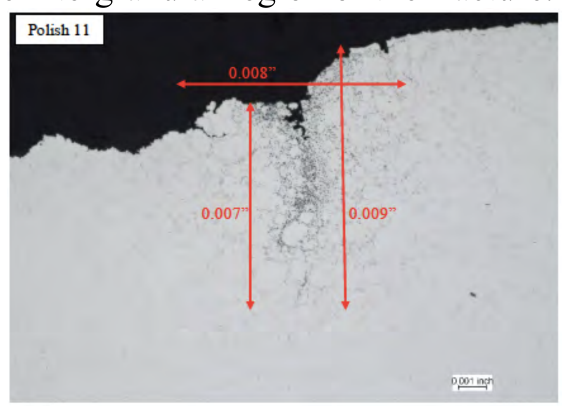

Picture 36

The inclusion area consisted of a region of distributed particles with Al-O and Al-Mg-O type chemistries. At one polish, a particle with the P-Ti-Ni-Co chemistry consistent with those in the main inclusion area on the fracture surface was observed.

b) Fragment 2

When using in-depth assessment and analysis methods to exam fragment 2, manufacturing defects were detected when carried out the following analysis methods:

- Visual and Binocular Review:

The Fracture A surface in the bore area on Fragment 2 was sectioned from the remainder of the hub via wire EDM. Binocular microscope examination of the fracture surface identified significant smearing and mechanical damage. The origin area was not readily apparent; however, remnant cyclic markers were observed throughout the progression. An adhered, smeared flap of material was observed in the vicinity of the origin area.

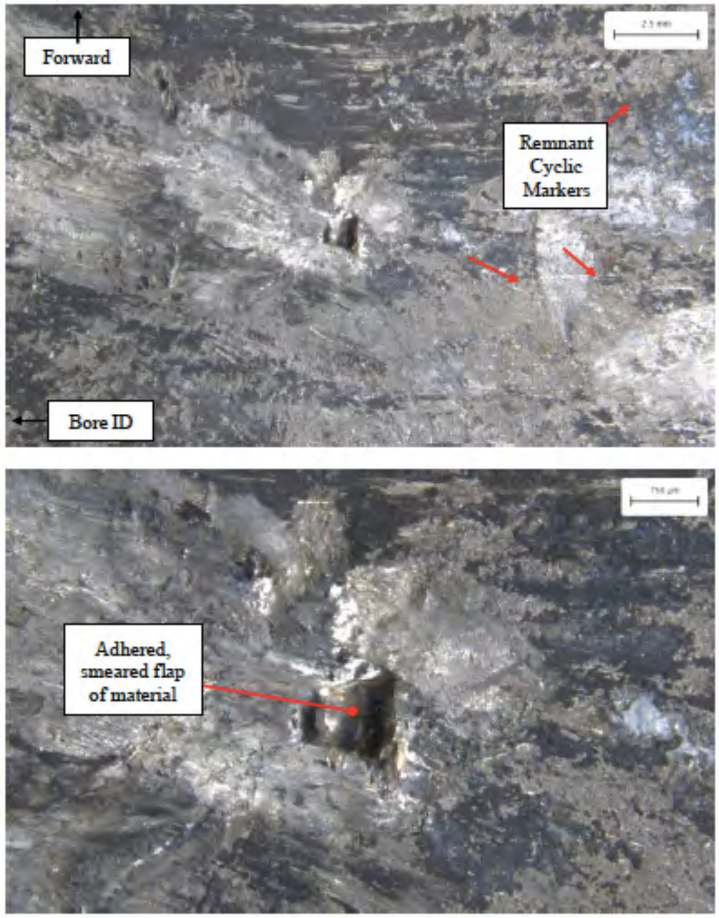

Picture 37

- SEM examination:

+ Binocular microscope examination of the fracture surface identified significant smearing and mechanical damage.

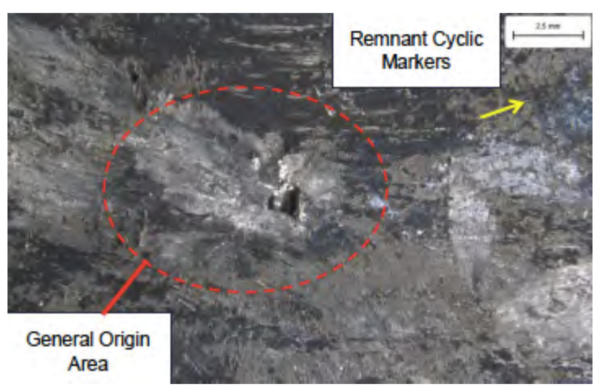

Picture 38

+ SEM evaluation of the fracture surface confirmed secondary damage and smeared features. There were no original fracture features remaining within the vicinity of the origin area.

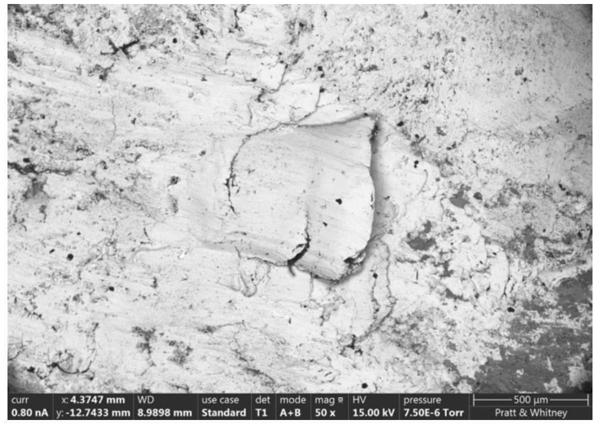

Picture 39

+ Micro-CT scans from the Fragment 2 origin area. No evidence of the inclusion was identified.

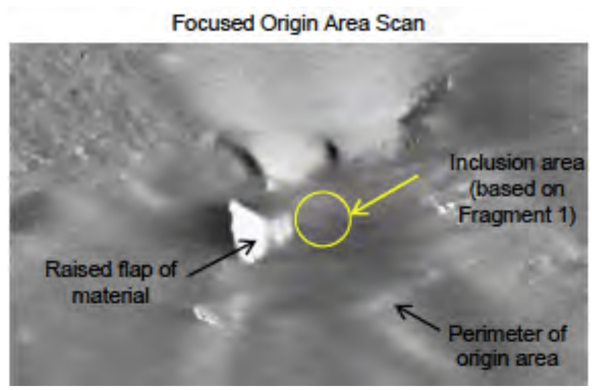

Picture 40

+ Results of the ultrasonic (UT) scans on the 0.1" thick section of Fragment 2. No indications associated with the known inclusion location were observed.

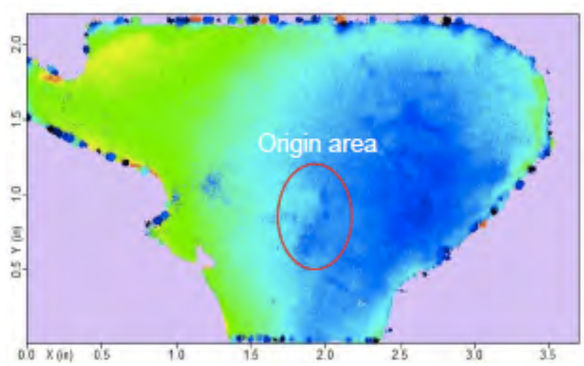

Picture 41

2.3 Flight recorder analysis result

The result of FDR data analysis of VN-A392 at the time of incident (09:04:07 UTC) is described as follow:

- All parameters of both Engines were normal;
- When an incident occurs, Engine #2 loses thrust, the aircraft tends to the right of runway center line, the longitudinal acceleration showed a reduction of acceleration, and lateral acceleration associated with drift showed a yaw to the right. At this time, the crew controls the aircraft to the runway center line and reject take-

off.

- After 09:04:07, Engine #2 parameters were NCD (Invalid) due to the Engine #2 damage.

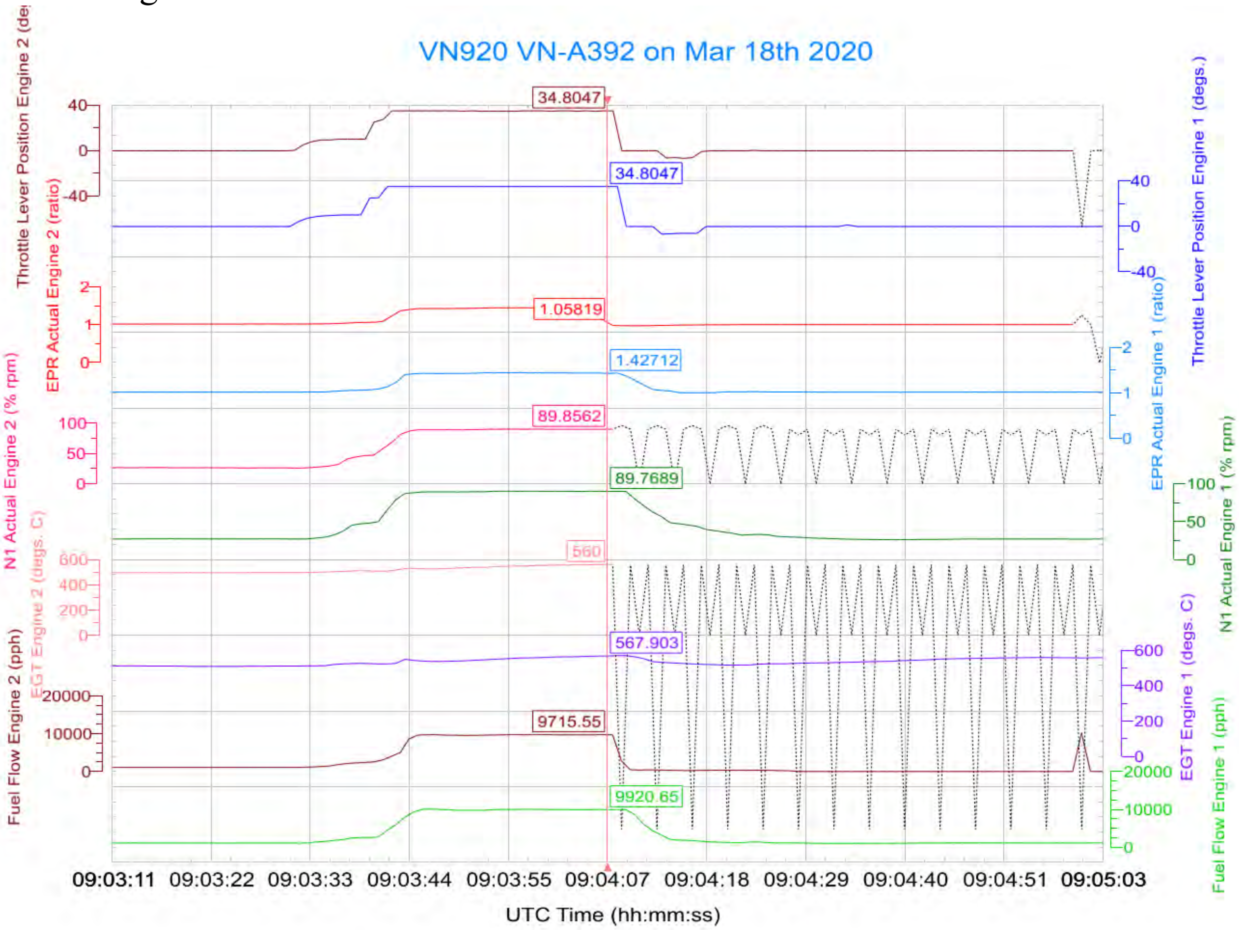

Picture 42

2.4 Aircraft Structure evaluation and action taken

a) After incident, Vietnam Airlines cordinated with Pratt&Whitney and Airbus for structure evaluation. The result of the damage assessment as follows:

- Engine #2 (Serial V16580) was almost destroyed and Manufacturer recommended to be replaced.

- Engine Nacelle includes: Air intake, Fan Cowlings, Thrust Reverser, CNA were heavily damaged. The manufacturer - Collins required replacement.

- RH pylon: Primary structure was damaged, the manufacturer - Airbus required replacement.

- Other damaged on RH wing, fuselage, Engine #1 (Scratch, nick, gouge,...) can be repaired and Vietnam Airlines has completed the structure repair order.

b) After the FAA issued directives related to the incident as well as received instructions from the engine and aircraft manufacturers, the Vietnam Airlines carried out repaired the damages as follows:

- Aircraft VN-A392 on ground for replace Engine #2 and repair aircraft as follow Pratt&Whitney and Airbus instructions:

+ Engine #2 completed replacement on 09/09/2021.

+ Aircraft repair completed on 30/09/2021 follow by Airbus RDAF 80768916/145/2021#A.

+ Flight test completed on 30/09/2021.

- Vietnam Airlines submited all of the documents to CAAV, after CAAV issued the Certificate of Airworthiness, the aircraft VN-A392 was returned to service.

2.5 Flight crew procedure assessment

The flight crew followed the correct procedure for reject take-off immediately occurred incident and controlled the aircraft to stop safely on the runway.

2.6 Corrective and preventive actions

1. Immediately after the incident, IAE AG requested an immediate recall of all discs of the same heat lot as the disc in the event engine being installed on A321 aircraft family to prevent similar incident and remove the affected disk from service.

2. The FAA had issued 03 ADs to prevent similar incident:

a) on March 21, 2020 the FAA had issued the Emergency Airworthiness Directive (No. 2020-07-51) which required actions: For affected IAE AG model turbofan engines with an engine serial number and HPT 1st-stage disk serial number listed in Table 1 to paragraph (g) of this AD, within 5 flight cycles after the effective date of this AD, remove the HPT 1st-stage disk from service, For all other affected IAE AG model turbofan engines, review the engine records within 3 calendar days after the effective date of this AD to determine if an HPT 1st-stage disk with serial number PKLBR37442, PKLBR38661, or PKLBR40207 is installed in the engine. If an affected HPT 1st-stage disk is installed, within 5 flight cycles after this determination remove the affected HPT 1st-stage disk from service.

b) On December 28, 2020, the FAA issued AD No. 2021-01-03, effective from January 21, 2021, which required actions: remove the V2500 HPT 1st and 2nd stage disc listed of this AD for improve safety.

c) On February 9, 2022, the FAA issued AD No. 2022-02-09, effective from March 15, 2022, which required the implementation of Ultrasonic Inspection method for Engine V2500 (specified in AD) for improve safety.

3. Engine manufacturers P&W and NTSB have researched and improved the production process, adding the HPT 1st stage disc inspection method to ensure detection and prevention of possible inclusion. materials in the manufacturing process as well as the ability to detect product irregularities before the product is shipped:

a) Addition inspection orientation (angle scan) to identify defects in alternate orientations, improving overall detectability. Incorporating into finished hardware and sonic shape for both HPC / HPT.

b) Time of flight (TOF) analysis of manufactured rotors to identify suspect sonic indications which are smaller defects than previous inspection methods (retrospectively and potentially proactively). .

c) Process improvements to remove sources of reactive Non-metallic inclusions (NMI) elements from melt practices reducing probability of occurrence. Closed loop inspection and quality requirements to monitor NMI content and remove process drift.

III. CONCLUSION

3.1 Findings

a) The flight crew, maintenance staff of VN920 had valid license and ratings and were fully qualified to undertake the flight.

b) As per the flight schedule, the crew had been given sufficient off duty period prior to the flight in accordance with existing fatigue management policy and Part 15 of Vietnam Aviation Regulations.

c) The aircraft VN-A392 had current Certificate of Airworthiness. The necessary inspections as per the approved maintenance programme were carried out. All aircraft systems operated normally.

3.2 Causes

By combining the methods used to analyze the 02 fragments of the HPT 1st stage disc and the review of the manufacturing process of this disc, the engine manufacturer P&W have found defects in the production process, the cause of the incidents as follows:

1. The manufacturer found inclusion mixed into the core of the metal ingot during the processing of the HPT 1st stage disc billet with dimensions of 0.016 inches x 0.0025 inches (0.4064 x 0.0635). mm), however, it could not be positively determined how the inclusion was mixed in during the manufacturing process of HPT 1st stage disc.

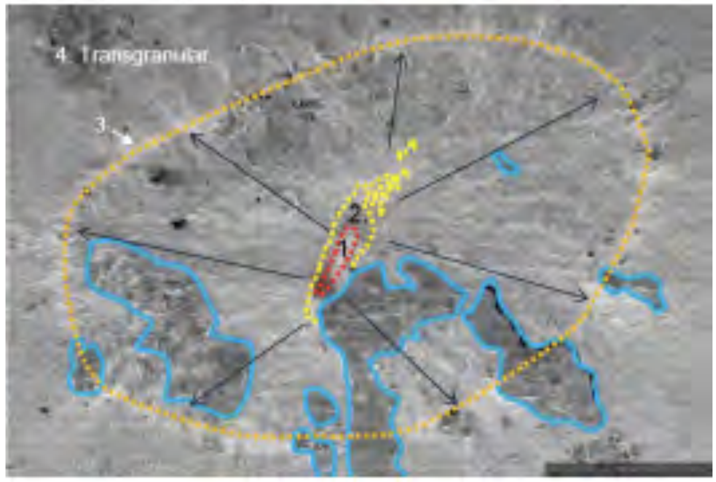

Picture 43

2. Investigative analysis showed that the Non-Metallic Inclusion and abnormal develops reaction zone had formed during thermal processing with dimensions 0.033 inches x 0.007 inches (0.8382 x 0.1778 mm).

3. Because of the presence of inclusion, an Intergranular crack-like anomaly forms during high-temperature manufacturing process. Sonic inspection did not identify a crack-like anomaly beyond acceptable limits at fracture location. The part is shipped with approx. 0.120” x 0.075” (3,048 x 1.905 mm) crack-like anomaly in bore.

4. The formation of crack-like irregularities in the bore of the HPT 1st stage disc combined with the engine operation has created tension on the bore of the HPT 1st stage disc and cause the disc rupture.

4. SAFETY RECOMMENDATIONS

4.1. Vietnam Operators

- Continuously update and comply with all Airworthiness directives of FAA, instructions of engine manufacturers to ensure safe operation of aircraft using engine V2500;
- Conducting a safety briefing about the incident and informing the conclusion of investigation to the entire flight crews and related individuals.

4.2 Engine Manufacturer - Pratt&Whitney

- Continue to review the production process and continuously research and add the HPT 1st and 2nd stage inspection method to ensure that it is able to detect and prevent inclusion into the material during the production process, as well as the ability to detect product abnormalities before release to service. Pratt&Whitney has done this recommendation. CLOSED - Acceptable Response.
- Add a detailed inspection method inside the engine to assit the operator detect defects and damage that can cause damage when the engine is operating. Pratt&Whitney has done this recommendation. CLOSED - Acceptable Response

- Review the impact of this production process issue on other Pratt & Whitney engines (PW1100, PW1500, etc…).

4.3 CAAV - Flight Safety Standard Department

- Monitoring the implementation of safety recommendations for Vietnam Airlines JSC.
- Codinate with NTSB to monitoring the implementation of safety recommendations for Pratt&Whitney.

APPENDIX I: FDR Analysis

Time (UTC)	Data
09:03:31	- Throttle Lever begin increase - Wheel speed: 1 knots - Longitude E $106^0$40’07.8’’, Latitude N$10^0$49’25.2” - Eng 1 EGT 511 degC, Eng 2 496 degC - Computed airspeed : no value - Vibration: + Eng 1 N1 0, N2 0.1 + Eng 2 N1 0, N2 0.3
09:04:01	- Computed Airspeed: 100 knots. - CVR: FO said 100 knots (CVR time 01:28:24)
09:04:05	- EEC 2 transfer from Channel B to Channel A. - Thrust Lever 34.8 (deg) / FLEX position - Wheel Speed: 127 knots - Eng 1 EGT 566 degC, Eng 2 558 degC - Computed Airspeed: 123 knots - Longitude E $106^0$39’45.2’’, Latitude N$10^0$49’15.8” - Vibration: + Eng 1 N1 0.4, N2 0.35 + Eng 2 N1 1.0, N2 0.3 - Oil pressure Eng 1 220 psi, Eng 2 206 psi - No warning, caution
09:04:07	- Throttle Lever 34.8047 (deg) and start decrease - Wheel speed: 132 knots (max). - Computed Airspeed: 125 knots, increase to 132 knots (09:04:09) and start decrease - Longitude E $106^0$39’40.7’’, Latitude N$10^0$49’14.1” - Vibration: + Eng 1: N1 max 0.4, N2 max 0.4 + Eng 2: N1 max 1.1, N2 max 0.9 - EGT: + Eng 1 568^0C, increase to max 570^0C (09:04:07) and start decrease. + Eng 2 max 5600C, after that the parameter became NCD (invalid) - Oil pressure Eng 1 221 psi, Eng 2 173 psi - CVR: loud explosion sound (CVR time 01:28:30).
09:04:10	- Master caution on, Eng 2 low oil pressure
09:04:12	- Thrust Lever start decrease below 0 deg / REVERSER - Wheel speed: 92 knots. - Computed Airspeed: 106 knots - Longitude E $106^0$39’30.3’’, Latitude N$10^0$49’10.3” - Vibration: + Eng 1: N1 0.25, N2 0.3 + Eng 2: N1 0, N2 0.7 - EGT: + Eng 1 534^0C

	+ Eng 2 parameter became NCD
09:04:14:	- Eng 1 Reverser unlocked, Eng 2 reverser still locked. - Eng 1 Reverser fully deployed, Eng 2 Reverser not deployed.
09:04:24	Aircraft Stop - Longitude E $106^0$39'18.7'' - Latitude N$10^0$49'06.7"

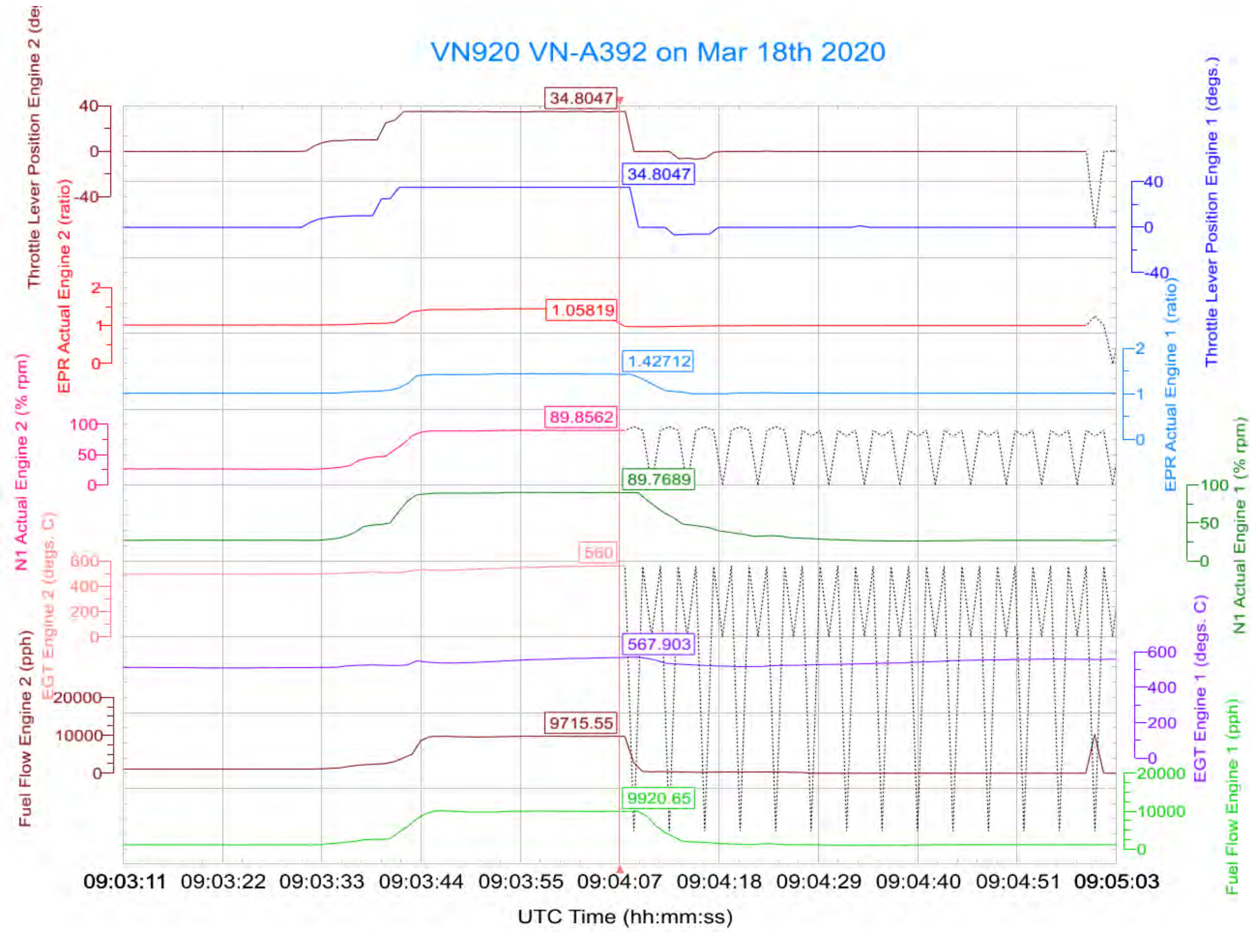

APPENDIX II: Metallurgical Investigation Final Report

Metallurgical Investigation Final Report

Pratt & Whitney
Materials & Processes Engineering
East Hartford, CT

Subject: **Metallurgical Investigation of V2500 HPT 1st Stage Hub from Engine V16580**

Date: **May 11, 2021**

Summary and Conclusions:

On March 18, 2020, Vietnam Airlines V2533-A5 engine V16580 experienced an uncontained event due to the fracture of the high pressure turbine 1st stage hub. The hub fractured into two pieces; one piece was approximately two-thirds of the hub, and the other was the remaining one-third. Both pieces were returned to Pratt & Whitney in East Hartford, CT for metallurgical examination under the supervision of the Civil Aviation Authority of Vietnam (CAAV) and the National Transportation Safety Board (NTSB) of the United States.

Visual review of the fracture surface identified an origin area in the middle of the bore. The origin area was intact on the larger hub fragment but was smeared due to event-related damage on the smaller fragment. Remaining features outside of the bore area appeared typical of rapid overstress/tearing.

Scanning electron microscope examination of the origin area identified an inclusion consisting of a region of voids and dispersed particles. Energy dispersive spectroscopic analysis of the particles identified three main chemistries: an Al-Mg-O type particle, an Al-O type particle with much less Mg, and a P-Ti-Ni-Co type particle. Surrounding the main inclusion area was the outer inclusion area, consisting of dispersed Al-Mg-O and Al-O particles. Outside of this region, crack features were intergranular, creating a roughly oval-shaped area that measured approximately 0.075" x 0.12" around the inclusion. A band of ductile dimple features measuring 0.001-0.005" wide, indicative of overstress, was observed at the extremity of the intergranular region; features extending from this region were transgranular. A mixture of striations and overstress features was observed in the transgranular progression, consistent with cracking due to engine operation at the reported operating conditions.

A series of metallographic polishes were prepared through both halves of the origin area. At each polish, the inclusion area was identified as a region of distributed particles, consistent with what was observed on the fracture surface. Additional electron microprobe analysis identified decreasing concentration gradients of silicon and phosphorous moving away from the inclusion, indicative of a reaction between the inclusion and the base metal.

1.0 Background

On March 18, 2020, a Vietnam Airlines (HVN) Airbus A321-231, powered by two International Aero Engines V2533-A5 engines, experienced an uncontainment of the No. 2 engine (V16580) during take-off roll from Tân Sơn Nhất International Airport in Ho Chi Minh City, Vietnam. Two fragments of the high pressure turbine (HPT) 1st stage hub were recovered and returned to Pratt & Whitney in East Hartford, CT, for metallurgical investigation. The investigation was conducted under the supervision of the Civil Aviation Authority of Vietnam (CAAV) and the National Transportation Safety Board (NTSB).

2.0 Details of Examination

2.1 Visual Review As-Received

Visual review of the hardware as-received found that the HPT 1st stage hub had fractured into 2 pieces. The hub had 2,636 hours and 1,910 cycles of engine operation since it had been installed. The larger piece, Fragment 1, consisted of approximately two-thirds of the hub. The smaller piece, Fragment 2, consisted of the remaining one-third of the hub (Figure 1). The two radial fracture paths between Fragments 1 and 2 were labeled Fracture A and Fracture B, as shown in Figure 1.

Visual review of Fragment 1 found that both the forward and aft sides of the hub exhibited smearing and other secondary, impact-related damage; damage to the bore was also observed, particularly in the vicinity of Fracture A. The inner diameter (ID) of the fragment appeared to have sprung open slightly. Thirty-eight (38) blade roots were retained in the blade slots; most airfoils had fractured off at or below the platform (Figures 2-3). Some of the blade roots were loose and could be removed by hand. The fragment and remnant blades weighed a total of 72.5 lbs (Figure 4). Review of the lugs identified the part markings as shown in Figure 5.

Visual review of Fragment 2 found that the piece exhibited a significant amount of damage on both the forward and aft sides of the part, as well as on the ID of the bore. Only four blade roots were retained on Fragment 2. The fragment and remnant blades weighed a total of 31.5 lbs (Figures 6-8).

During review of both Fragment 1 and Fragment 2, it was noted that Fracture A exhibited a planar path within the bore area. The bore region of Fragment 1 appeared largely intact with isolated smearing. Cyclic features were observed progressing from a subsurface, oval-shaped origin area within the bore. The fracture surface outboard of the bore area was completely obscured by secondary damage. On the Fragment 2 side of Fracture A, features in the bore were smeared/damaged; however, remnant cyclic markers were observed. Outboard of the Fragment 2 bore area, the surface exhibited rougher features and shear lips consistent with overstress/rapid tear (Figures 9-11).

Fracture B did not exhibit as planar of an axial-radial fracture path as Fracture A. Review of the Fragment 1 side of Fracture B found rough, directional features and shear lips consistent with overstress/rapid tear. The Fragment 2 side of Fracture B was completely obscured by secondary damage (Figure 12). Fracture B was determined to be secondary to Fracture A.

2.2 Visual and Binocular Review – Fragment 1

The Fracture A surface on Fragment 1 was sectioned from the remainder of the hub via wire electrical discharge machining (EDM). Best effort measurements to the origin area were taken; the origin was located approximately 1.5" from the aft surface of the bore, 1.1" from the ID surface of the bore, and approximately 5.25" from the blade slot bottom. Damage on the external reference surfaces prohibited a precise measurement to the origin location (Figure 13).

Further visual and binocular review of the fracture surface identified cyclic markers throughout the crack progression surrounding the oval shaped origin area. The oval shaped origin region appeared rougher textured compared to the surrounding area. This region measured approximately 0.120" x 0.075" (Figures 14 – 15).

2.3 SEM Examination – Fragment 1

The Fragment 1 fracture surface was rinsed with water and isopropanol to clean it for scanning electron microscope (SEM) examination. SEM examination of the oval-shaped origin area identified an inclusion roughly centered in this region. Via back scatter electron imaging, the inclusion appeared as a region of darker gray/black particles (Figures 16 – 17). Initial energy dispersive spectroscopy (EDS) analysis of the inclusion region identified an increased concentration of oxygen, magnesium, aluminum, phosphorous, and titanium (O, Mg, Al, P, and Ti). Additional elements were also identified however it could not be determined if they were due to the inclusion or other event-related contamination sources (Figures 18-19). Outside of this inclusion, crack features within the oval shaped area appeared intergranular. This intergranular region 0.120" x 0.075" in size was surrounded by a band of ductile dimples ~0.001 to 0.005" wide. Transgranular features were observed progressing in all directions from the ductile dimple band (Figure 20).

In order to fully characterize the fracture surface via SEM and EDS, several acetate replicas were pulled from the surface to remove loose debris. The sample was subsequently ultrasonically cleaned in a mild detergent to remove additional surface contamination.

Further SEM characterization of the fracture surface following cleaning was completed to map out the features within the bore area. Five main regions were identified: the main (inner) inclusion area, the outer inclusion area, the intergranular area, the ductile dimple band, and the transgranular area. Additionally, regions of smeared features due to secondary event-related damage were observed within and outside of the origin area (Figures 21-22).

2.3.1 Main (Inner) Inclusion Area

The main inclusion area consisted of a concentrated area of voids and foreign particles. This area measured 0.016" x 0.0025" on the fracture surface (Figures 22-23).

SEM/EDS analysis of individual particles identified three distinct particle types. The two most common types were a primarily Al-O type with a small amount of Mg and an Al-Mg-O type particle, with much more magnesium. The third type of particle, found rarely within the main inclusion area, consisted of a phosphorous-titanium-nickel-cobalt chemistry (Figure 24).

2.3.2 Outer Inclusion Area
The outer inclusion area was a non-continuous region of dispersed particles surrounding the main inclusion area. This area appeared medium gray and speckled via backscatter SEM examination. The continuous part of this region measured 0.033" x 0.007"; however, additional regions were observed over a distance of more than 0.041". Fracture features appeared to be dominated by the presence of these ceramic particles, forming ductile regions around them (Figure 25).

SEM/EDS analysis of the particles identified the two common chemistries also observed in the main inclusion area – Al-Mg-O and Al-O with much less Mg. The P-Ti-Ni-Co type particle was not observed in the outer inclusion area (Figure 26).

2.3.3 Intergranular Area
Surrounding the outer inclusion area, fracture features were intergranular, consistent with cracking having occurred at temperatures above reported operational temperatures. The fracture surface appearance and topography did not appear consistent with fatigue fracture (Figure 27).

2.3.4 Ductile Dimple Band
At the extremity of the intergranular region, a discrete band of ductile dimple features was observed. This band varied in width from approximately 0.001" – 0.005". Within this region, the ductile dimple features were the predominant mode of fracture. The band was observed around the entirety of the intergranular region (Figure 28).

2.3.5 Transgranular Area
SEM examination of the region outside of the oval-shaped origin area found that the fracture progressed away from the origin in all directions via transgranular features. Near the ductile dimple band, a mixture of striations and ductile features was observed. The ductile features were indicative of cyclic tearing and comprised greater than 50% of the fracture surface in these areas (Figures 29-30). A crack growth rate assessment could not be performed as the ductile features comprised a majority of the crack features.

Further review of the progression extending away from the origin area confirmed unstable/cyclic tearing features throughout (Figure 31). As distance from the origin increased, more ductile overstress features were observed. The transgranular features appeared consistent with cracking due to an unstable mode of low cycle fatigue (LCF).

2.4 White Light Scanning – Fragment 1

Focused white light scanning of the Fragment 1 origin area was completed to characterize the topography of this region (Figure 32).

2.5 Visual and Binocular Review – Fragment 2

The Fracture A surface in the bore area on Fragment 2 was sectioned from the remainder of the hub via wire EDM (Figure 33). Binocular microscope examination of the fracture surface identified significant smearing and mechanical damage. The origin area was not readily apparent; however, remnant cyclic markers were observed throughout the progression. An adhered, smeared flap of material was observed in the vicinity of the origin area (Figure 34).

2.6 White Light Scanning – Fragment 2

Similar to Fragment 1, focused white light scanning of the origin area was completed to characterize the topography of the fracture surface (Figure 35). While the scan was heavily biased due to the damage on the fracture surface, remnant high and low features could be observed. A comparison of the Fragment 1 and Fragment 2 topography maps allowed for identification of the approximate inclusion location on the Fragment 2 fracture surface. The inclusion location was adjacent to the adhered, smeared flap of material (Figure 36).

2.7 SEM Examination - Fragment 2

The Fragment 2 fracture surface was rinsed with water and isopropanol prior to SEM examination. SEM evaluation of the fracture surface confirmed secondary damage and smeared features. There were no original fracture features remaining within the vicinity of the origin area (Figure 37).

2.8 Micro-CT/UT Scans

The bore regions of both Fragment 1 and Fragment 2 were scanned via micro computed tomography (micro-CT) and ultrasonic (UT) methods to characterize the origin.

Initially, the Fragment 1 sample measured approximately 3” x 2” x 0.75”. The scan was completed over this section at a voxel resolution of 46 µm (~0.0018”) to provide the best penetration through the sample. A second, focused scan of a region on the sample measuring approximately 1.2” x 1.2” surrounding the origin was completed at a voxel resolution of 15 µm (~0.0006”). Due to the large sample size, contrast was limited within the scan. As a result, the scan primarily captured surface topography. While the focused scan did capture more detail within the origin area, it was still too noisy to identify the inclusion area (Figures 38 – 39).

The Fragment 1 bore region was further sectioned to a 1” x 1” x 0.1” piece via EDM. The origin was located in the center of this section.

Additional micro-CT examination of the 1” x 1” x 0.1” section from Fragment 1 was completed. A focused scan completed at a voxel resolution of approximately 6 µm (0.0002”) was centered on the origin. A slight difference in density believed to be associated with the inclusion area was observed. This area extended approximately 0.005” – 0.007” into the metal. No other areas with similar features were observed on the rest of the scan (Figure 40).

Micro-CT examination was additionally completed on the 3.5” x 2” x 0.1” thick Fragment 2 section. A focus scan aimed at the origin area was completed at a voxel resolution of 10 µm (~0.0004”). No inclusion within the origin area could be identified. Secondary damage to the fracture surface may have obscured the evidence of the inclusion from the micro-CT scan (Figure 41).

Ultrasonic (UT) examination was completed on the 1” x 1” x 0.1” Fragment 1 section. The UT method utilized high frequency ultrasonics at 25MHz, 50MHz and 100MHz in order to obtain higher sensitivity. No indications associated with the known inclusion location were observed. However, indications were found that correlated with the perimeter of the intergranular region. No other indications were observed outside of the origin area (Figure 42).

Additional UT scans were completed on the 0.1” thick Fragment 2 section at 50 MHz and 100 MHz. No indications associated with the known inclusion location were observed (Figure 43).

2.9 Metallographic Examination

A metallographic section was prepared through an intact region of the bore approximately one to two inches away from the origin area (See Figure 13). This sample was reviewed as-polished and via three different etchants for general microstructure conformance. The distribution of gamma prime phase, grain size, distribution of carbides, and amount of micro-porosity all conformed to the material requirements (Figure 44).

A sample of material was removed and sent off-site for chemistry analysis to capture the full chemical composition. The material composition conformed to the requirements for powder metal IN-100 material.

2.10 Fragment 1 Serial Polish

A metallographic section was prepared perpendicular to the main area of the inclusion on Fragment 1 in order to understand the size, shape, and morphology by progressively (serial) polishing into it. The Fragment 1 section was mounted in clear epoxy so that the progress of the polish plane across the fracture surface could be visually observed. Polishing started outside of the origin area and progressed into the area of the inclusion (Figure 45). The section was initially polished at increments of ~0.01” until the plane of the inclusion was reached; then the polishing increment was decreased to ~0.002” per polish. At each plane of polish, the section was examined as-polished and via two different etchants to characterize the microstructure.

The first confirmed sighting of the inclusion was at Polish 8; it was continually observed through Polish 13 at which point the serial polishing process was stopped to preserve remaining evidence. At each of these locations, the inclusion was roughly centered within the intergranular region of the fracture. While some of the surface appeared smeared, the inclusion area was largely intact (Figures 46-47).

Review of each of the polish planes as shown in Figure 47 in the as-polished condition identified the inclusion area as a region of distributed particles. The particles appeared dark gray to black when compared to the surrounding base metal. Many of the particles appeared to be concentrated on the prior particle boundaries in the material. This appearance was consistent with what was observed on the fracture surface as part of the outer inclusion area. The densest region of this area was measured as the particle cloud dimension; maximum size measured at Polish 11 was 0.008" wide by 0.009" deep (Figure 48).

Starting at polish 11, the voided area of the inclusion was observed. The voided region was observed on polishes 11-13 and measured up to 0.003" in depth.

The sample was etched with a mixed acids etchant to reveal the gamma prime phase. At the center of the inclusion, an area denuded of the primary gamma prime phase was observed. This area was contained within the particle cloud and typically was smaller than the particle cloud. Secondary and tertiary gamma prime phases were still visible within this region (Figure 49).

SEM/EDS analysis of the metallographic section at each of Polishes 8 – 13 was completed. EDS maps of the particle cloud showed the distribution of elements within the region. The particle cloud itself consisted of the Al-O and Al-Mg-O type chemistries. This was consistent between polishes (Figures 50-53).

At Polish 11, a discrete particle was observed within the voided region as shown in Figure 51. This particle had the P-Ti-Ni-Co chemistry consistent with those observed in the main inclusion area on the fracture surface.

2.11 Fragment 1 Electron Microprobe Analysis

Electron microprobe analysis (EMP) was completed on the metallographic section at Polishes 11 and 13 to gain higher fidelity chemistry data within and away from the inclusion area by use of wavelength dispersive spectroscopy (WDS). EMP EDS/WDS maps of the particle cloud revealed chemistry consistent with what was observed via initial SEM/EDS analysis, including high concentrations of oxygen, aluminum, magnesium, phosphorous, and titanium. Elevated levels of silicon were observed at discrete points, but these may have been due to contamination from sample preparation (Figures 52 – 53).

A series of points, or line scans, were taken following multiple paths away from the inclusion; chemistries at each point were analyzed to understand material composition and look for small amounts of reactive elements, with a focus on silicon and phosphorous. On both Polish 11 and Polish 13, the initial line scans extended for 200 – 250 µm from the inclusion in two directions. On Polish 13, an additional line scan extending approximately 1250 µm from the edge of the inclusion was completed. This scan extended through the particle cloud, intergranular area, and into the transgranular area.

Examination of the results found that on all paths, a decreasing concentration gradient of silicon was observed extending from the inclusion, indicative of a reaction between the inclusion and the base metal. Maximum weight percent ranged from 0.2 – 0.3 percent; values exceeding that were believed to be due to surface contamination from sample preparation. This concentration gradient appeared to die out within the first 150 – 200 µm from the inclusion area until it reached a value consistent with what was observed in the bulk material. It should be noted that while this data can be used to understand general trends, the absolute value of the weight percent measurement is uncertain due to a lack of calibration of the electron microprobe at the levels observed.

Review of the scans on both polishes 11 and 13 for phosphorous found that the phosphorous weight percent generally appeared to stay steady with a slight downward trend. Review of the 1250 μm scan on polish 13 found that phosphorous exhibited a decreasing concentration gradient over the first 400-500 μm away from the inclusion. Again, while this data can be used to understand general trends, the absolute value of the weight percent measurement is uncertain due to a lack of calibration of the electron microprobe at the levels observed. In particular, weight percent values less than 0.03 for phosphorous should be considered undetectable via microprobe since the value at that level cannot be distinguished from the noise (Figures 54 – 56).

2.12 Fragment 1 EBSD

Electron backscatter diffraction (EBSD) analysis was completed on the metallographic section of Fragment 1 at Polish 13. The initial EBSD scan, centered on the inclusion area, found no discernable difference in grain size between the transgranular and intergranular regions; no clusters of similarly oriented grains were detected (Figure 57). The sample was further prepared by polishing it overnight on a colloidal silica solution for higher resolution examination and a focused review of the inclusion area was completed. The higher resolution examination found no discernable differences in grain size between the inclusion area and the regions surrounding it. The orientation of grains appeared random; no clusters of similarly oriented grains were detected. The scans show some evidence of missing data (black pixels); these appeared to correlate with the ceramic particles within the particle cloud (Figure 58).

2.13 Fragment 2 Serial Polish

A metallographic section was prepared through Fragment 2 in order to understand the size, shape, and morphology of the inclusion via serial polishing. The Fragment 2 section was mounted in clear epoxy so that the progress of the polish plane across the fracture surface could be visually observed. The location of the inclusion area had been roughly identified using the comparison of the topography of Fragment 1 (Figure 59). At each plane of polish, the section was examined as-polished and via two different etchants to characterize the microstructure.

A total of 23 polishes were completed on the metallographic section. Polishes occurred at increments of 0.002” – 0.010”, depending on location, with finer increments used to polish into and through the inclusion. The first confirmed sighting of the inclusion was at Polish 5; the last confirmed sighting was at Polish 18, as shown in Figure 60. This corresponded to a minimum inclusion length of 0.025” as measured in the polish direction.

Review of each of the polish planes in the as-polished condition identified the inclusion area as a region of distributed particles. The particles appeared dark gray to black when compared to the surrounding base metal. Many of the particles appeared to be concentrated on the prior particle boundaries in the material. This appearance was consistent with what was observed on the fracture surface as part of the outer inclusion area and on the Fragment 1 serial polish. The most dense region of this area was measured as the particle cloud dimension; minimum size observed at Polish 16 measured 0.001” x 0.005”; maximum size measured at Polish 8 was 0.005” x 0.004” (Figure 61). Additionally, cracking was observed at multiple polishes on this section. However, due to the secondary damage to the surface, it was not possible to determine whether the crack was pre-existing or due to secondary damage after the fracture event.

SEM/EDS analysis of the metallographic section at each of Polishes 5 and 7 was completed. EDS maps of the particle cloud showed the distribution of elements within the region. The particle cloud itself consisted of the Al-O and Al-Mg-O type chemistries (Figure 62). This was consistent on both polishes.

2.14 Fragment 2 Electron Microprobe Analysis

The metallographic section through Fragment 2 was analyzed via electron microprobe. Two line scans extending up to 275 µm away from the inclusion were completed. Review of the data found decreasing concentration gradients of silicon and phosphorous, indicative of a reaction between the inclusion and the base metal. The relative concentrations decreased at increased distance from the inclusion (Figure 63). The gradient was similar to that seen on the prior analysis of Fragment 1.

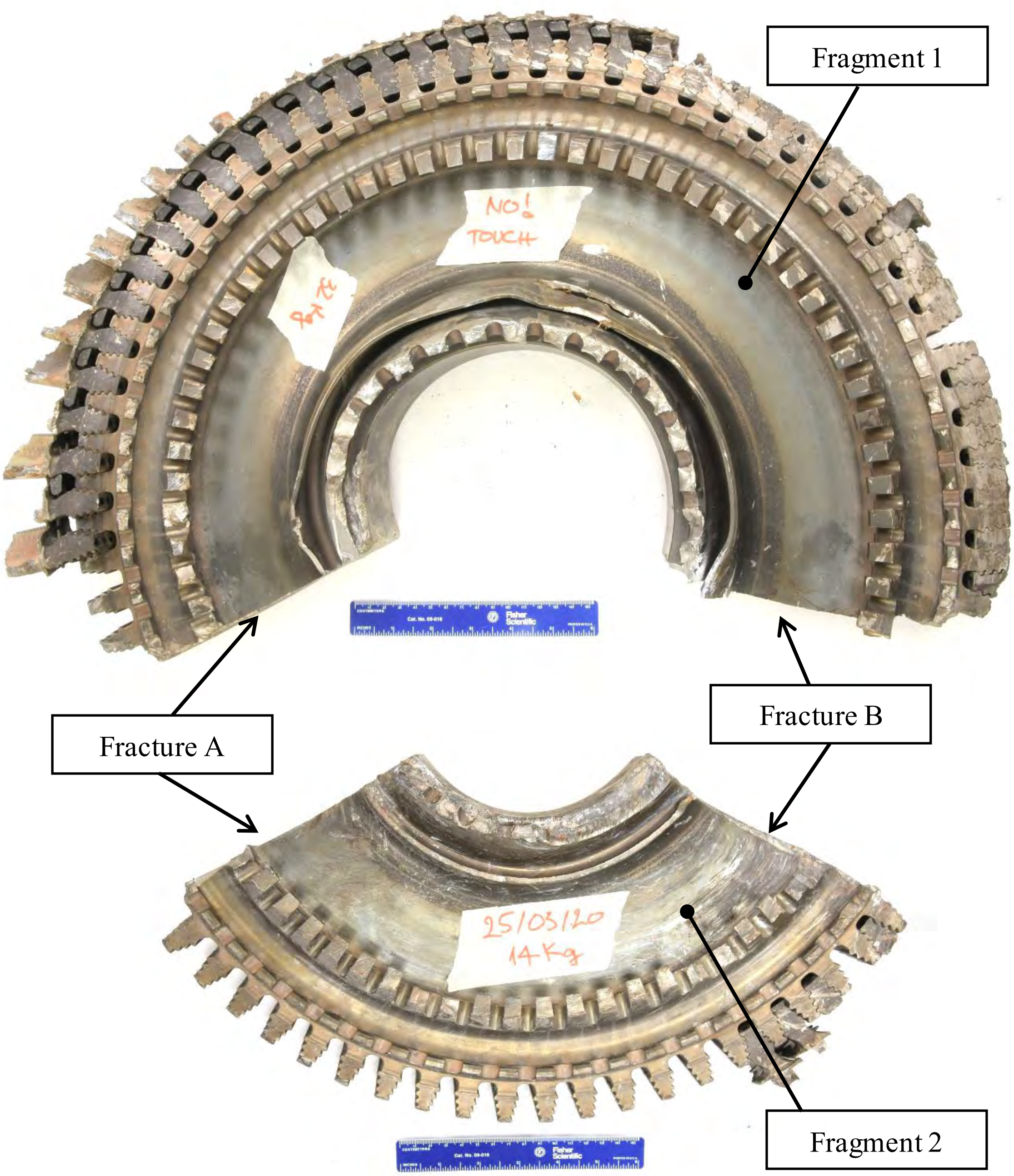

Figure 1: Overall images showing the forward sides of Fragments 1 and 2 in the as-received condition. Fracture surfaces A and B on each part are notated as shown.

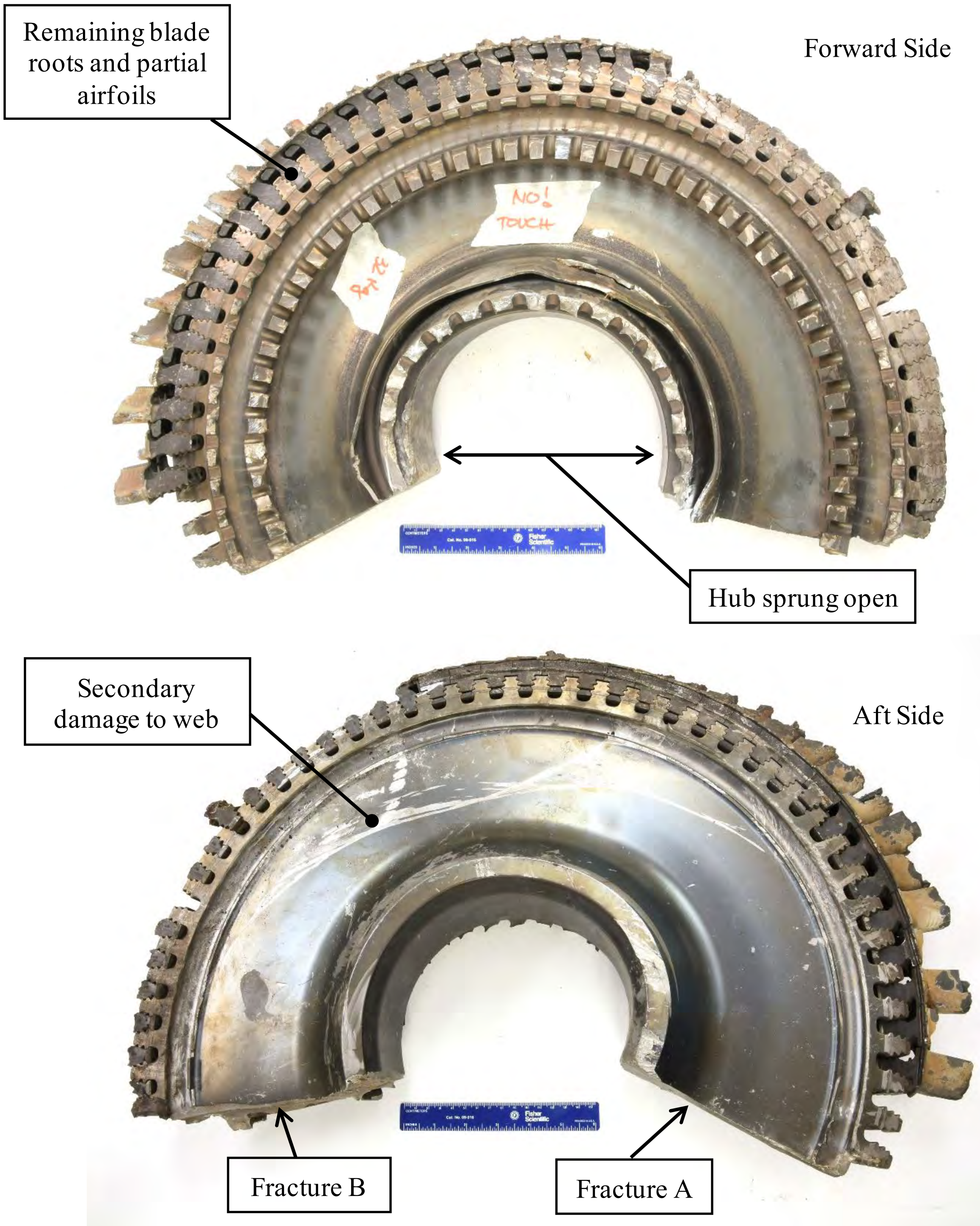

Figure 2: Forward (top) and aft (bottom) sides of Fragment 1. Secondary damage was observed on both sides of the hub.

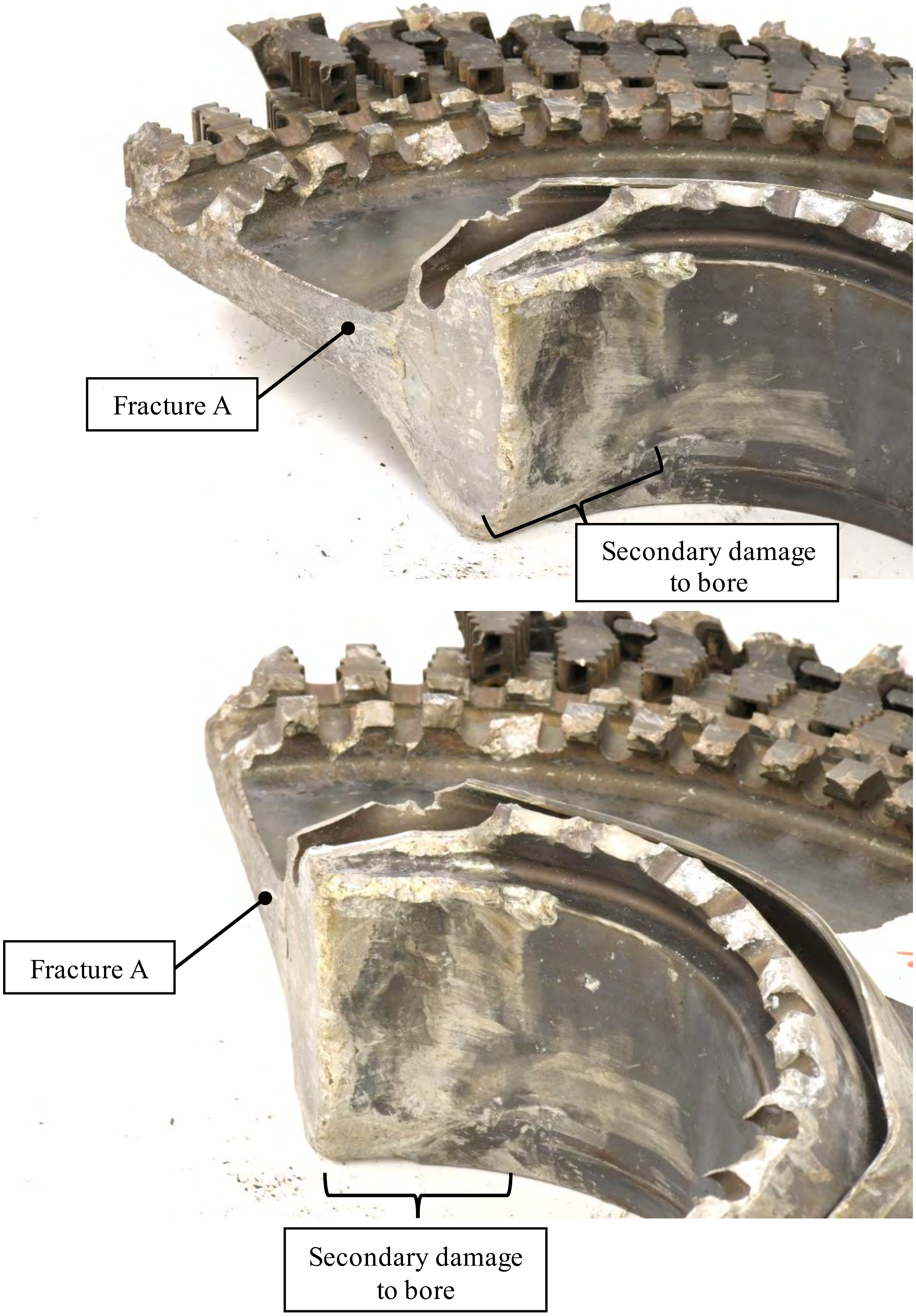

Figure 3: Images showing damage to the bore and hub section at the Fracture A end of Fragment 1.

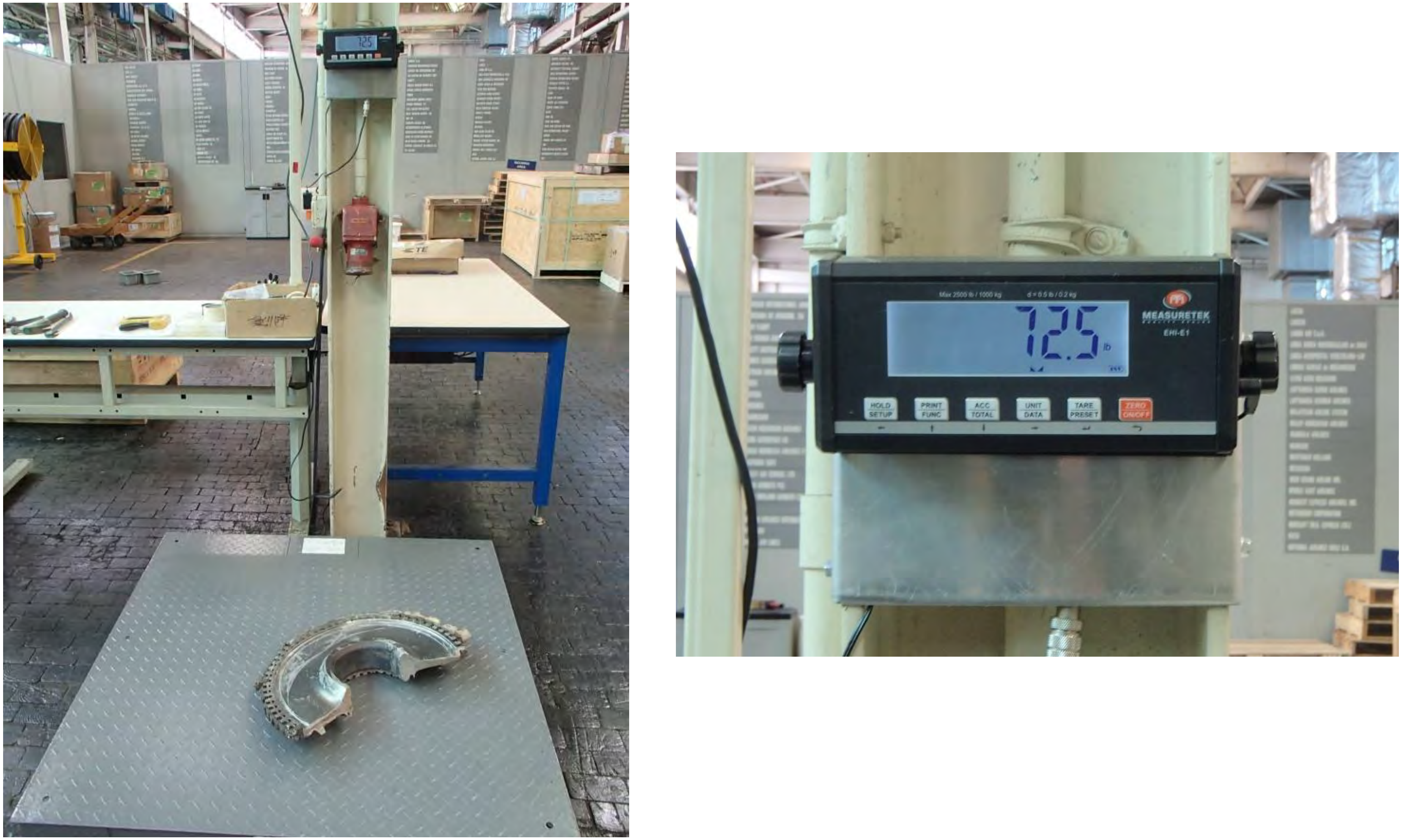

Figure 4: The weight of Fragment 1 and the remaining blades as-received measured 72.5 lb.

Figure 5: Hub part markings on Fragment 1.

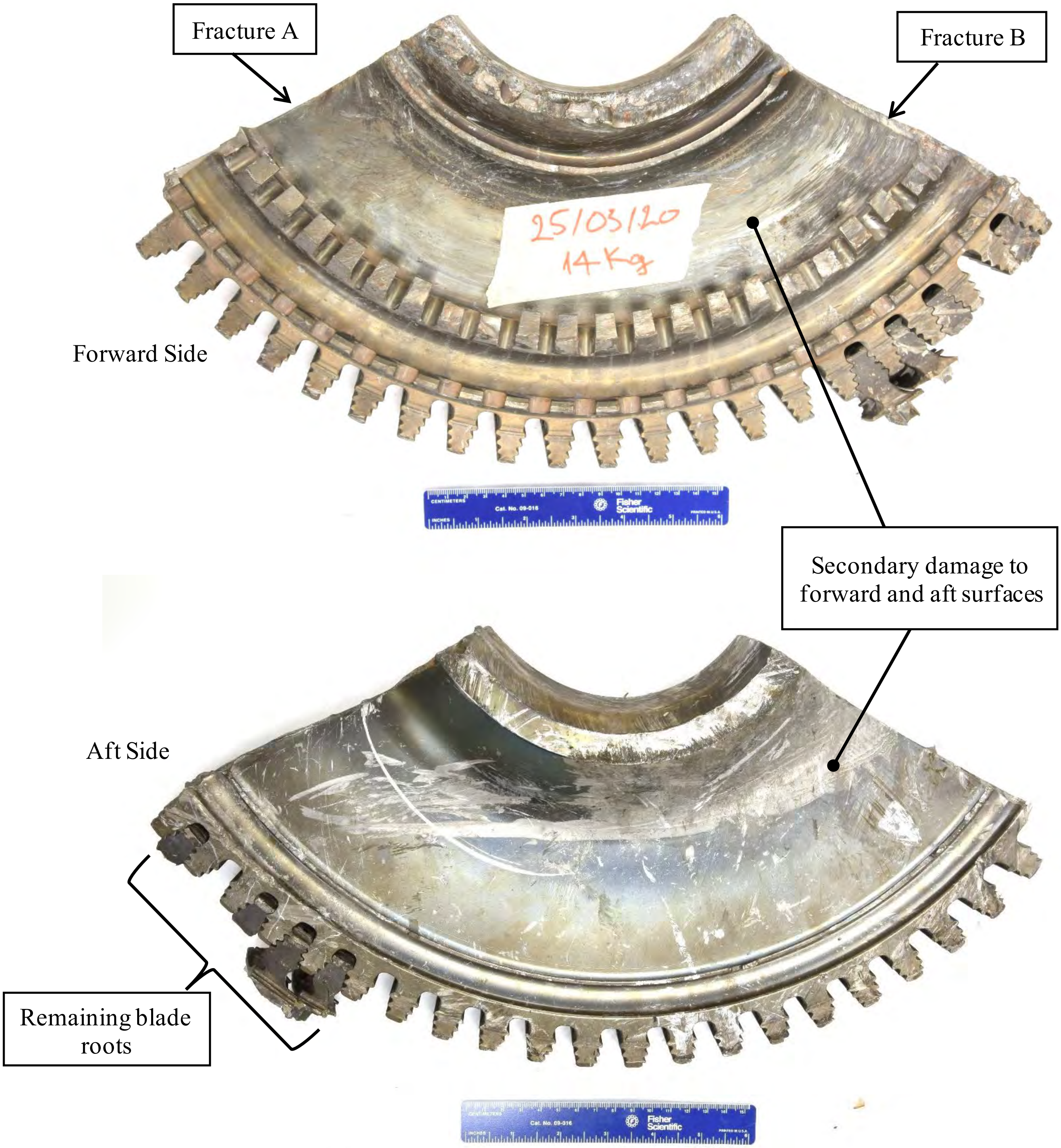

Figure 6: Forward (top) and aft (bottom) sides of Fragment 2.

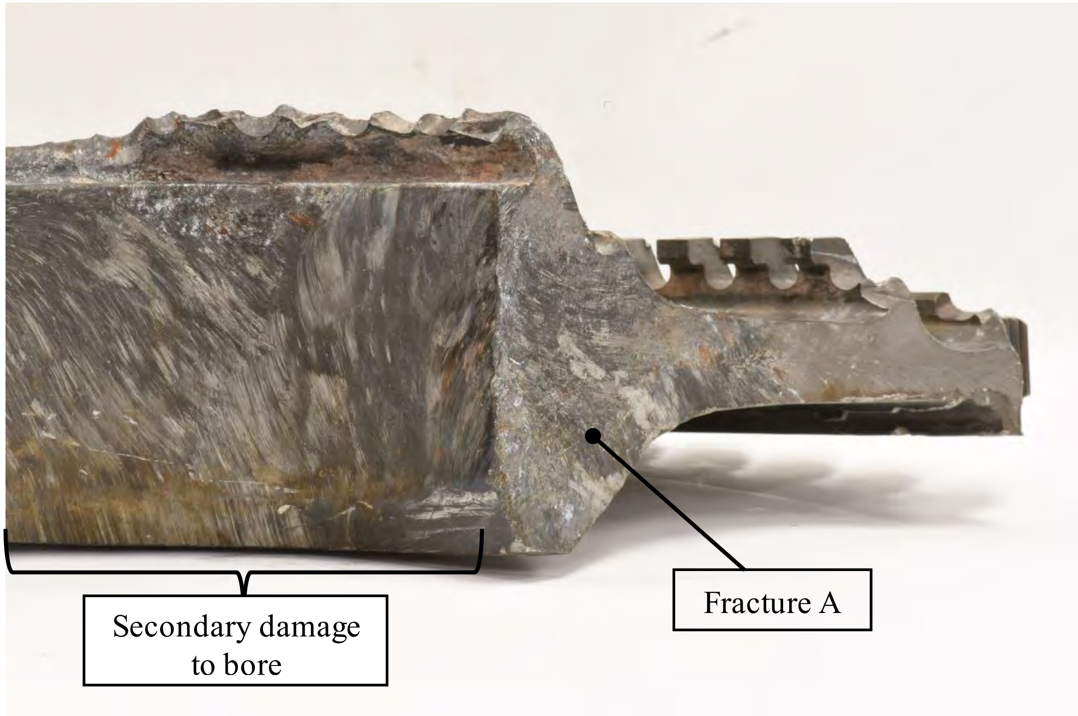

Figure 7: Images showing damage to the bore at the Fracture A side of Fragment 2.

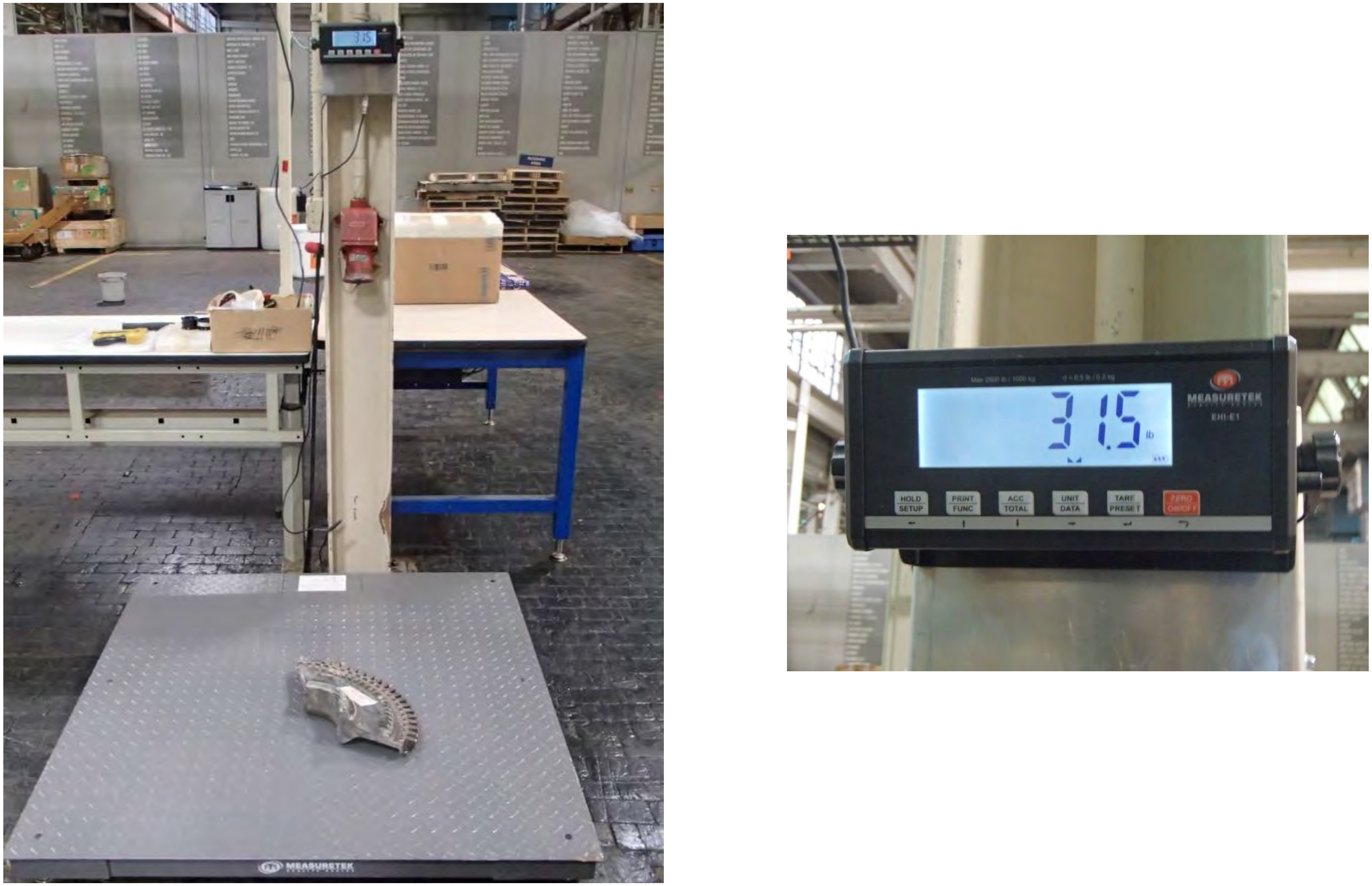

Figure 8: The weight of Fragment 2 and the remaining blades as-received measured 31.5 lb.

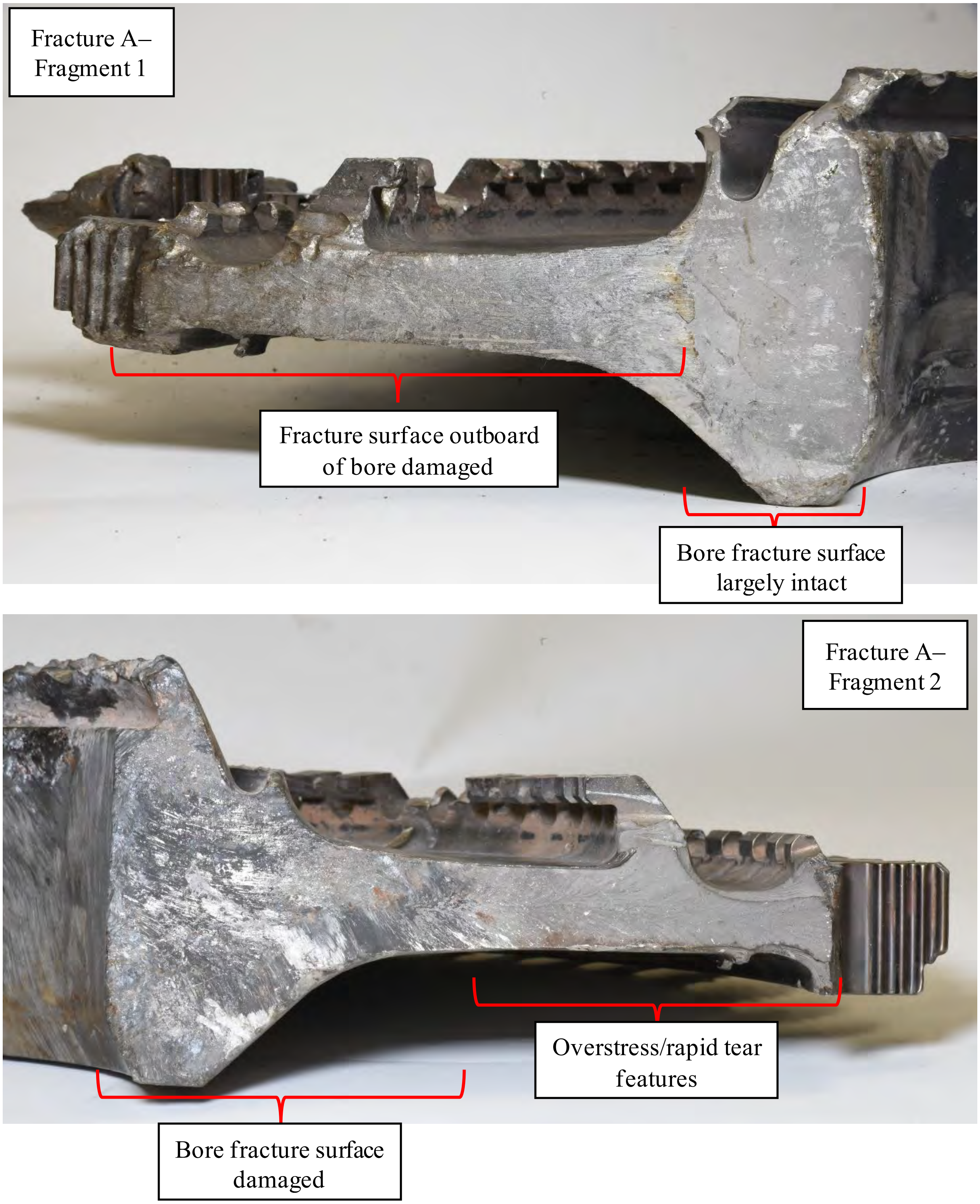

Figure 9: Mating sides of Fracture A on Fragment 1 (top) and Fragment 2 (bottom). The fracture appeared relatively planar in the axial-radial plane in the bore area.

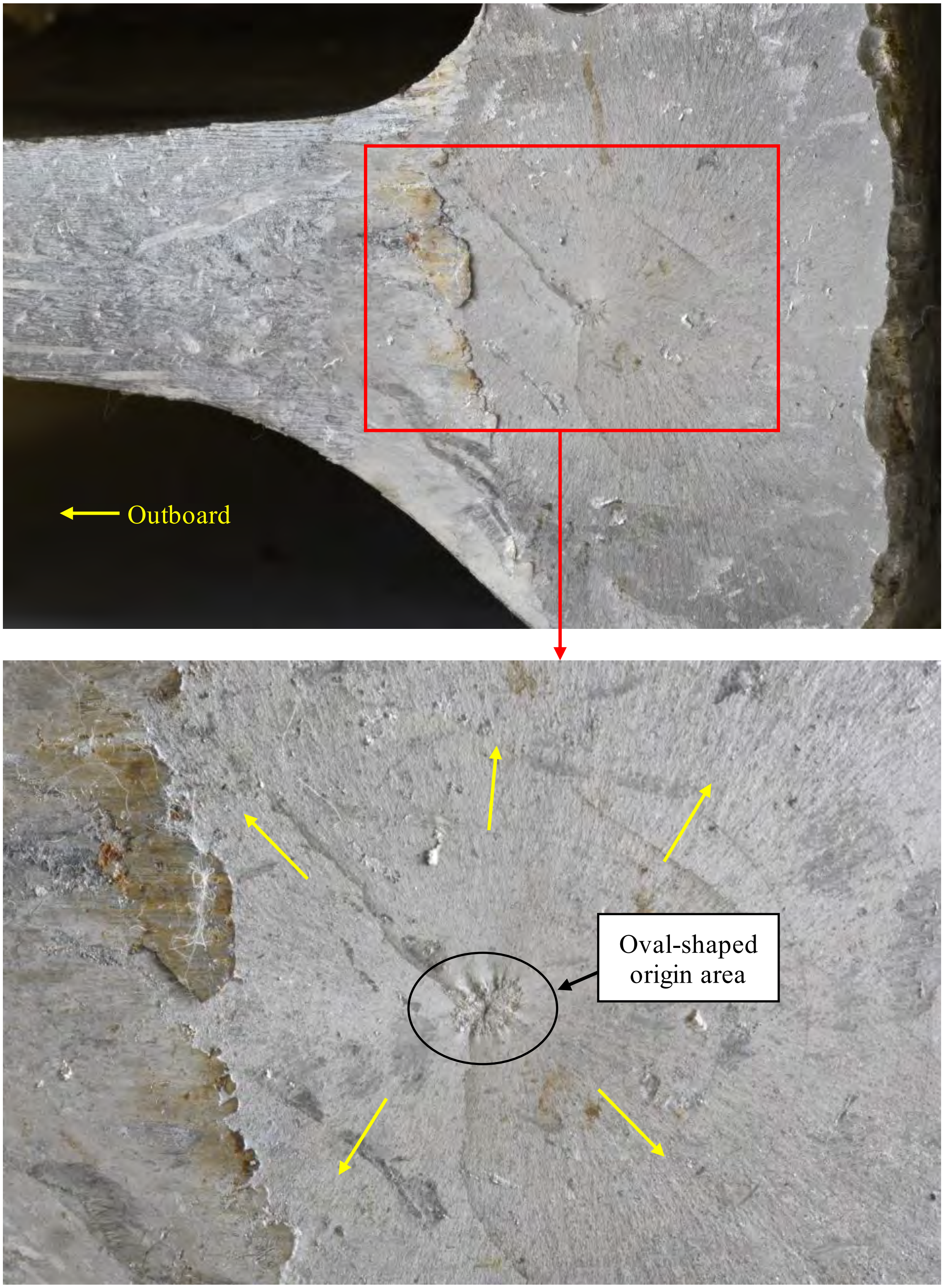

Figure 10: Origin area on the Fragment 1 side of Fracture A. Yellow arrows indicate general direction of fracture progression.

Figure 11: Origin area on the Fragment 2 side of Fracture A; the fracture surface was smeared/damaged; however, remnant cyclic markers were observed.

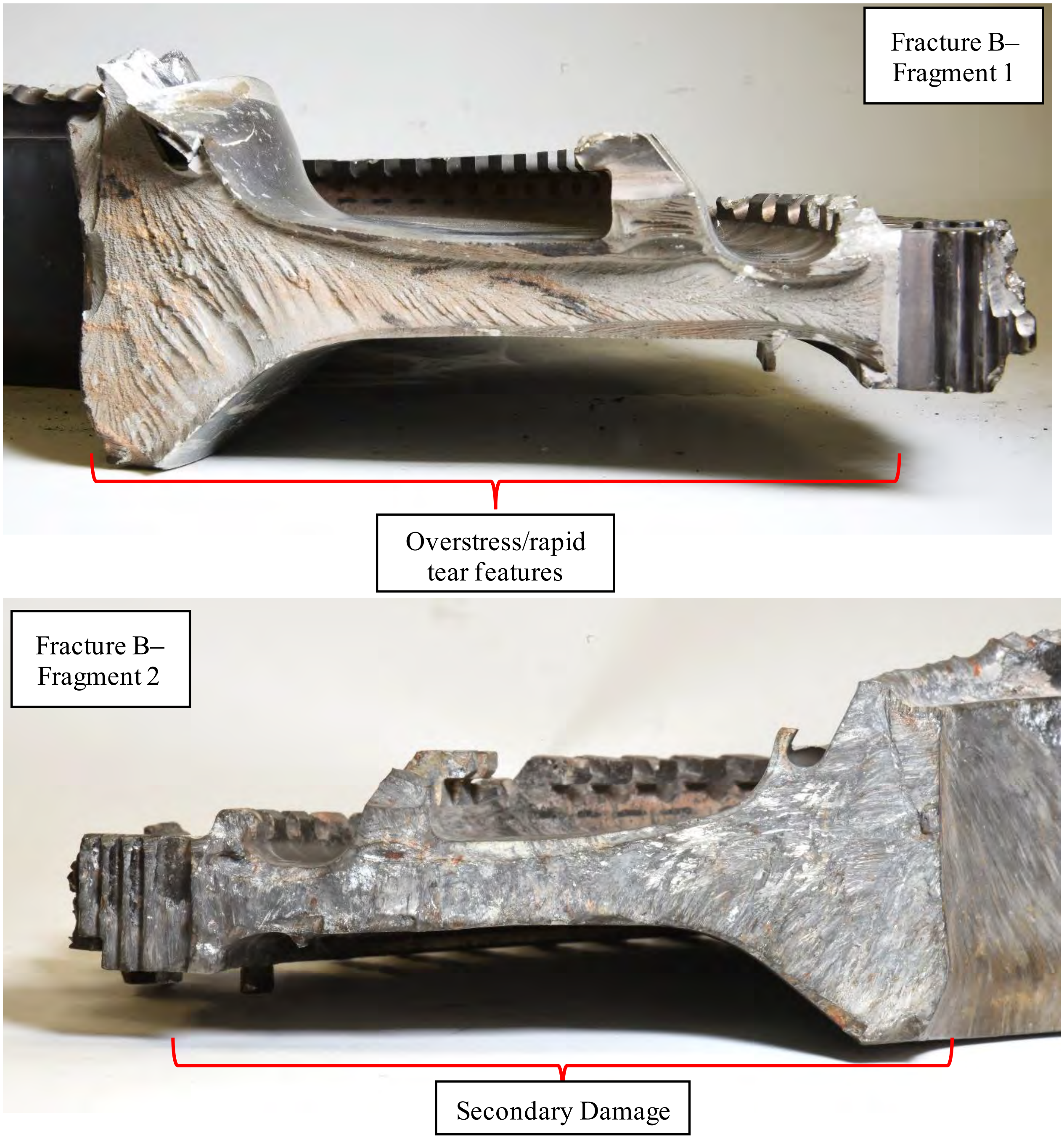

Figure 12: Mating sides of Fracture B on Fragment 1 (top) and Fragment 2 (bottom).

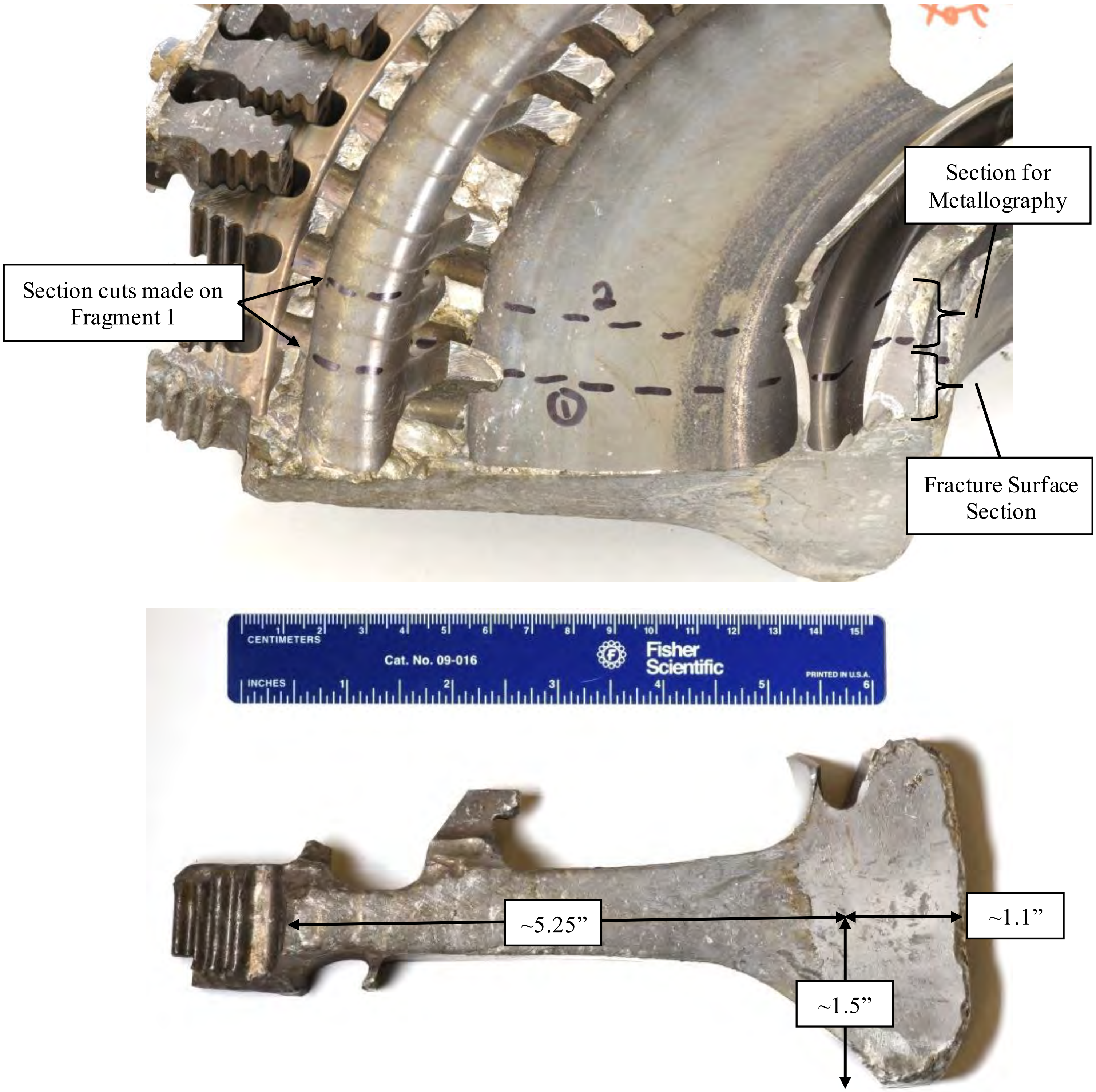

Figure 13: The Fracture A surface on Fragment 1 was sectioned from the remainder of the hub. Approximate dimensions to oval shaped origin area shown above.

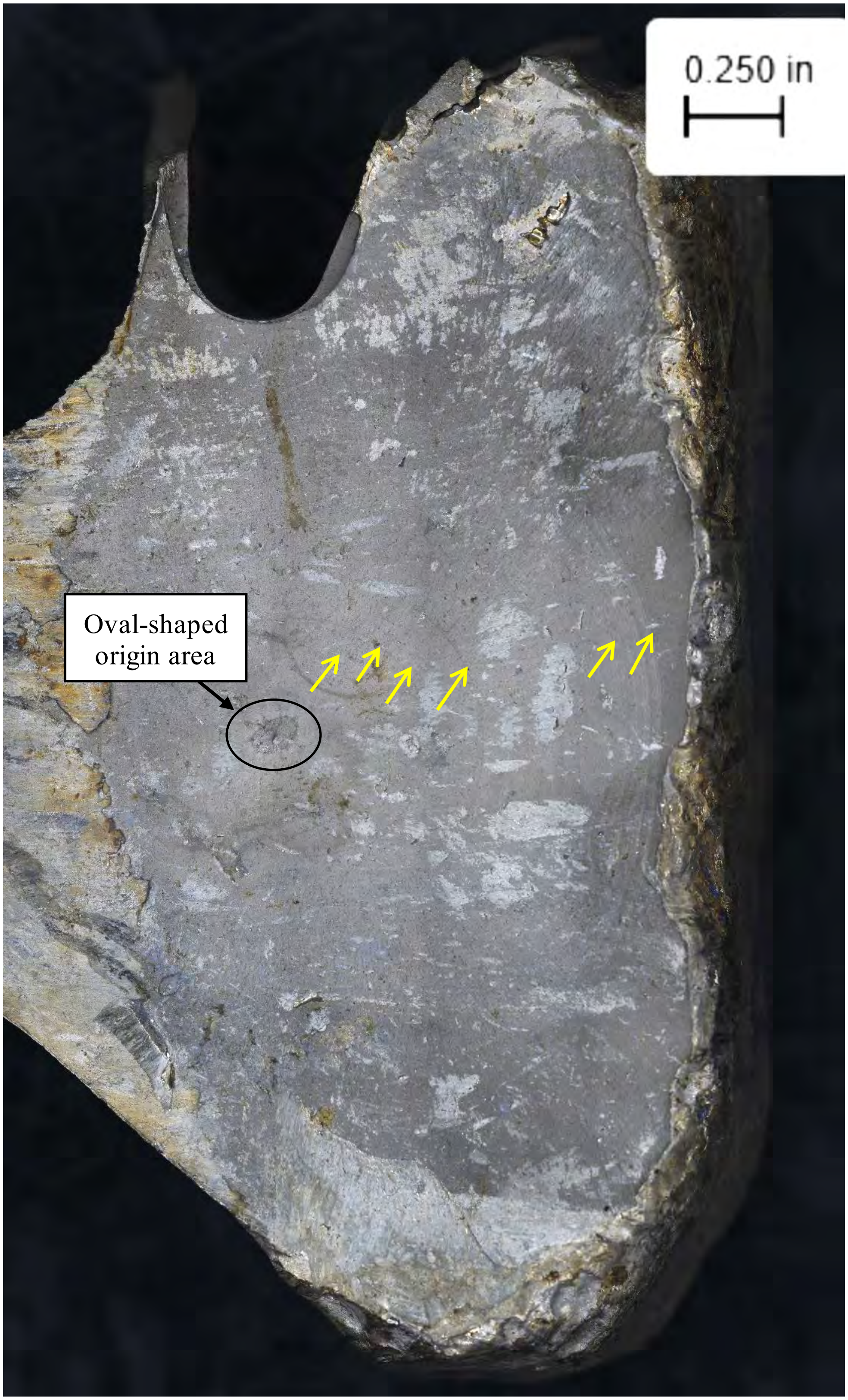

Figure 14: Bore area on Fragment 1 Fracture A. Cyclic markers emanating from the oval shaped origin area were observed (some notated by yellow arrows).

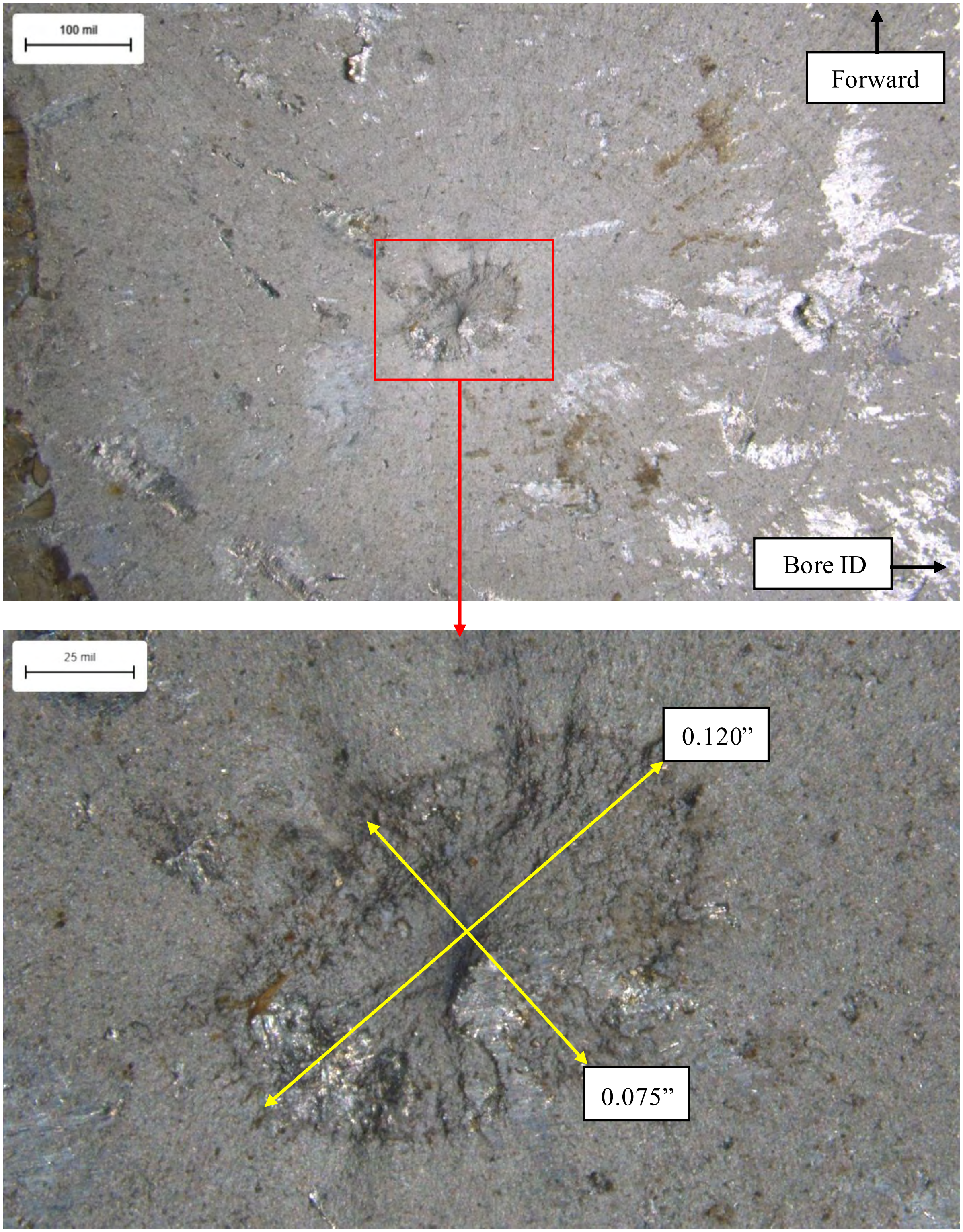

Figure 15: Higher magnification images showing the origin area on Fragment 1.

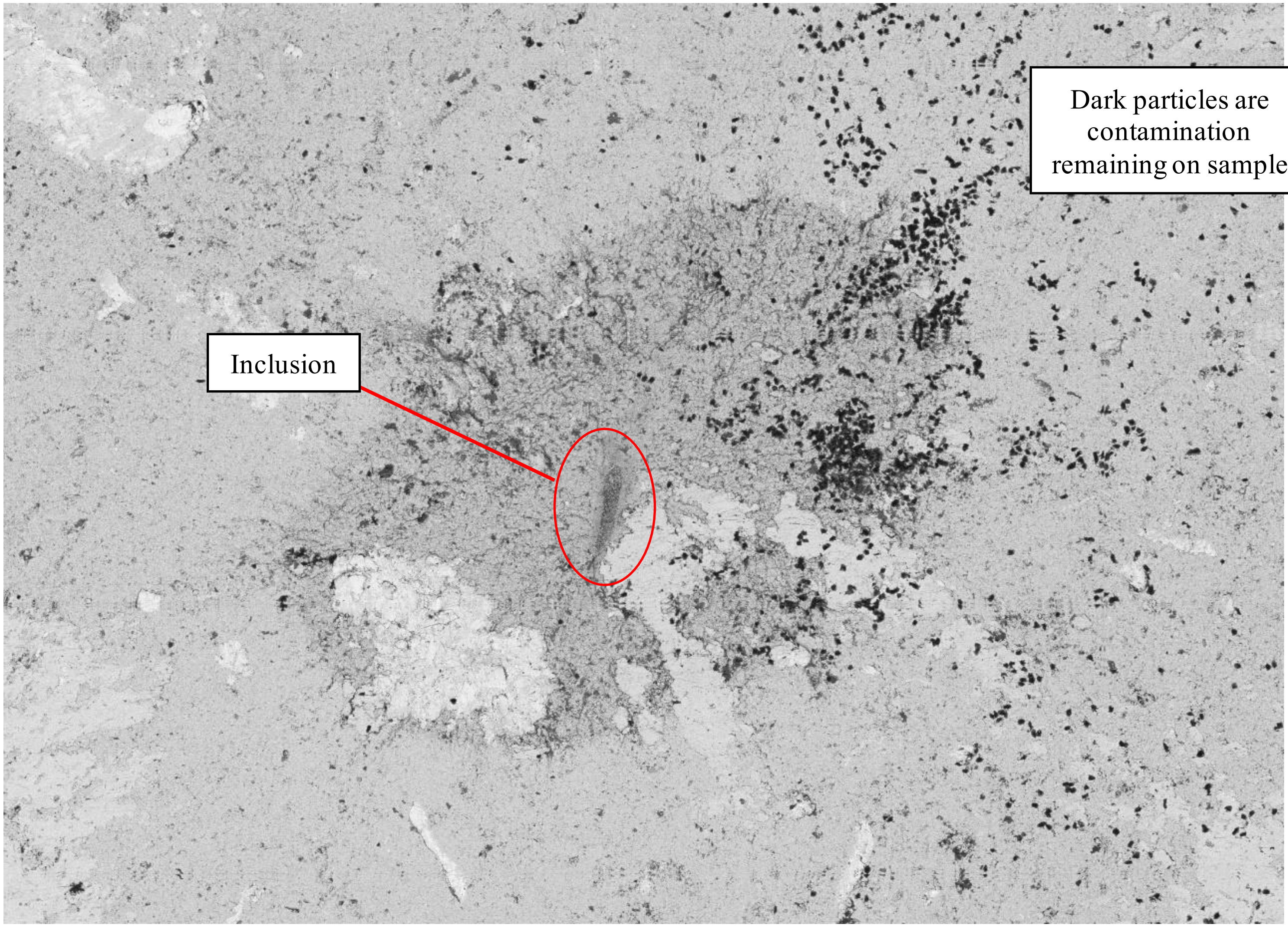

Figure 16: Initial SEM examination following a water and isopropanol rinse identified an inclusion roughly centered in the oval-shaped origin area.

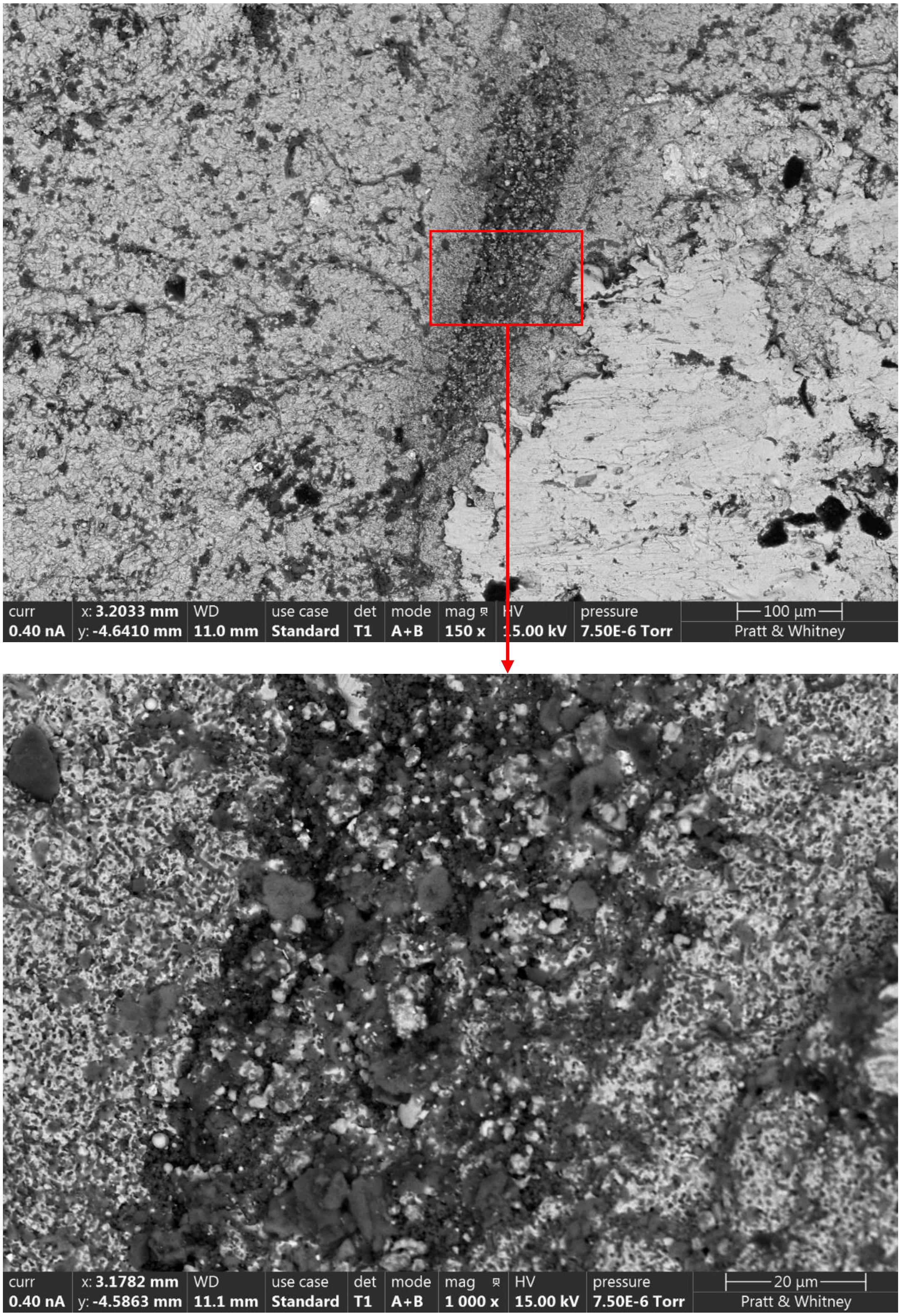

Figure 17: SEM images showing the region of darker gray/black particles within the inclusion as viewed via back scatter electron imaging.

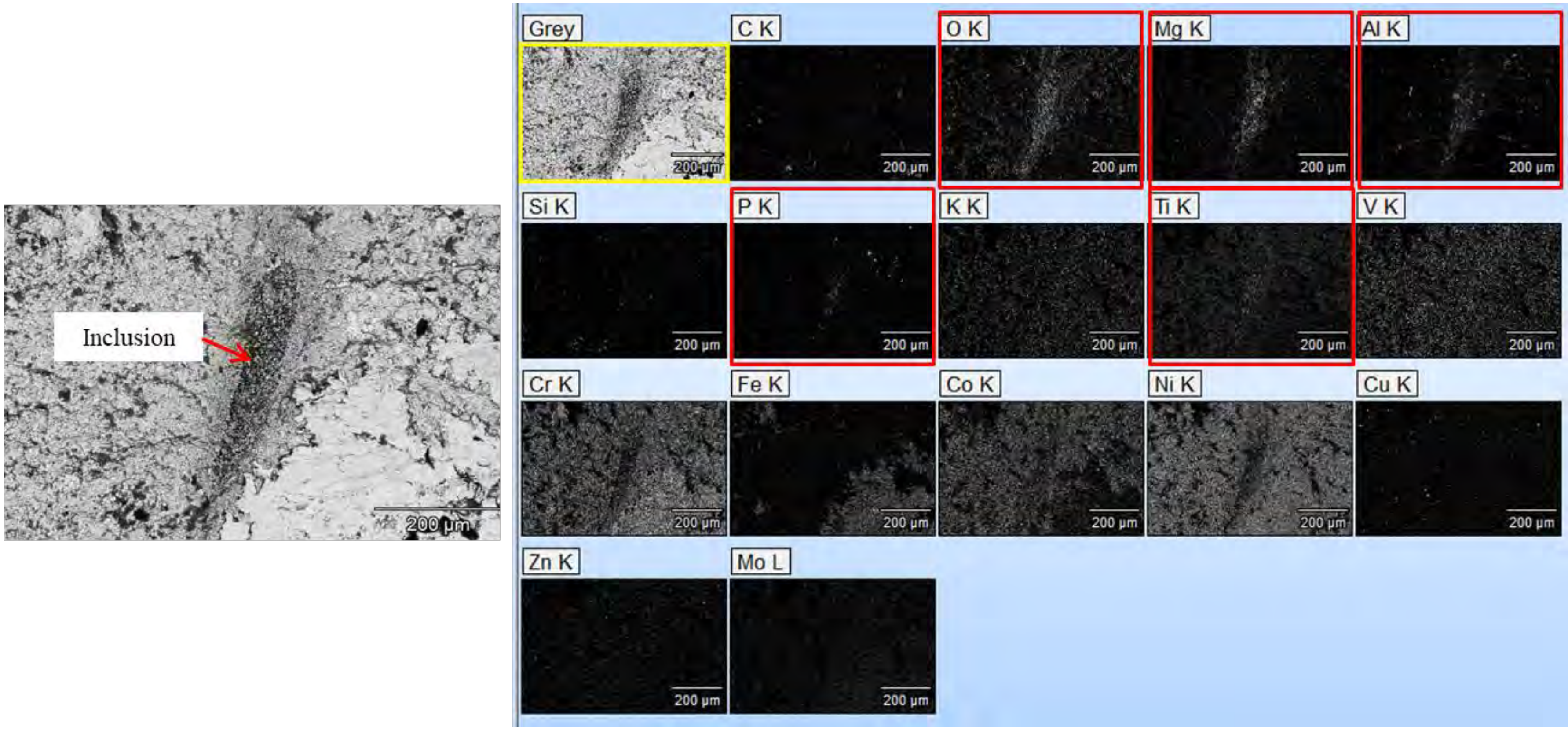

Figure 18: Initial SEM/EDS examination of the inclusion area identified locally higher concentrations of O, Mg, Al, P, and Ti (red outlines, above). Lighter color in maps on right indicates a higher concentration of the given element.

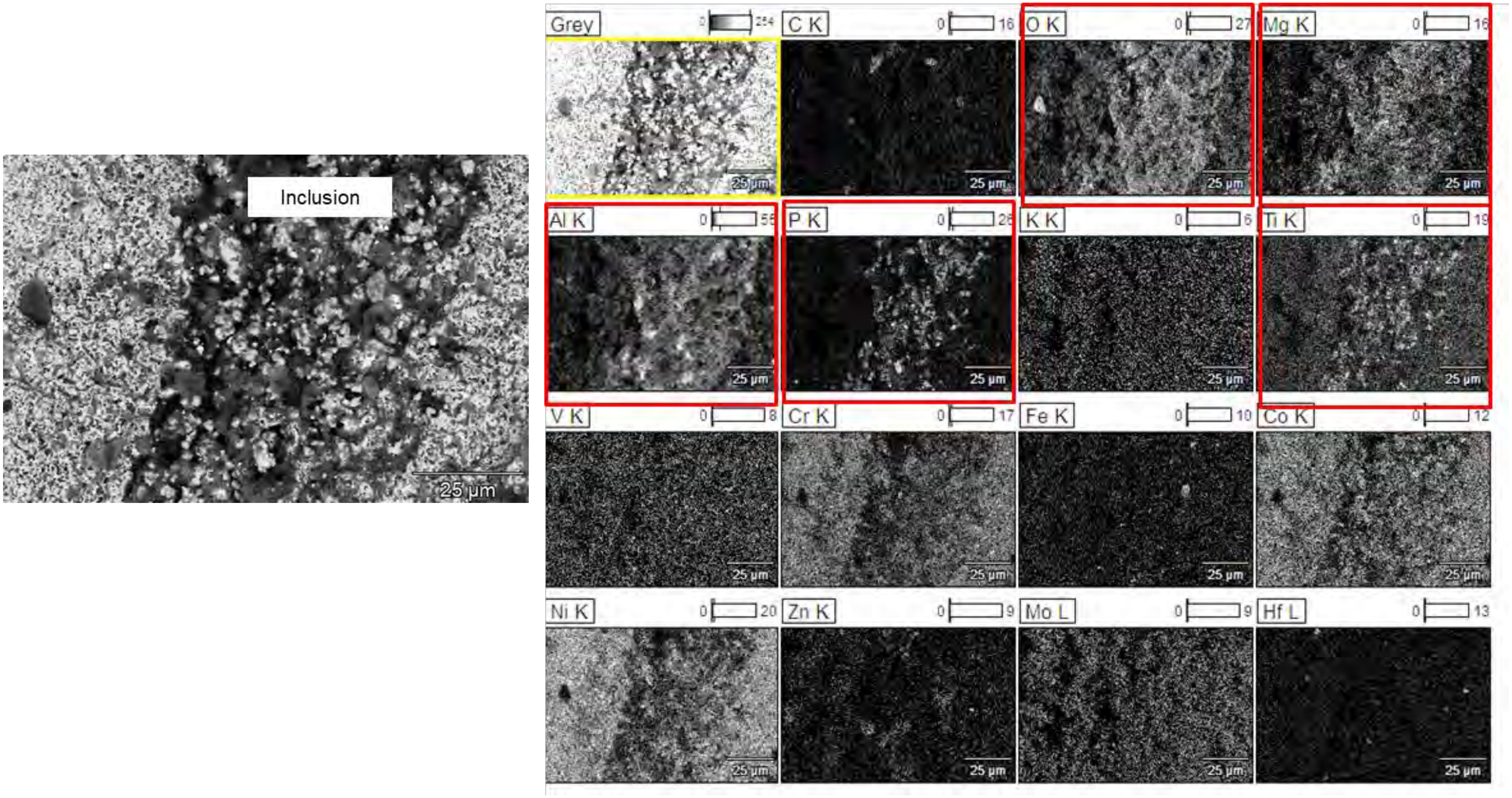

Figure 19: Higher magnification SEM/EDS maps showing locally higher concentrations of O, Mg, Al, P, and Ti (red outlines, above). Lighter color in maps on right indicates a higher concentration of the given element.

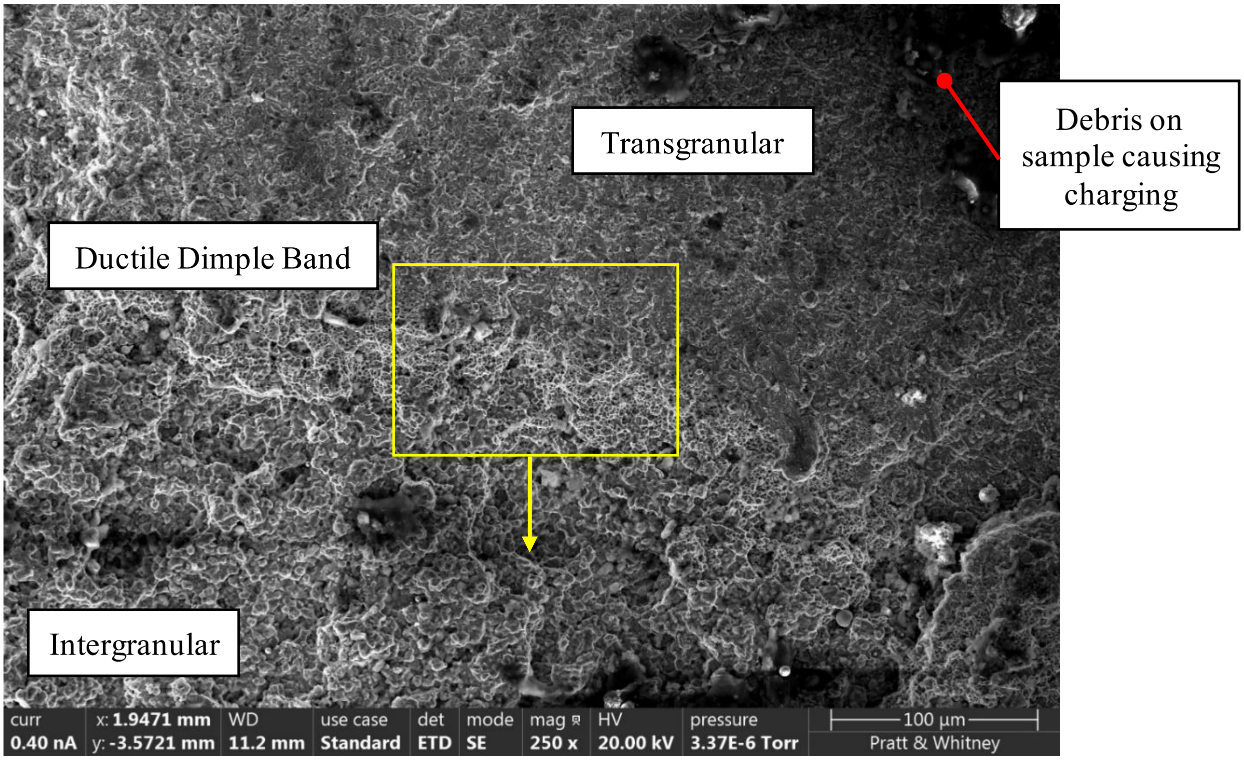

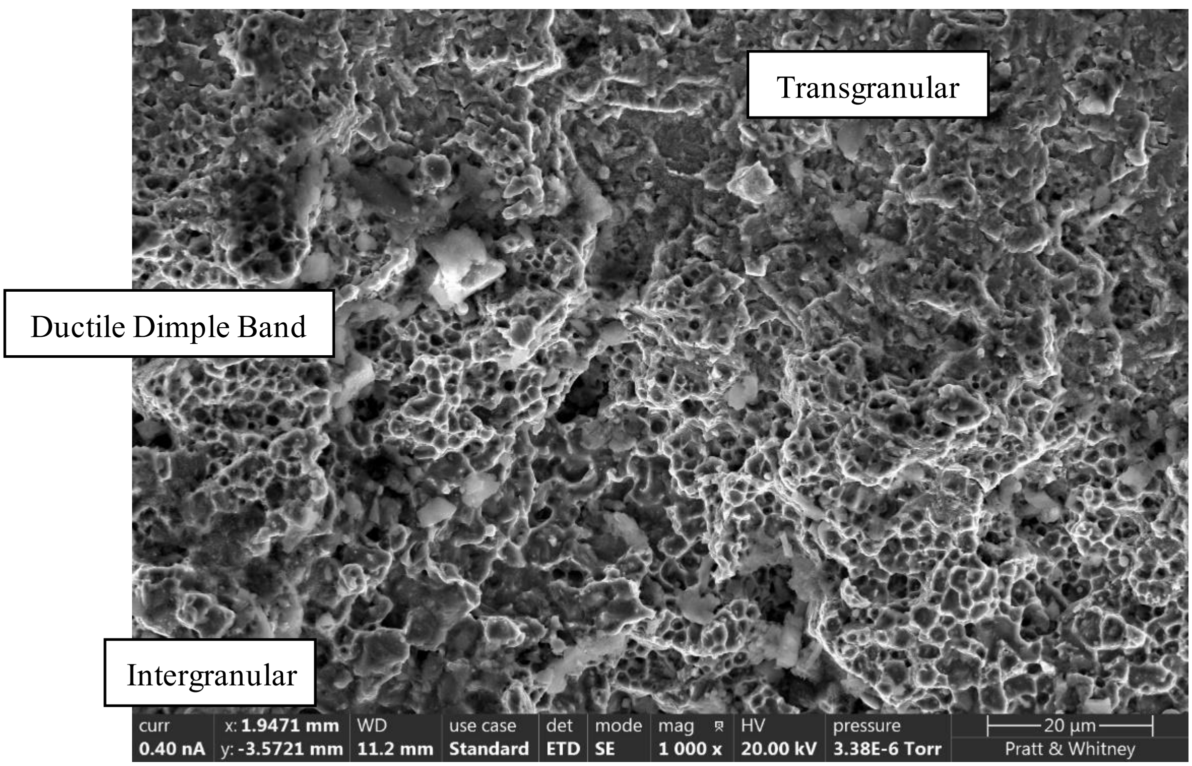

Figure 20: SEM images showing intergranular, ductile dimple, and transgranular features observed at the perimeter of the 0.120” x 0.075” origin area, following water and isopropanol rinse.

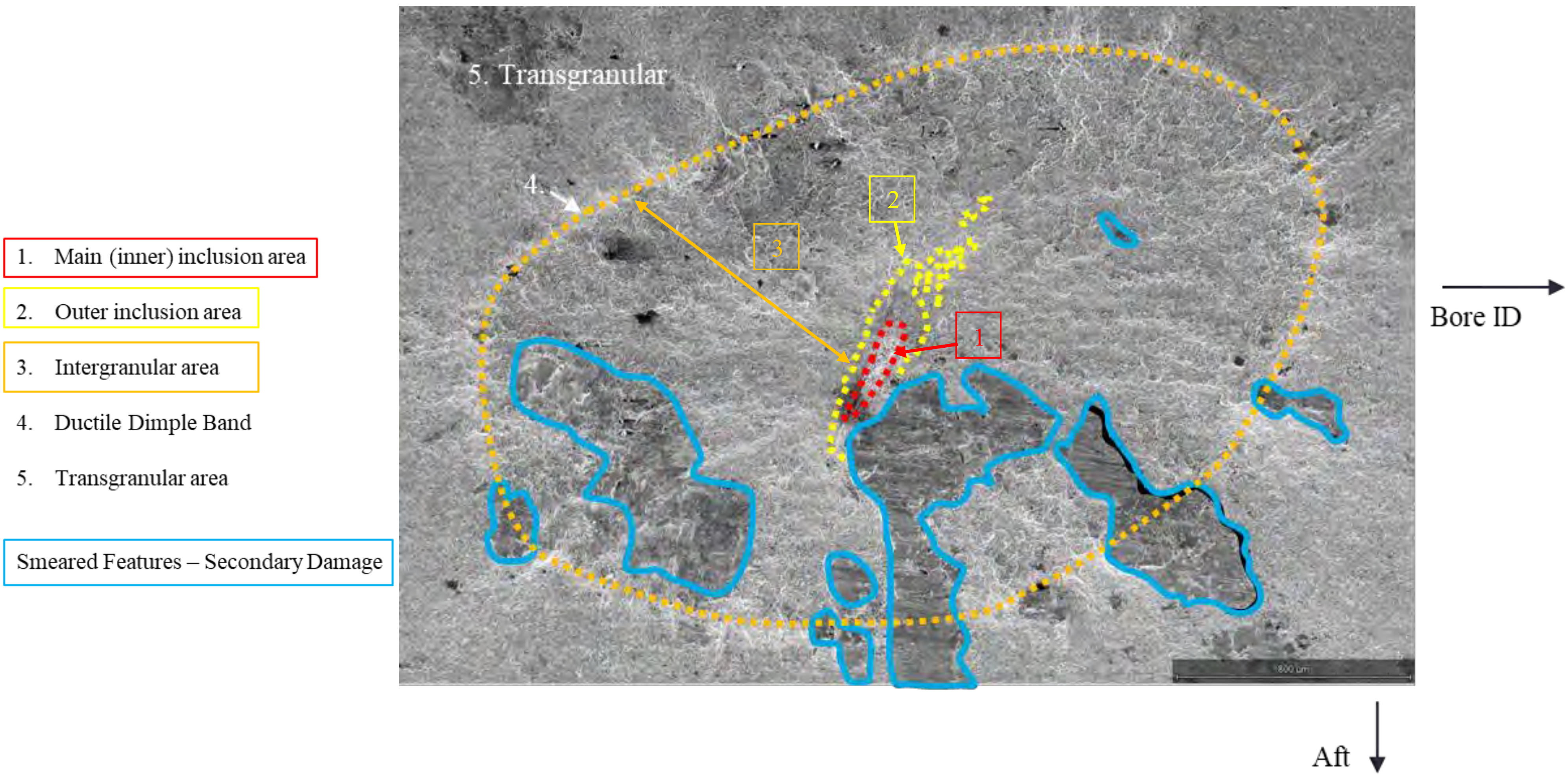

Figure 21: SEM map showing the 5 main regions observed within and adjacent to the origin area. In addition to the five regions of crack progression, areas of secondary damage were observed.

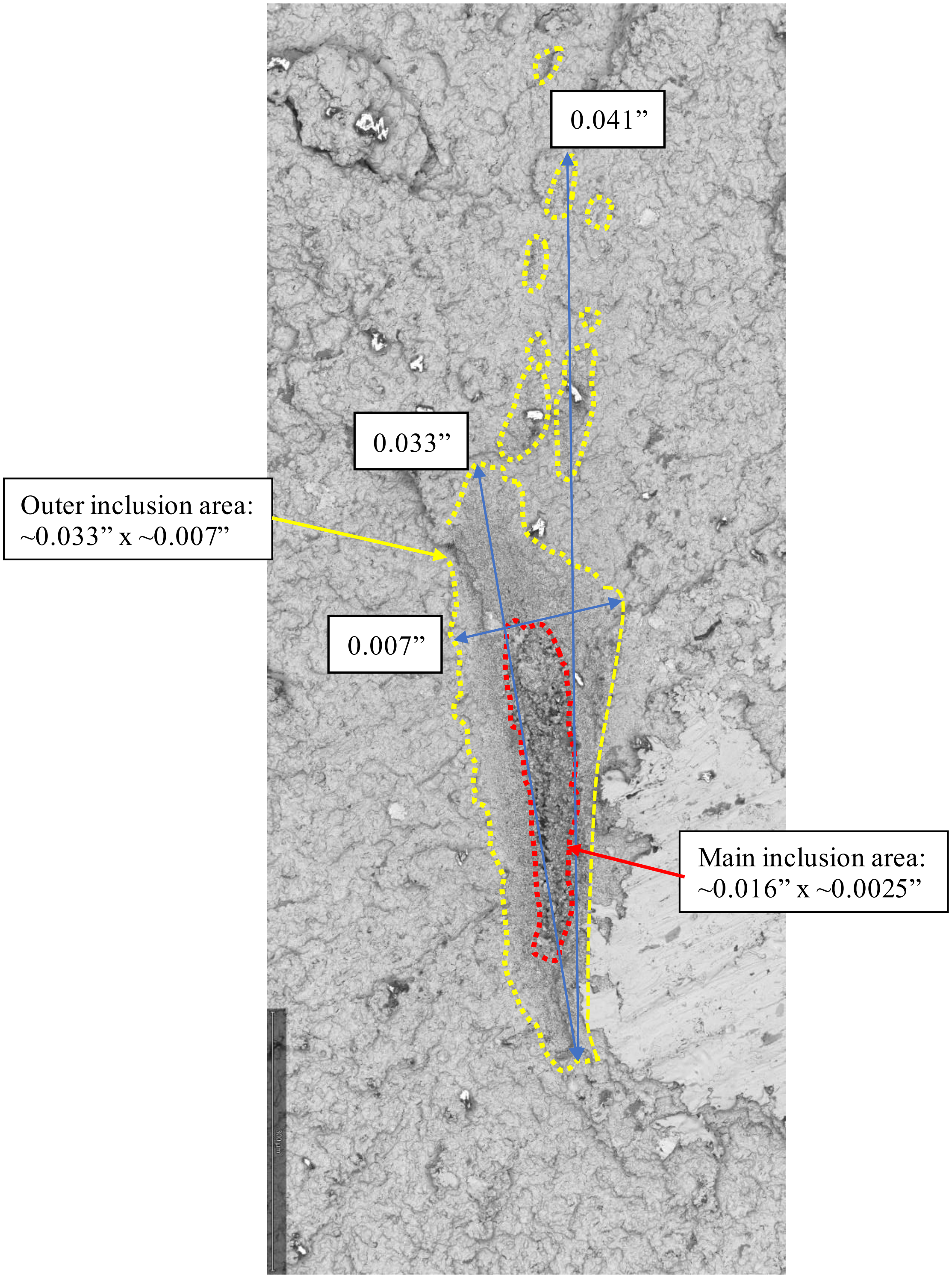

Figure 22: Map of the main (red dashed lines) and outer (yellow dashed lines) inclusion area, rotated from Figure 21. The main inclusion area consisted of a concentrated area of voids and foreign particles while the outer inclusion area was a non-continuous region of dispersed particles.

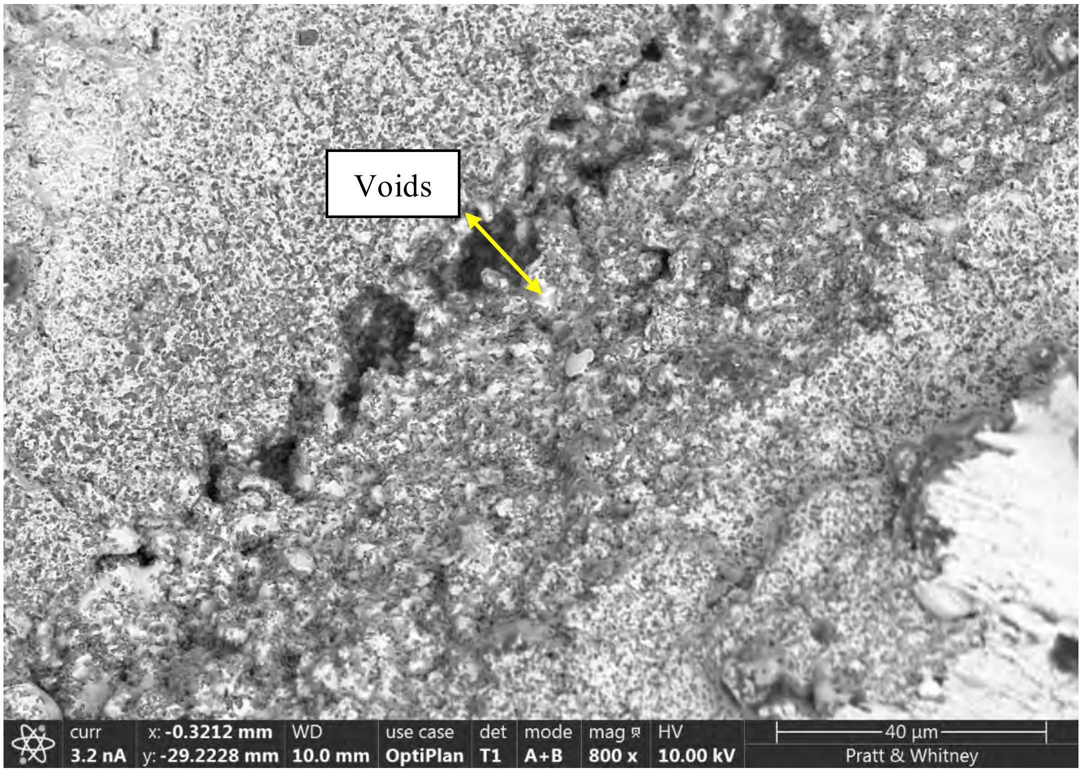

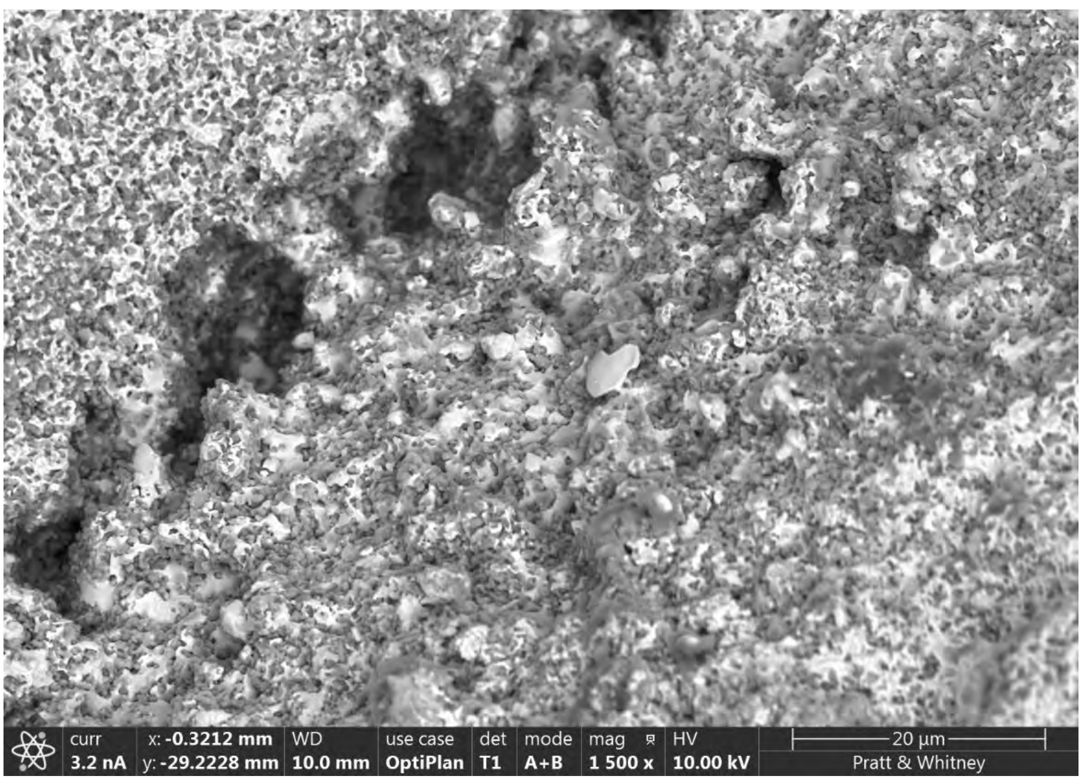

Figure 23: SEM images showing appearance of the main (inner) inclusion area. The inner inclusion area consisted of voids and foreign particles (dark particles, above).

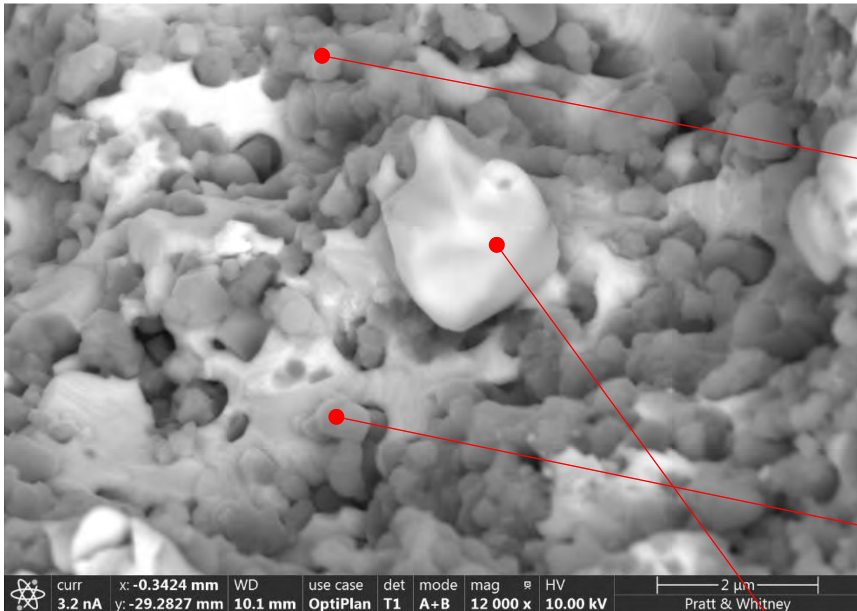

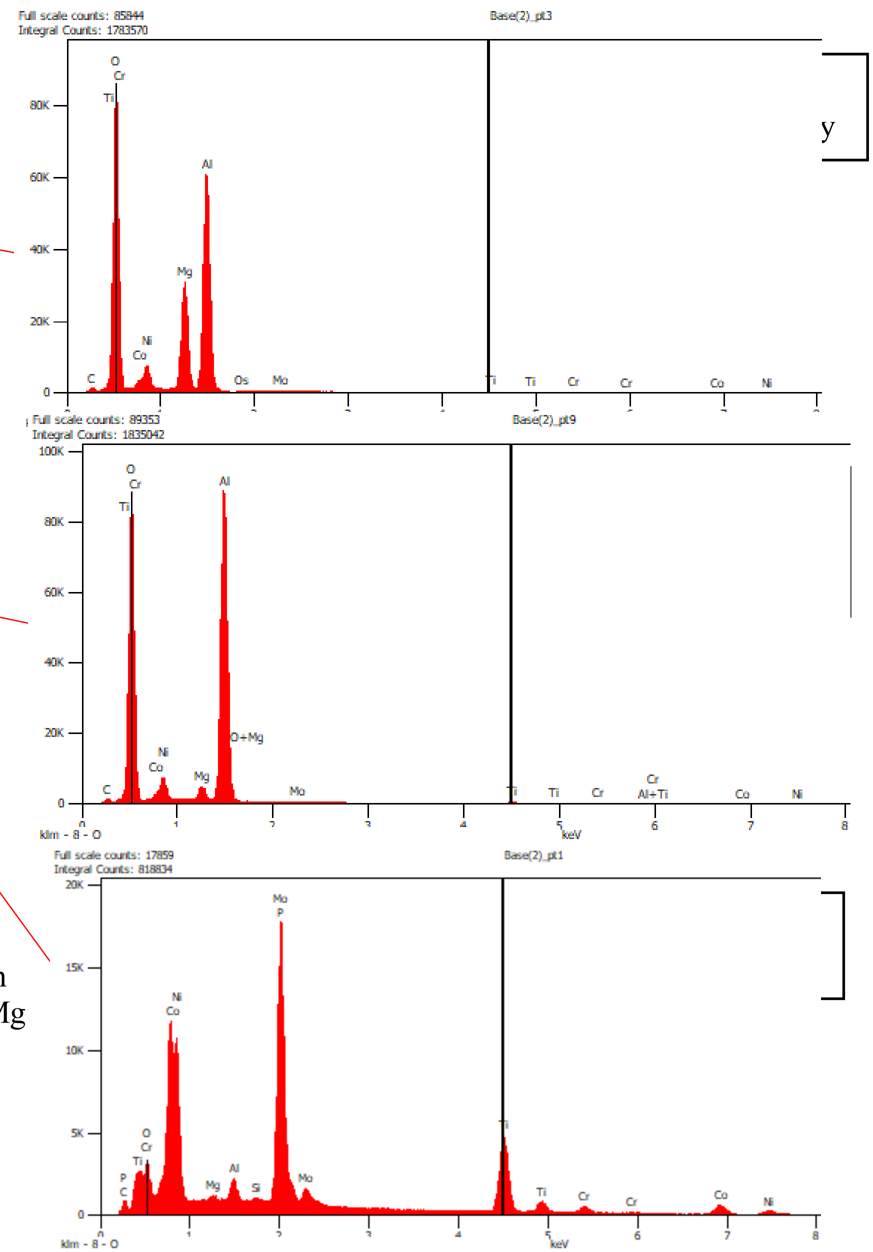

Figure 24: Typical particle chemistries observed in the inner inclusion area included the Al-Mg-O type (top right), the Al-O with much less Mg type (middle right), and the P-Ti-Ni-Co type (bottom right).

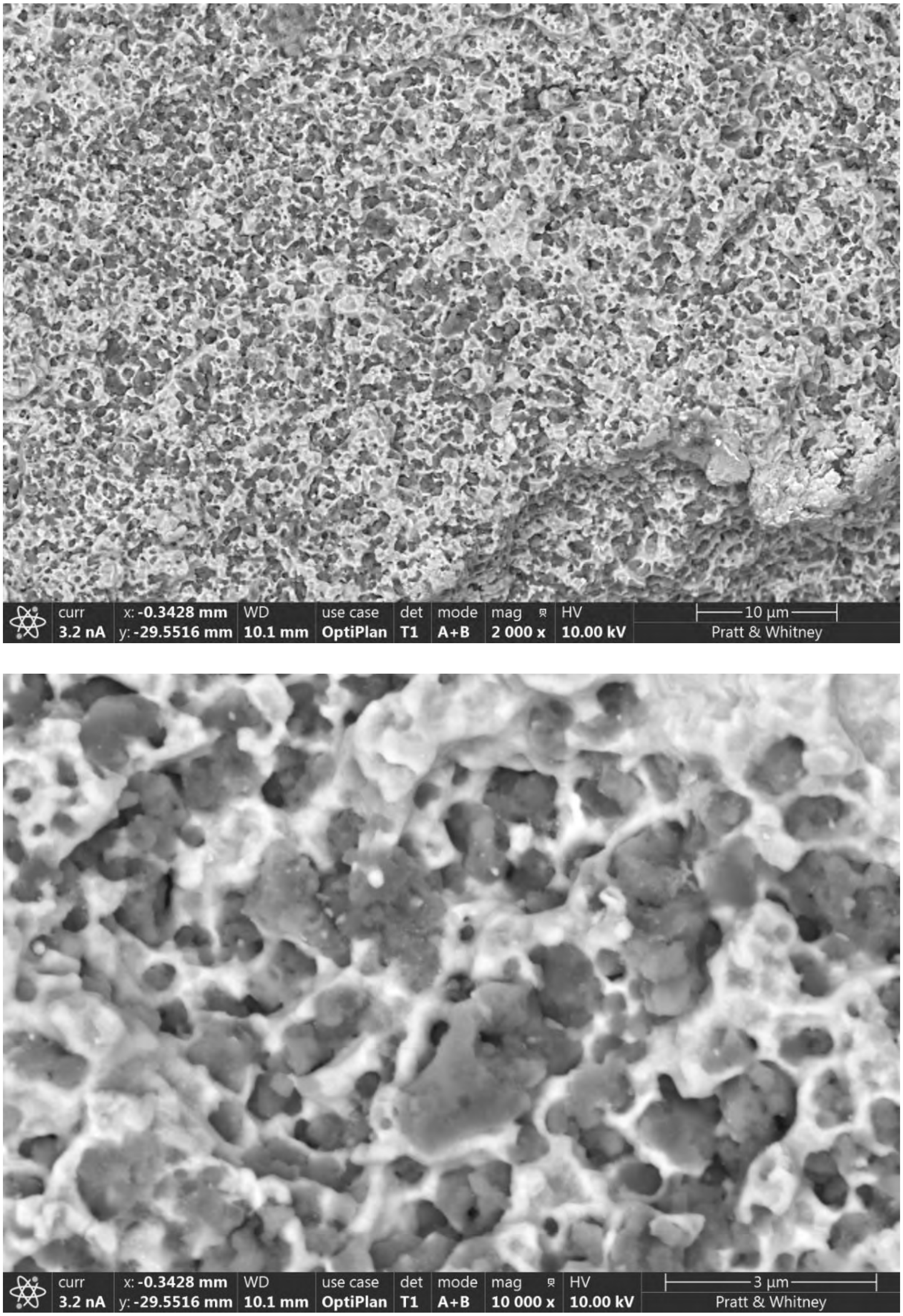

Figure 25: SEM images showing fracture appearance within the outer inclusion area. Features appeared ductile surrounding the inclusion particles.

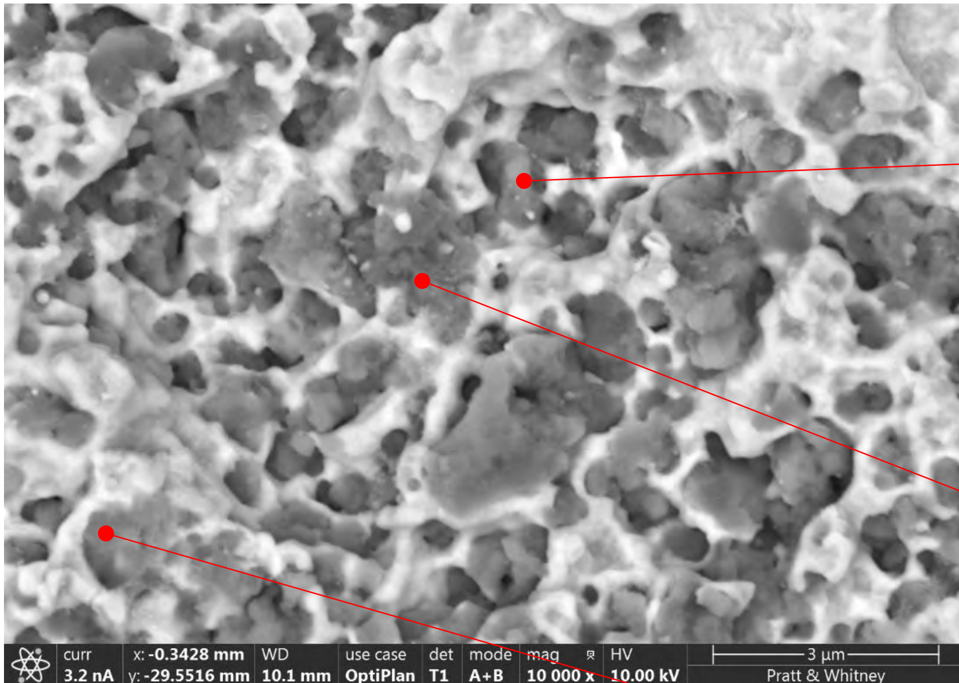

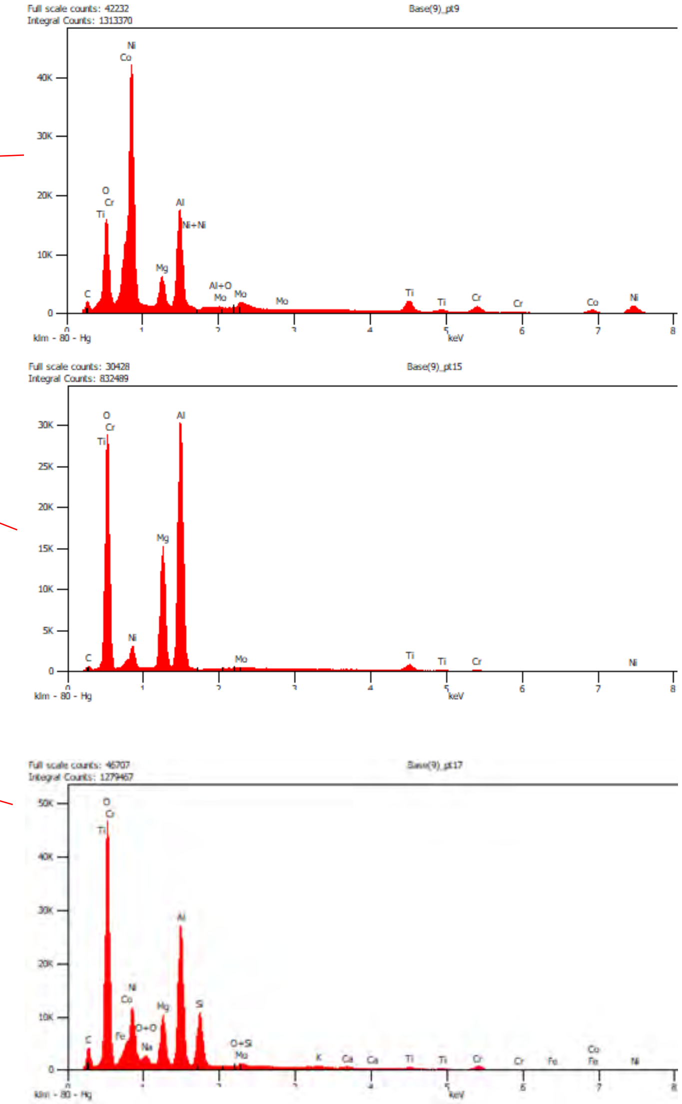

Figure 26: Typical particle chemistries observed in the outer inclusion area.

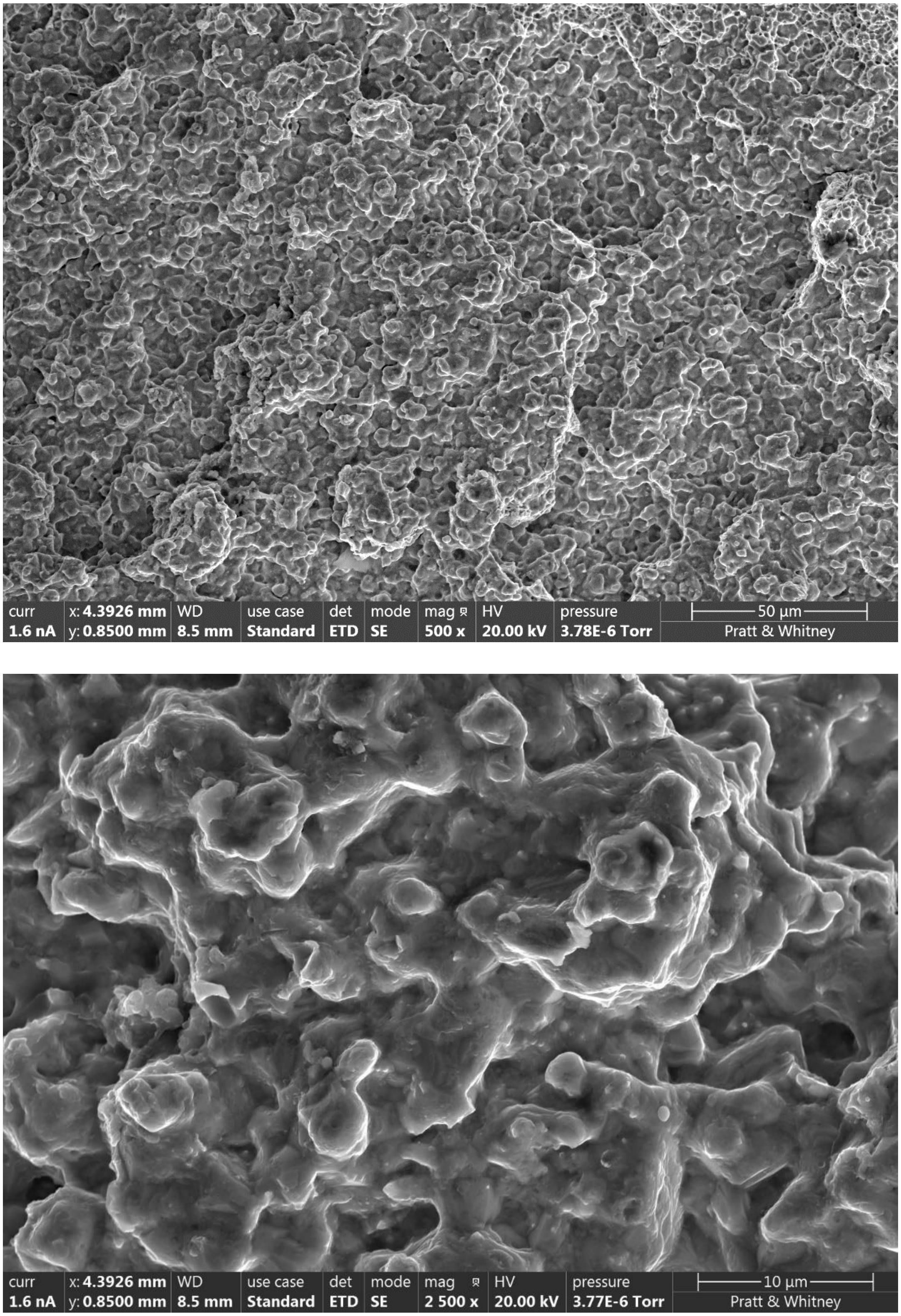

Figure 27: SEM images showing intergranular features observed.

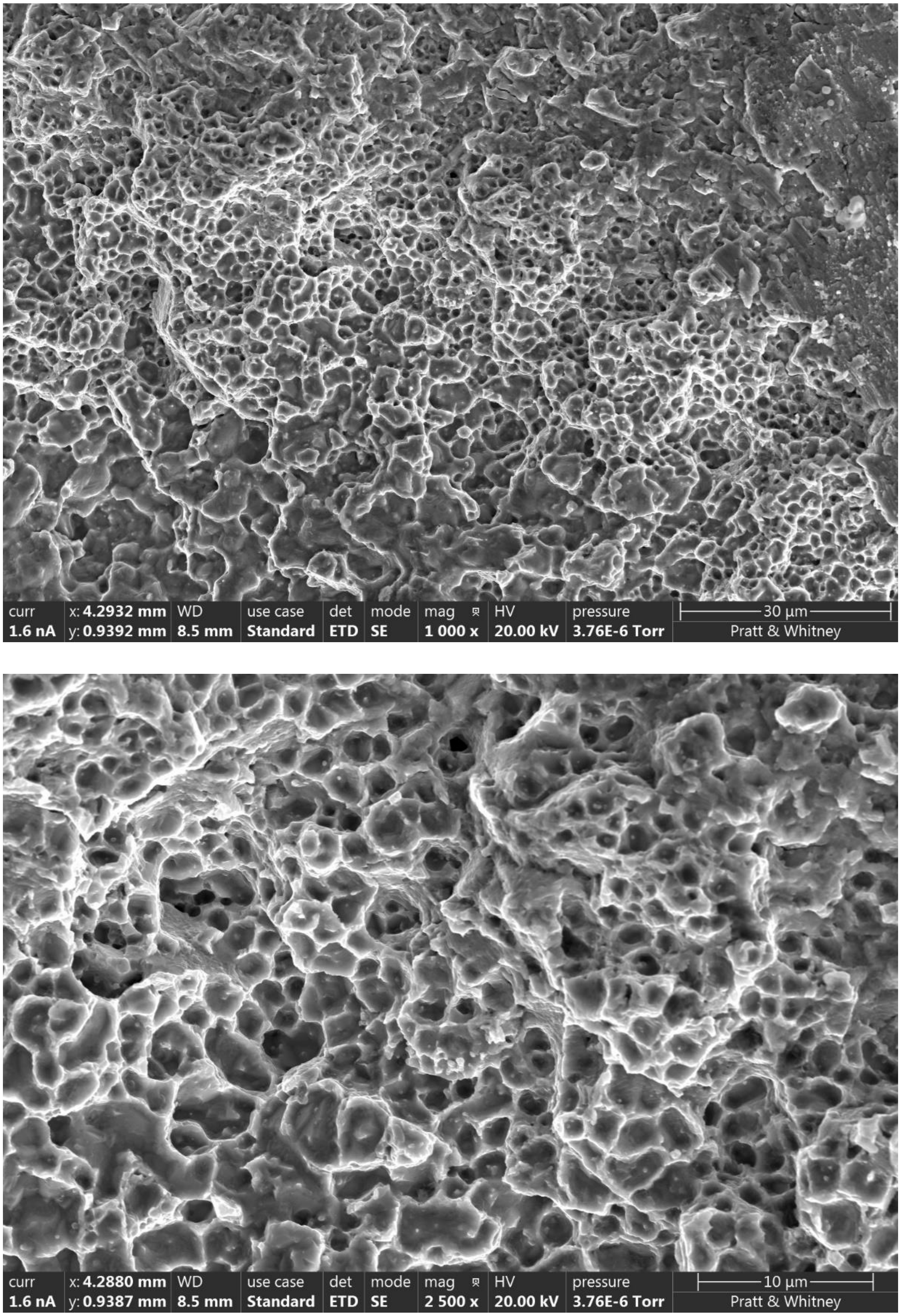

Figure 28: SEM images of fracture surface within the ductile dimple band.

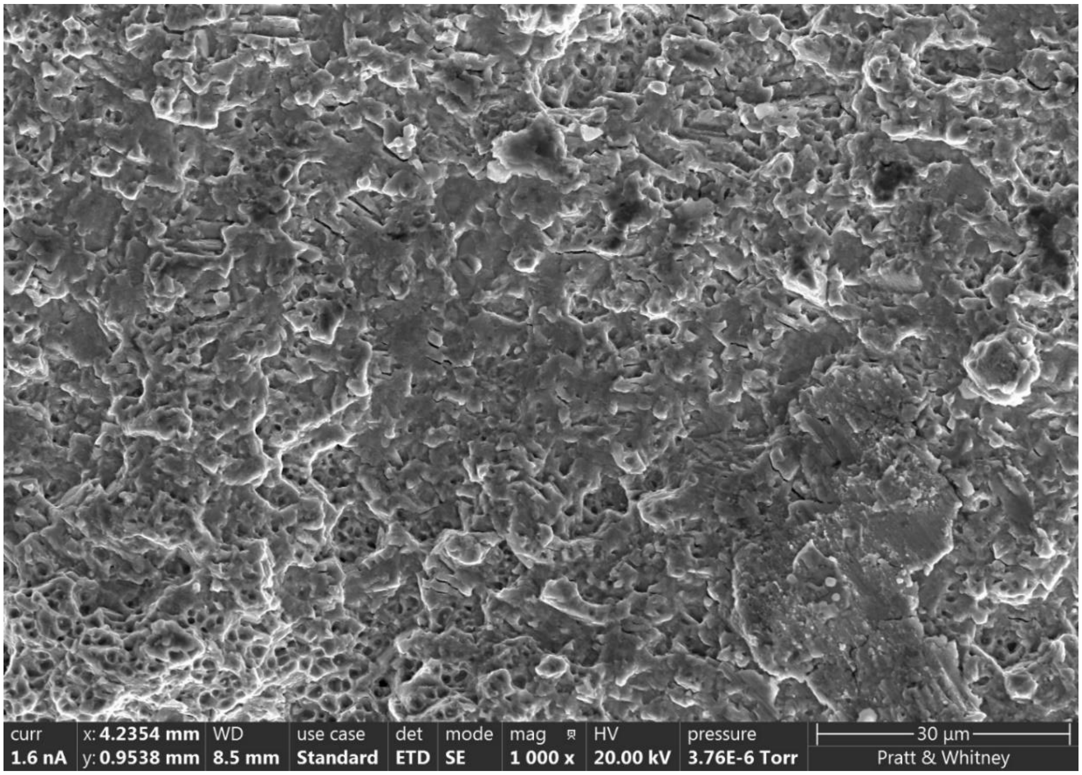

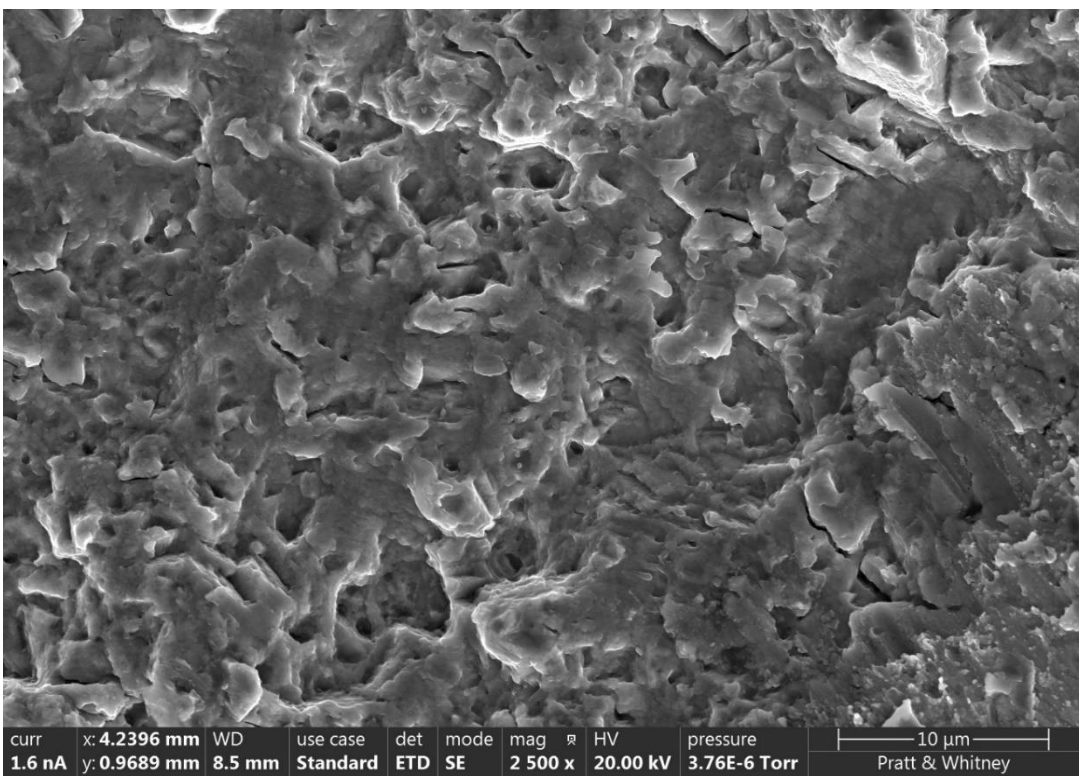

Figure 29: SEM images of transgranular progression outside the origin area. Progression was a mixture of striations and ductile dimple features.

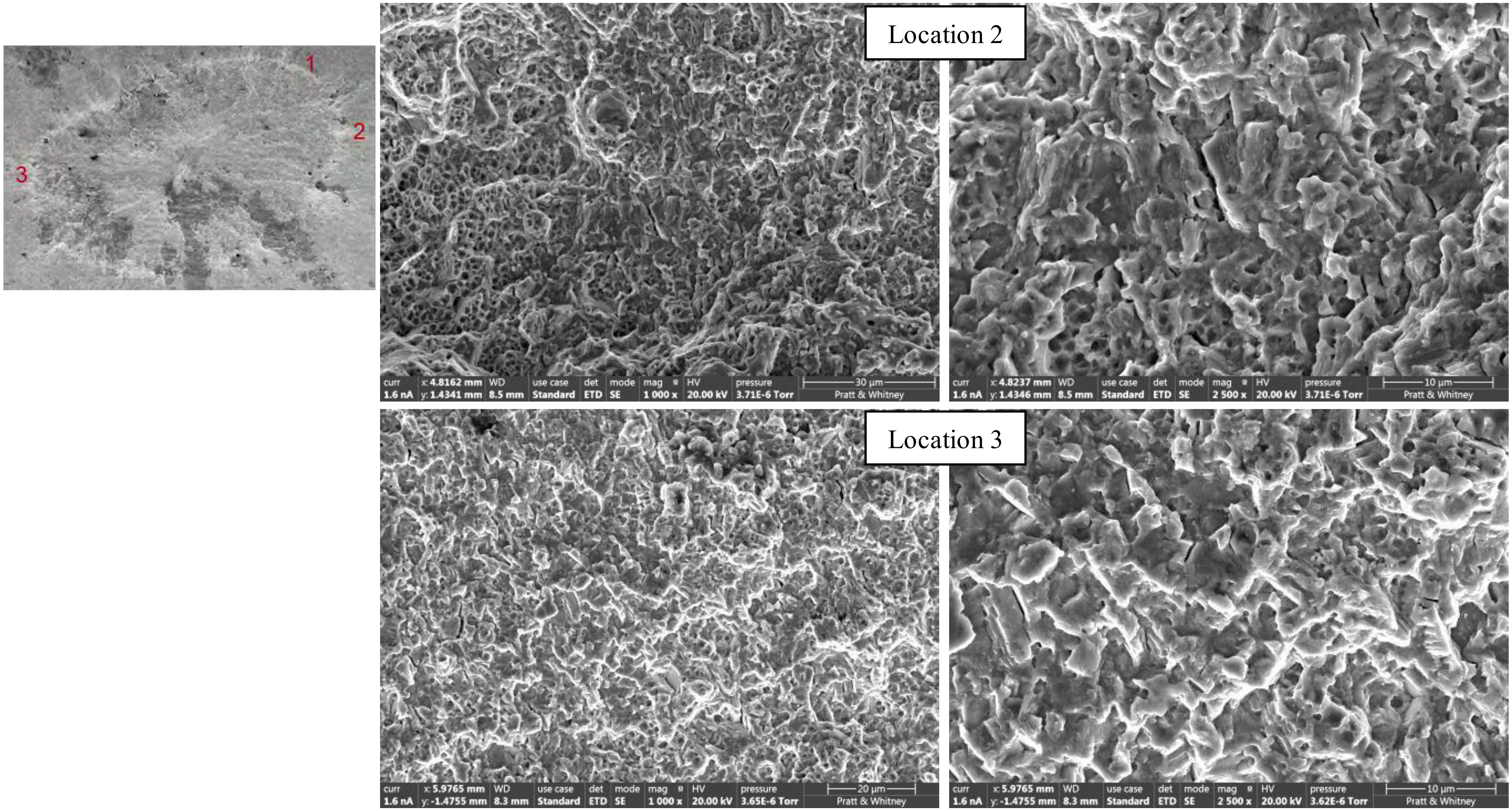

Figure 30: Additional regions of transgranular cracking (striations and ductile dimples) immediately outside of the oval-shaped origin area, as shown at upper left.

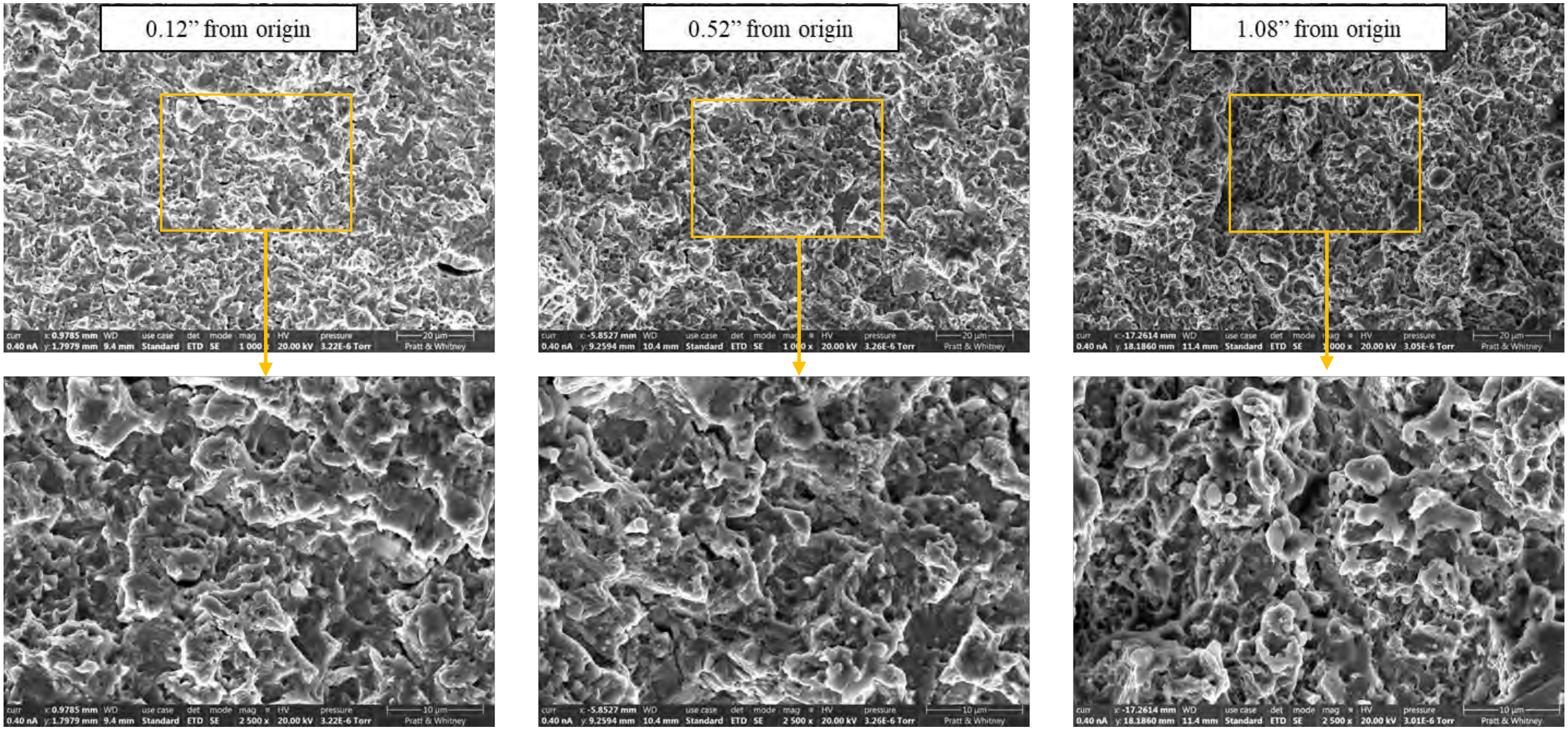

Figure 31: SEM images showing transgranular progression further away from the origin. Further away from the origin, crack features were dominated by ductile dimples.

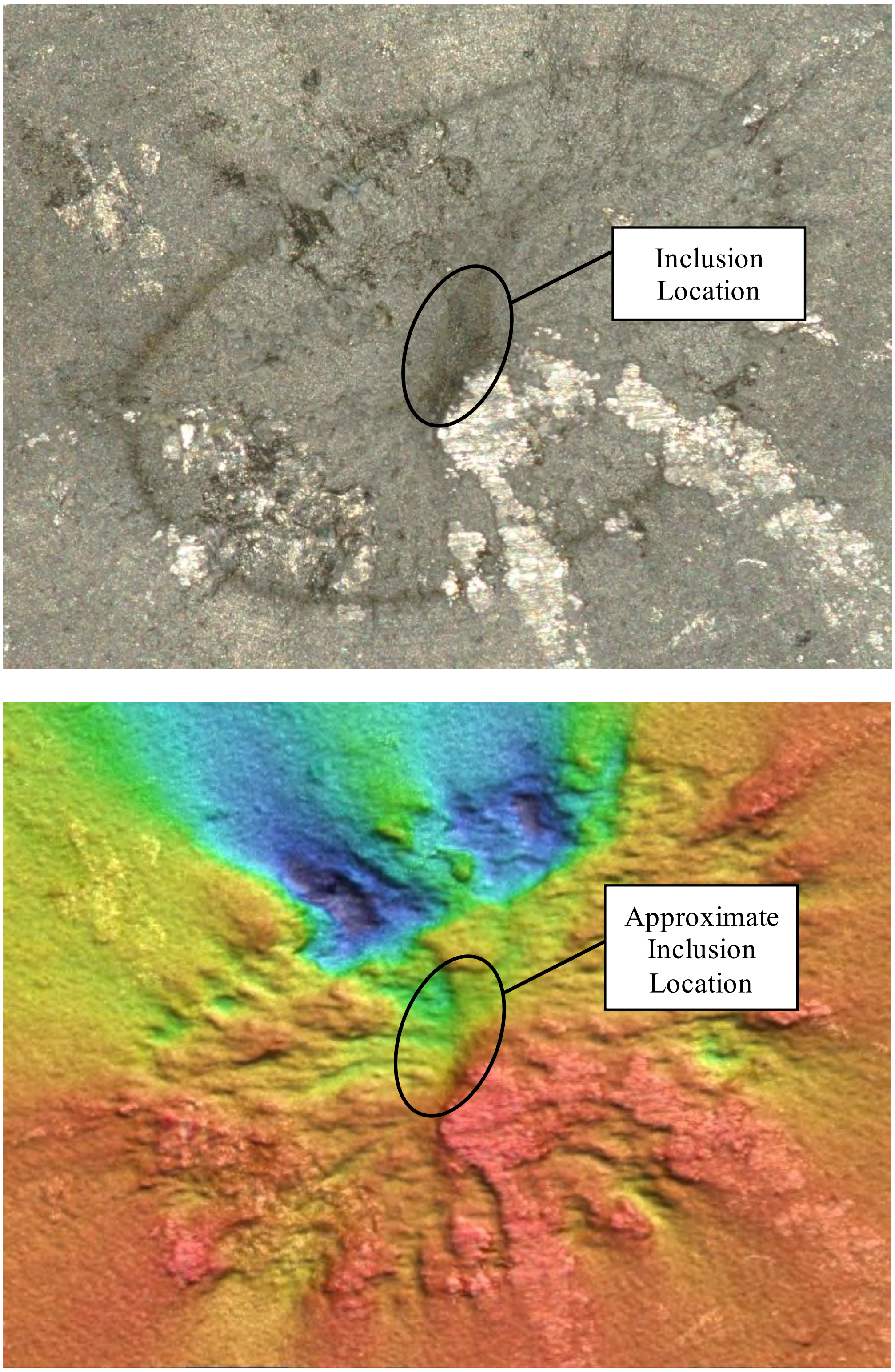

Figure 32: Higher magnification view of origin (top) and topography map superimposed on image (bottom). The red areas in the map were high and the blue areas were low.

Figure 33: The Fracture A surface on Fragment 2 was sectioned from the remainder of the hub via wire EDM (top). The section was then cut down to a 0.1” thick slice (bottom).

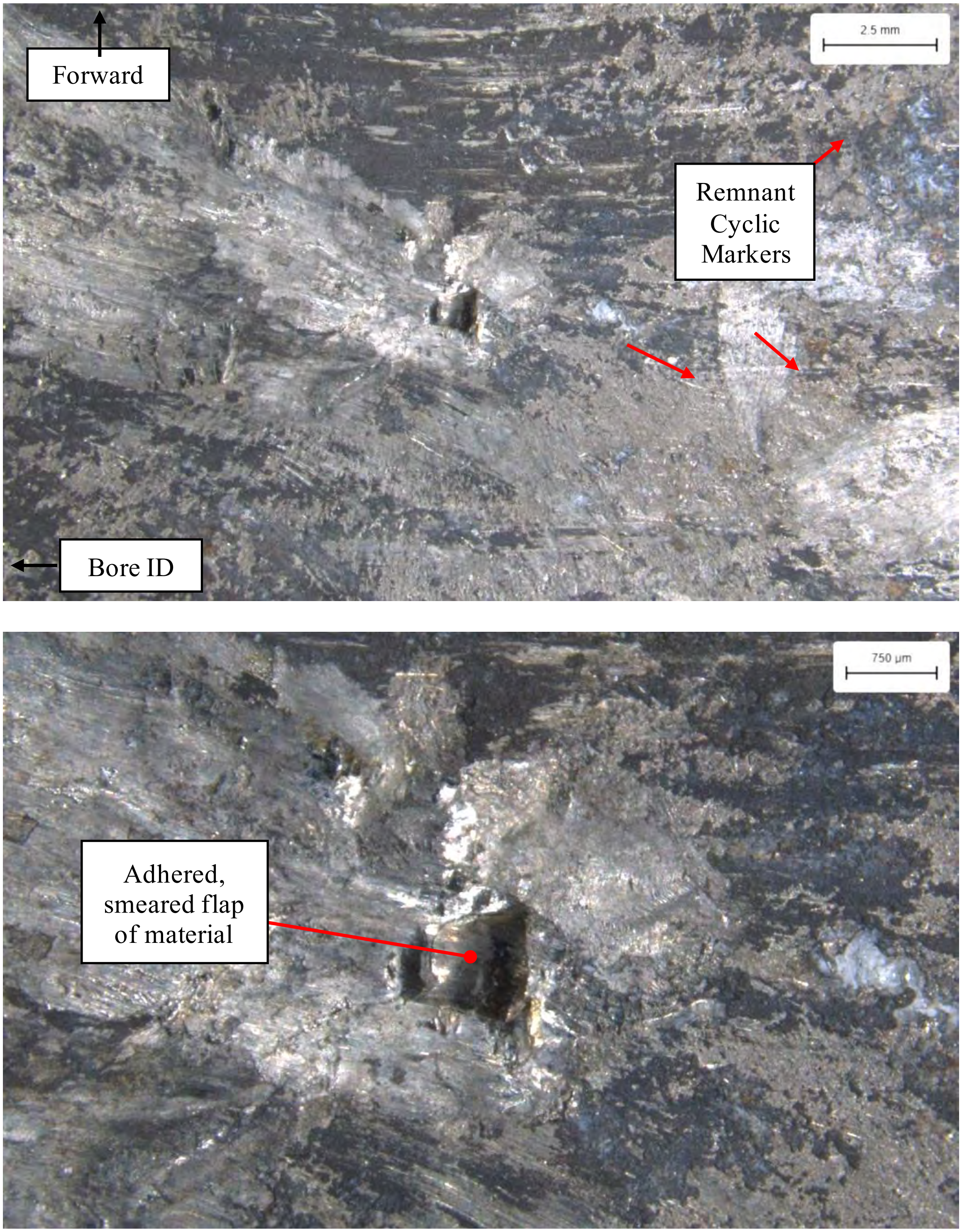

Figure 34: Origin area on the Fragment 2 side of Fracture A; the fracture surface was smeared, however remnant cyclic markers were observed. An adheared, smeared flap of material was observed near the presumed origin area.

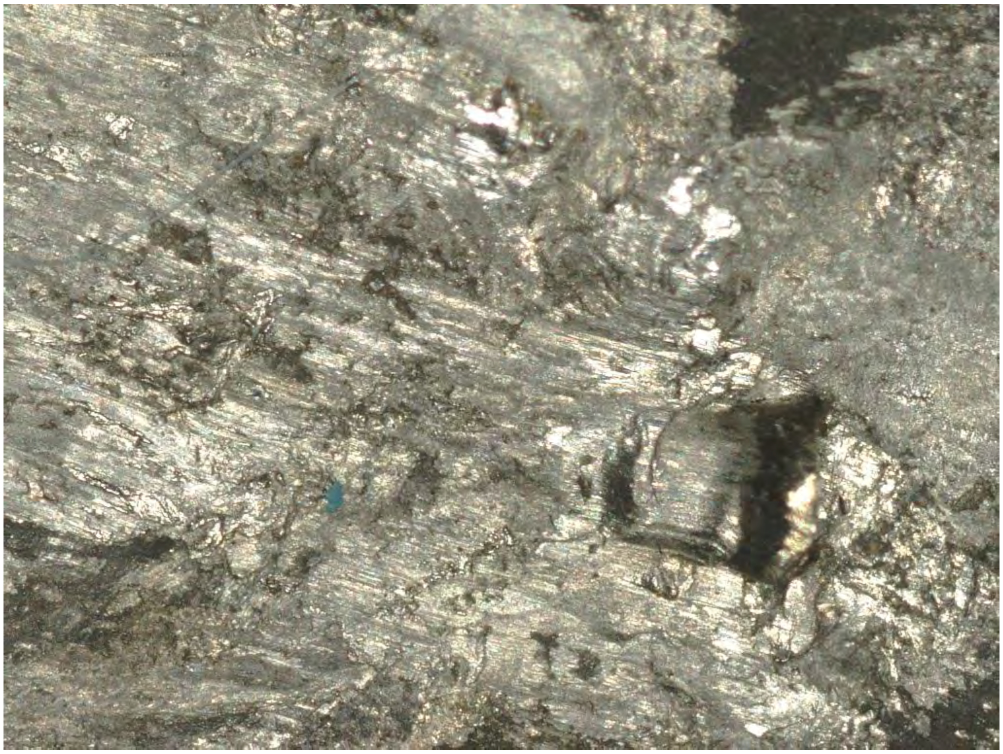

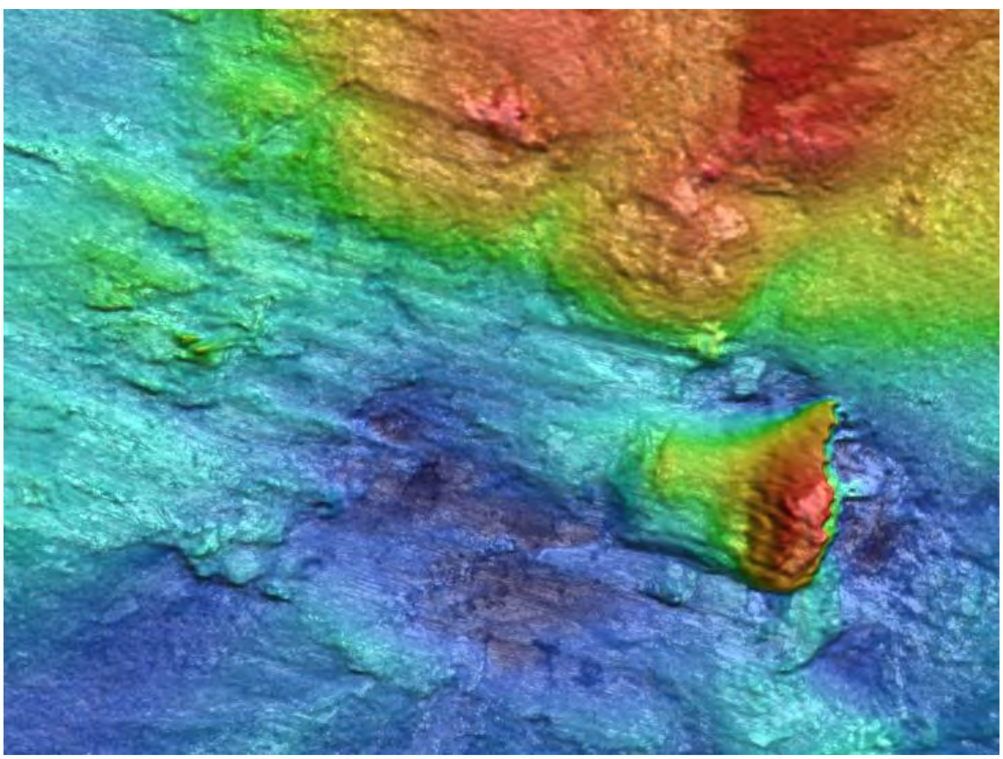

Figure 35: Higher magnification view of the origin area on Fragment 2 (top) and topography map superimposed on image (bottom). The red areas in the map were high and the blue areas were low.

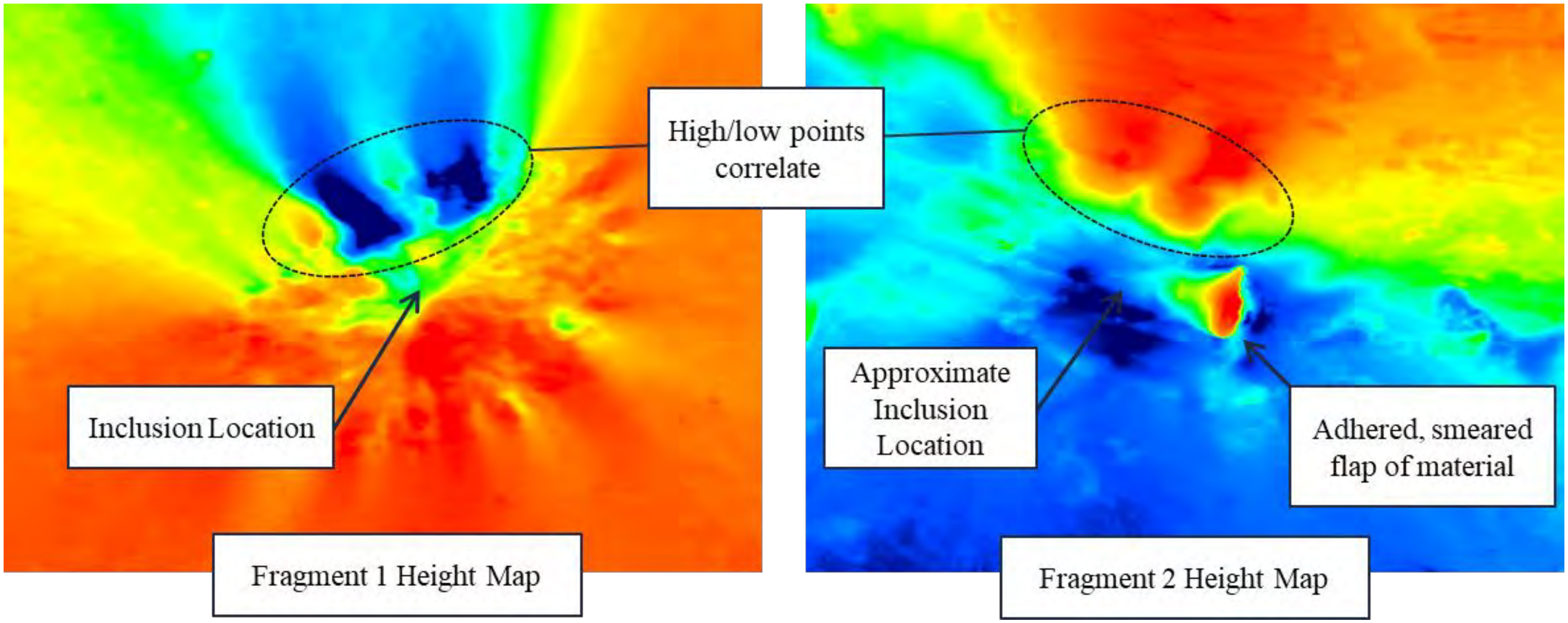

Figure 36: Comparison of Fragment 1 and Fragment 2 topography maps to determine approximate inclusion location. Red areas represent high points; blue areas represent low points.

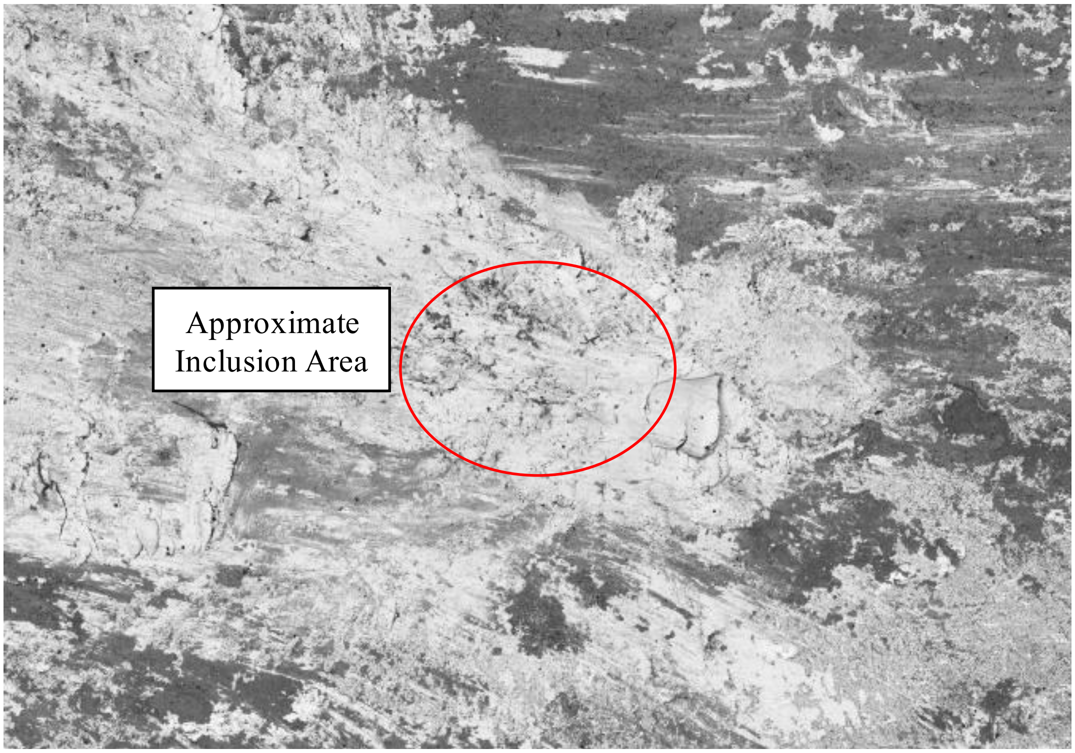

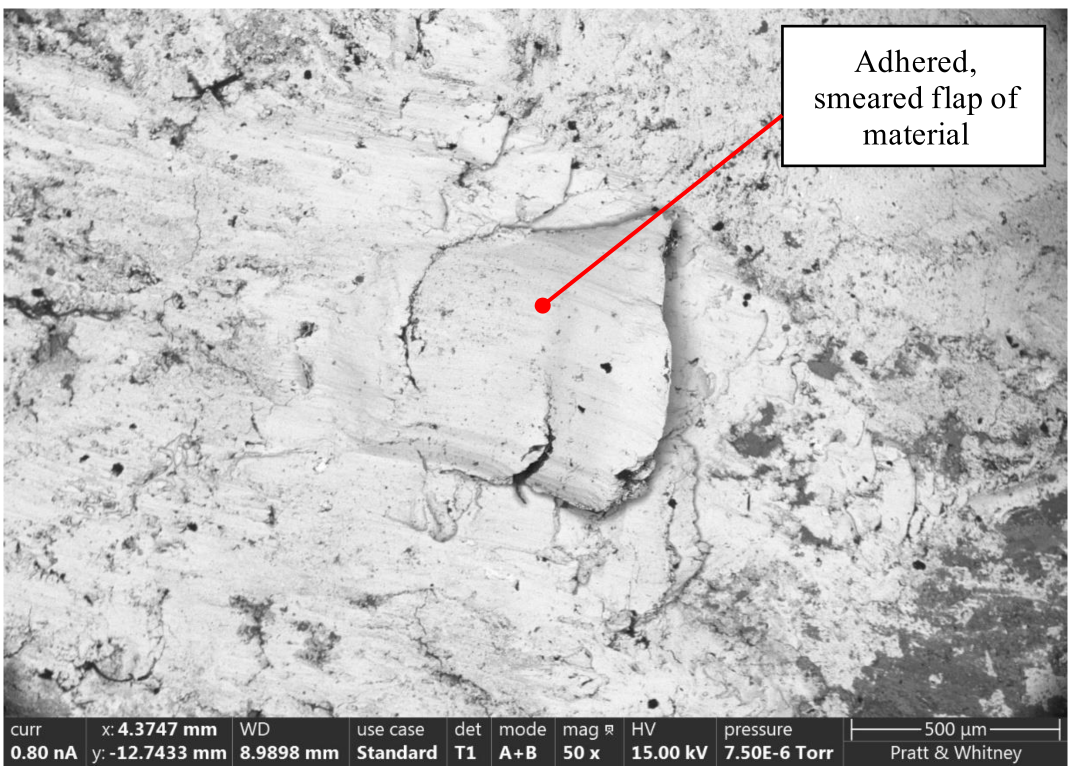

Figure 37: SEM images of Fragment 2 fracture surface. No original fracture features were observed within the origin area; the surface was smeared due to secondary damage.

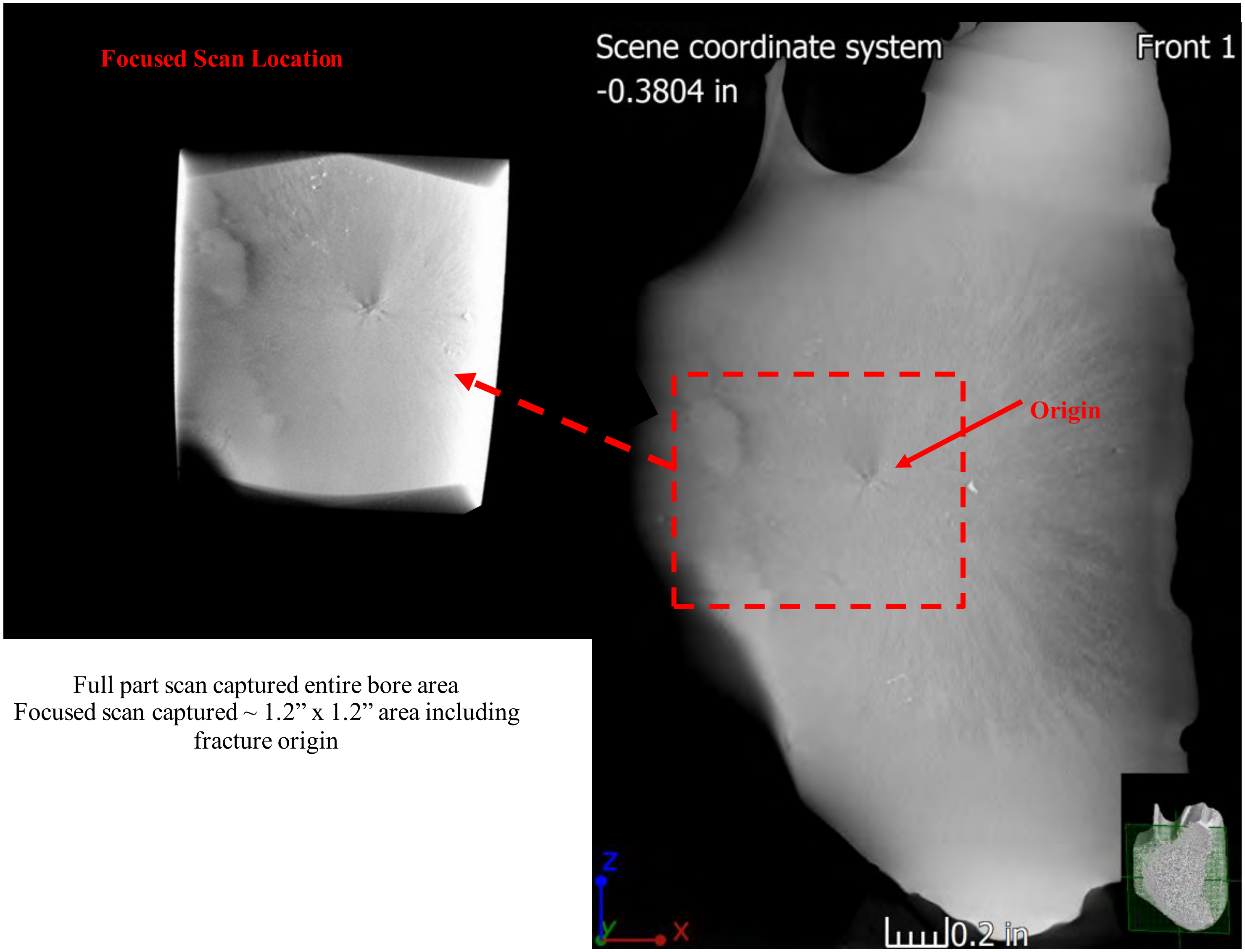

Full part scan captured entire bore area
Focused scan captured ~ 1.2” x 1.2” area including fracture origin

Figure 38: Initial micro CT scan images of the full bore section and a focused scan showing the origin area. Due to the large sample size, contrast was limited within the scan and it mostly captured the surface topography of the sample.

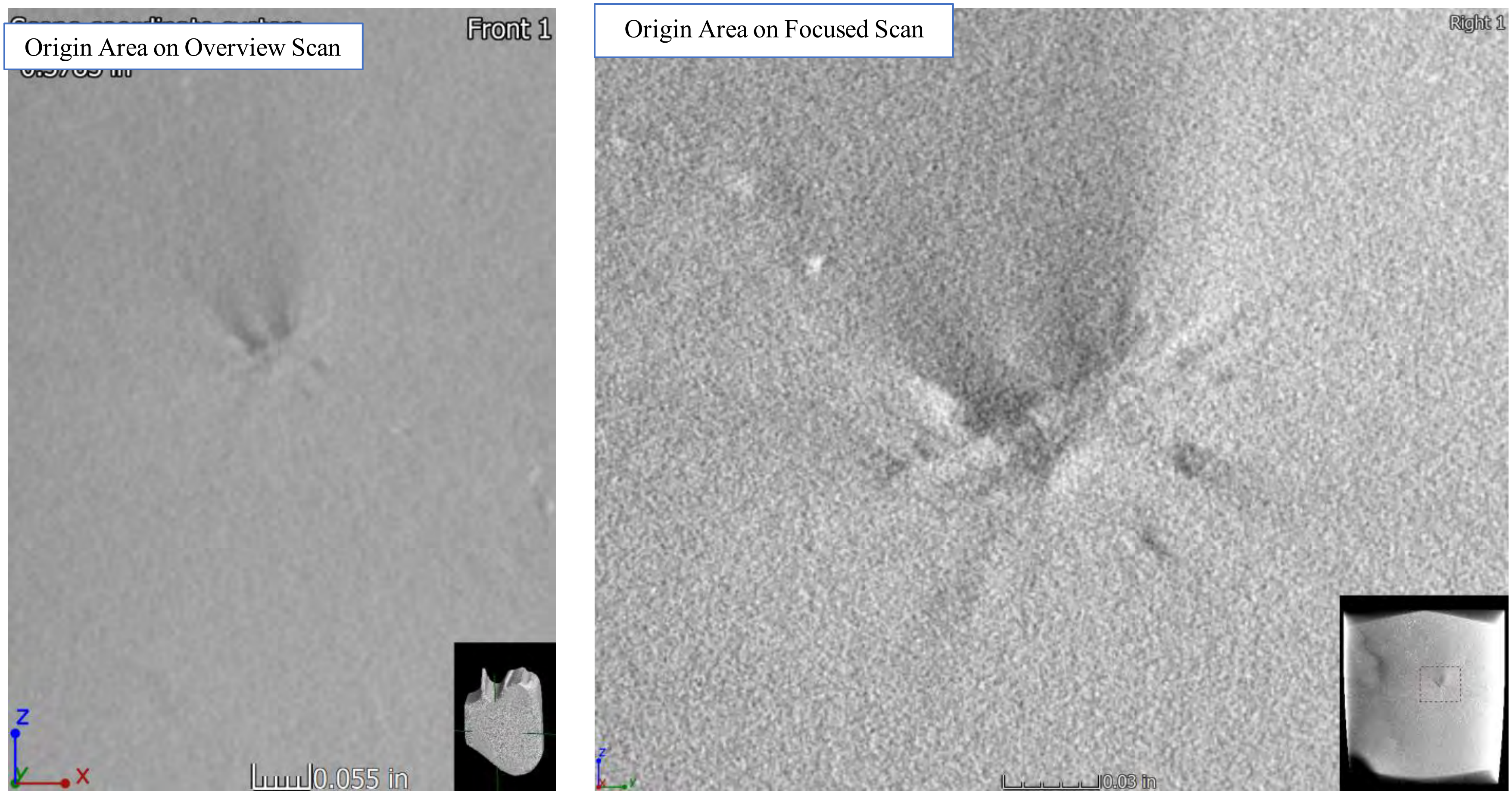

Figure 39: Views of the origin area on the overview micro CT scan (left) and the focused scan (right). The focused scan captured more detail within the origin area, however, was too noisy to identify and characterize the inclusion area.

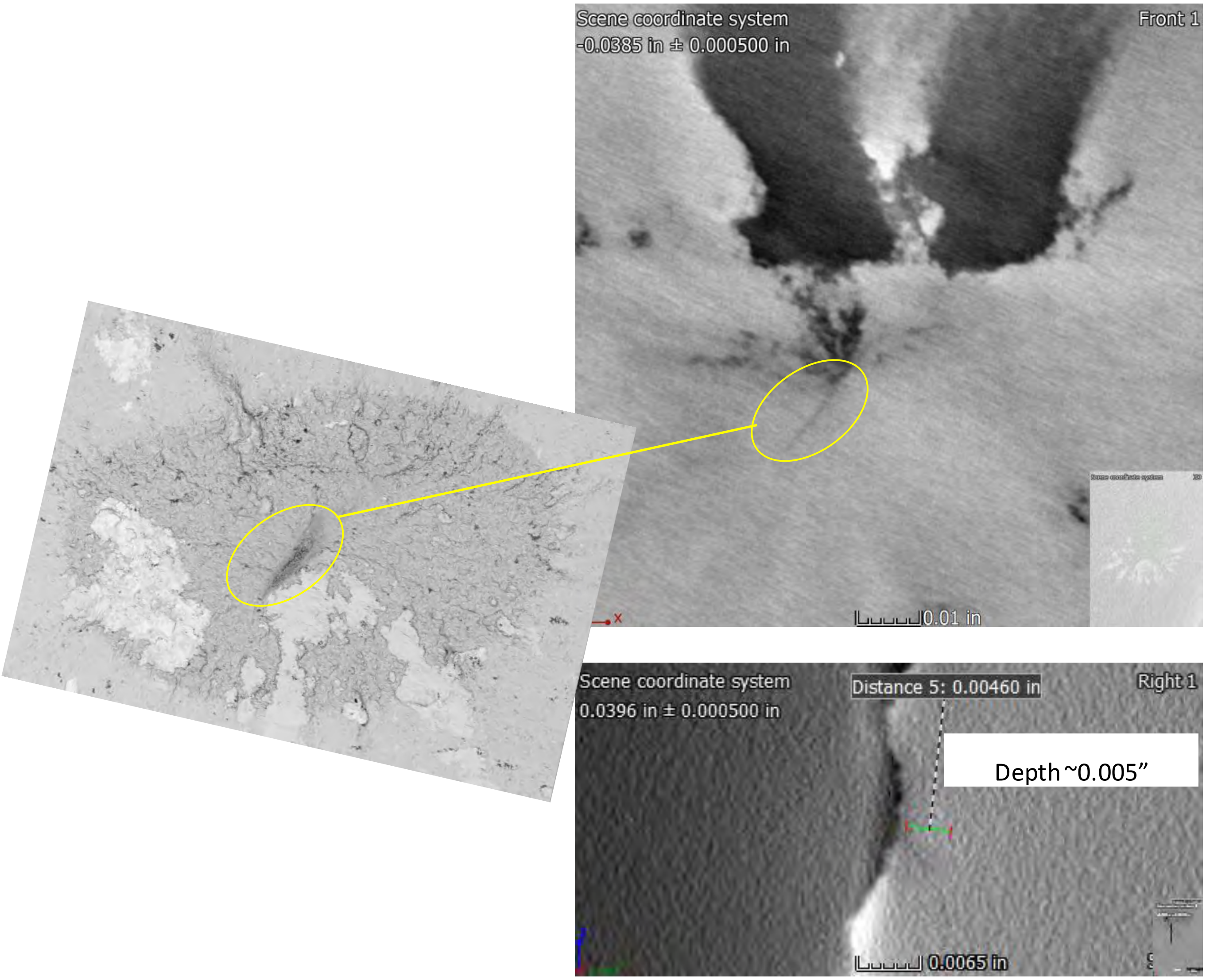

Figure 40: Micro CT scan images after sectioning the Fragment 1 origin area to a 0.1" thick section. The focus scan at the origin area identified a region extending approximately 0.005" – 0.007" into the sample at the location of the inclusion that exhibited a difference in density when compared with the surrounding base metal. No other indications were found within the rest of the scan.

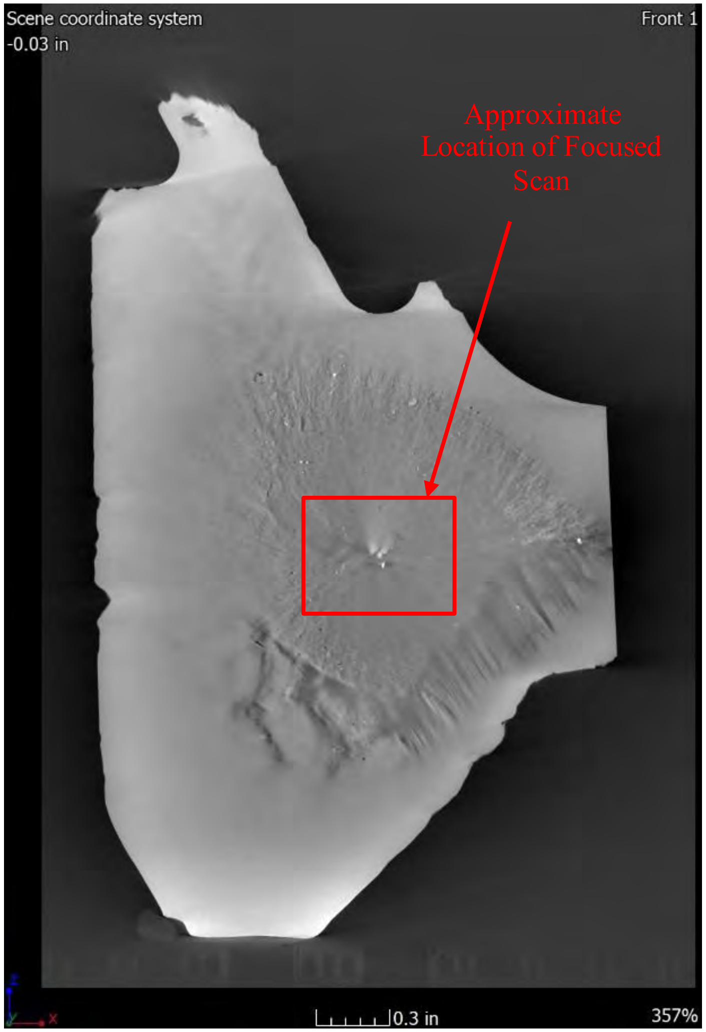

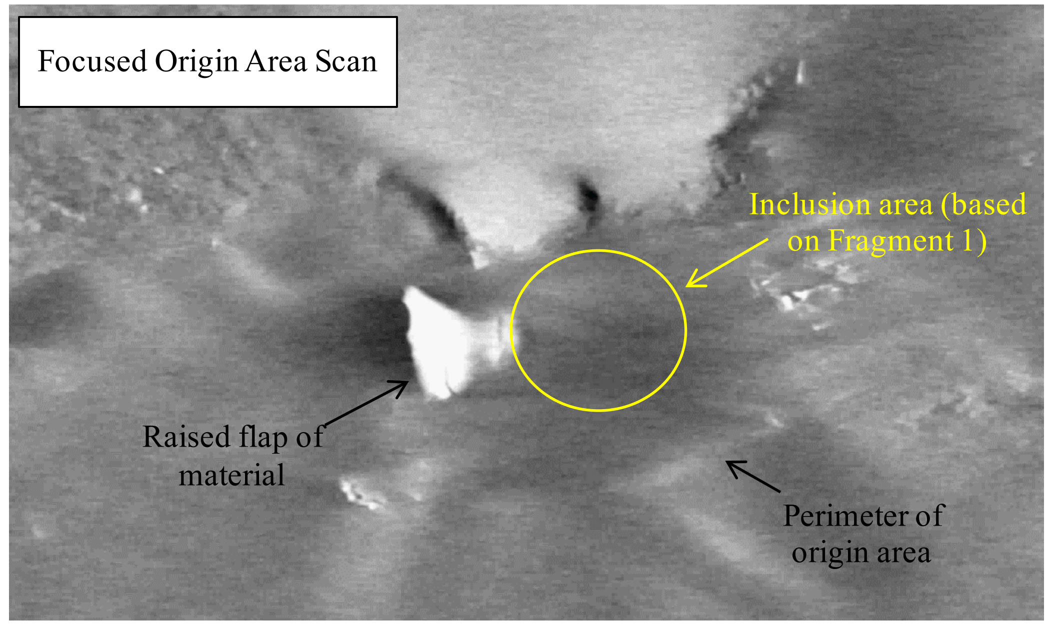

Figure 41: Micro-CT scans from the Fragment 2 origin area. No evidence of the inclusion was identified; secondary damage to the fracture surface may have obscured the evidence of the inclusion.

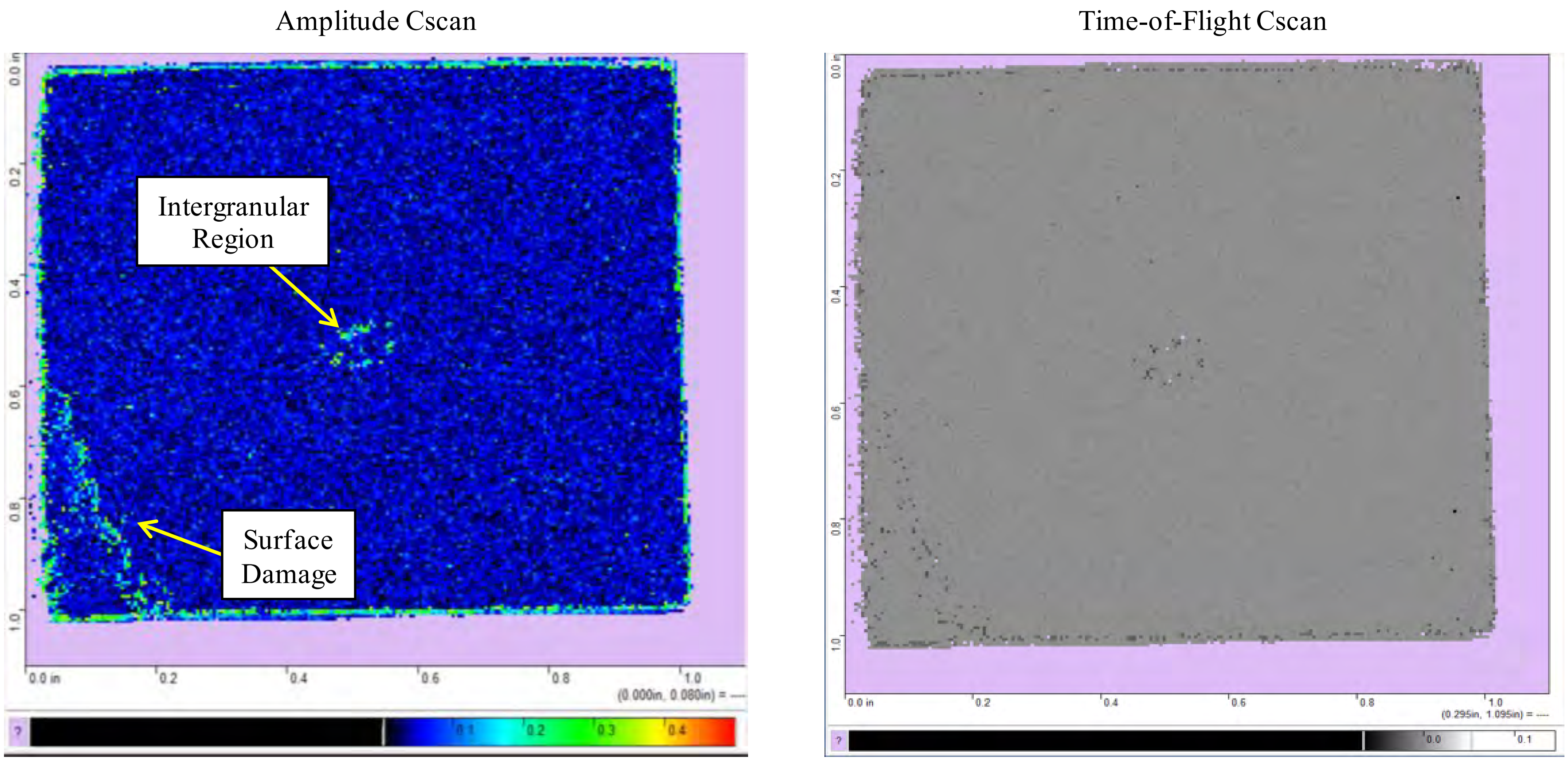

Figure 42: Results of the ultrasonic (UT) scans on the 0.1" thick section of Fragment 1. Indications were found that correlated with the perimeter of the intergranular region; no other indications were observed.

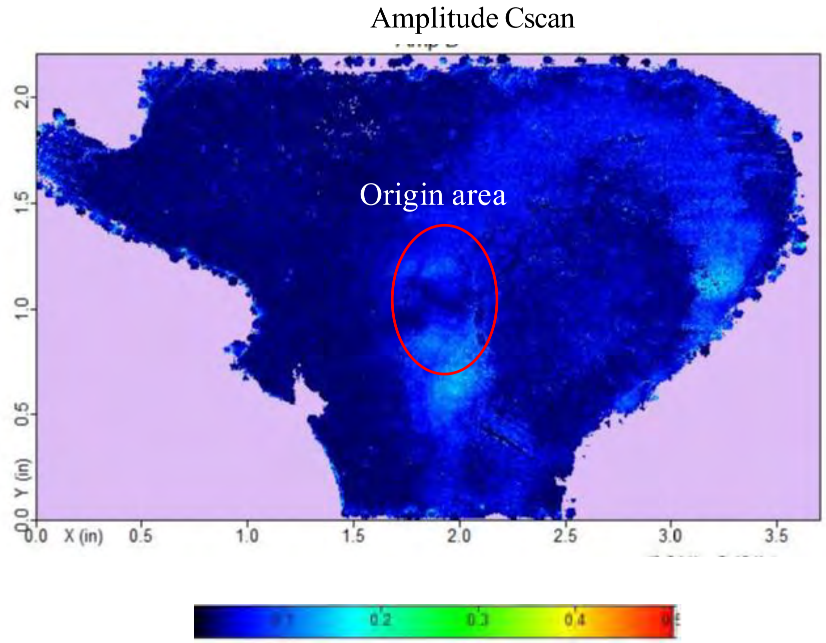

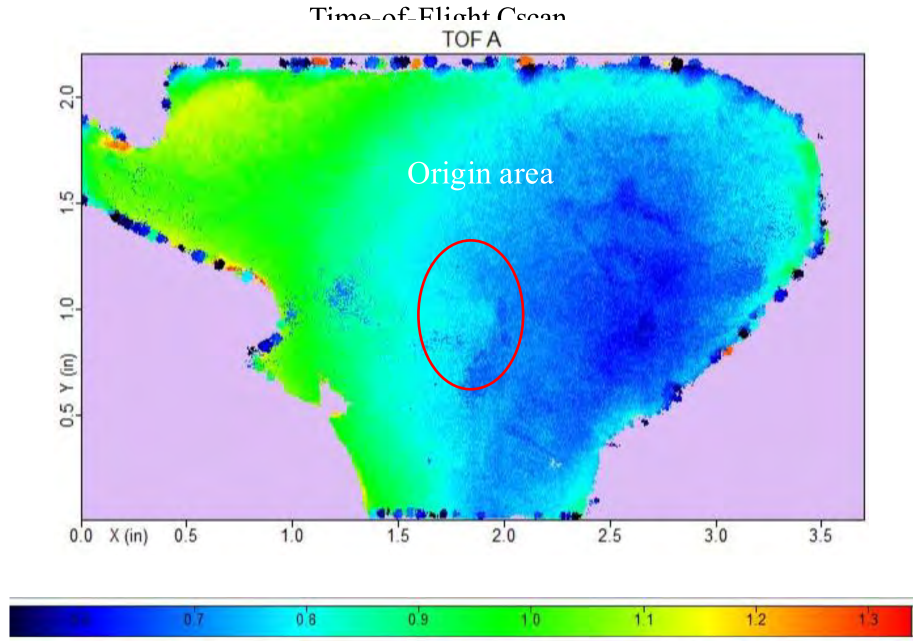

Thickness varied from 0.084" to 0.144"

Figure 43: Results of the ultrasonic (UT) scans on the 0.1" thick section of Fragment 2. No indications associated with the known inclusion location were observed.

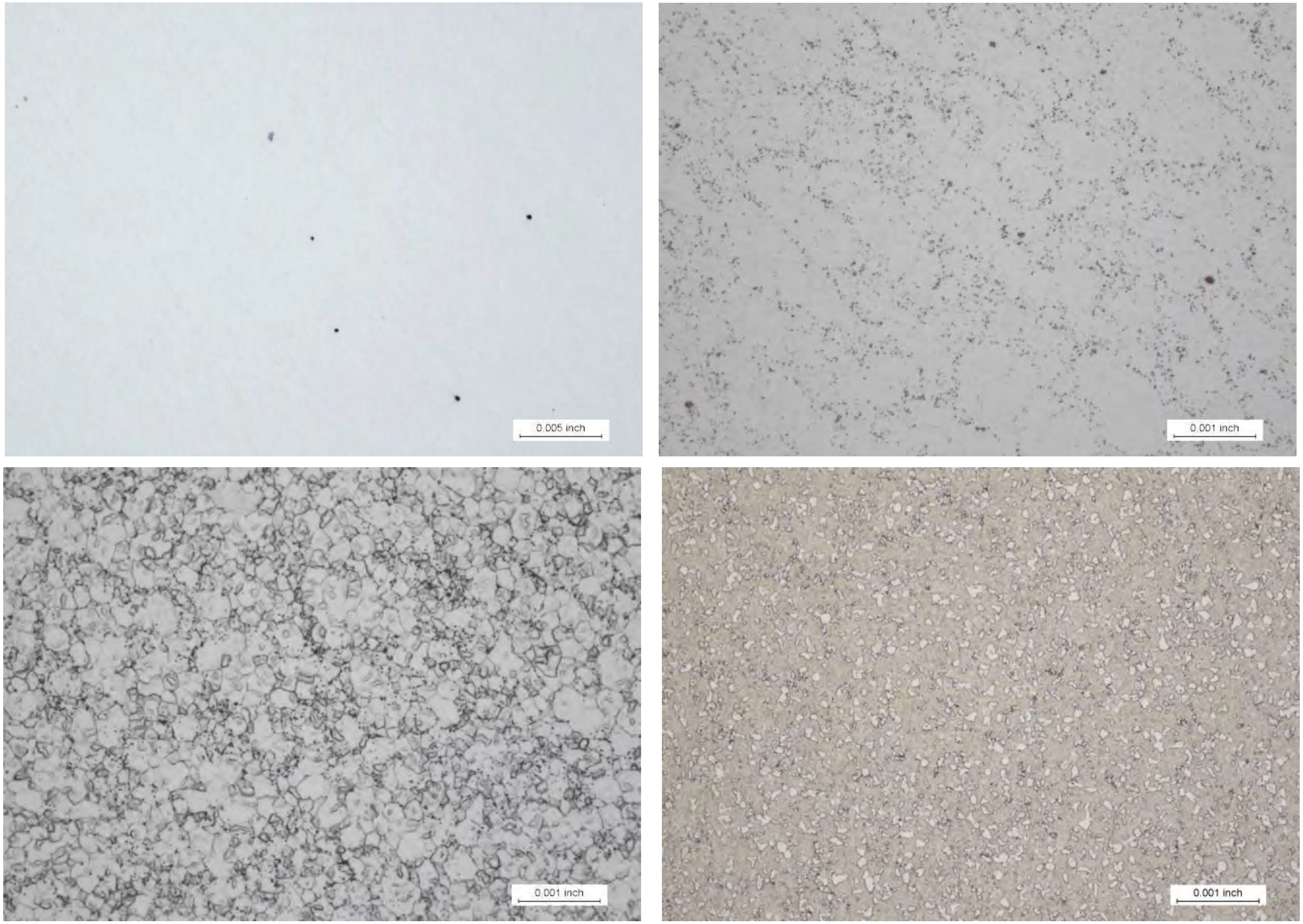

Figure 44: Bulk microstructure appearance in the bore approximately one to two inches away from the origin area. The distribution of gamma prime phase, grain size, distribution of carbides, and amount of micro-porosity all conformed to the material requirements.

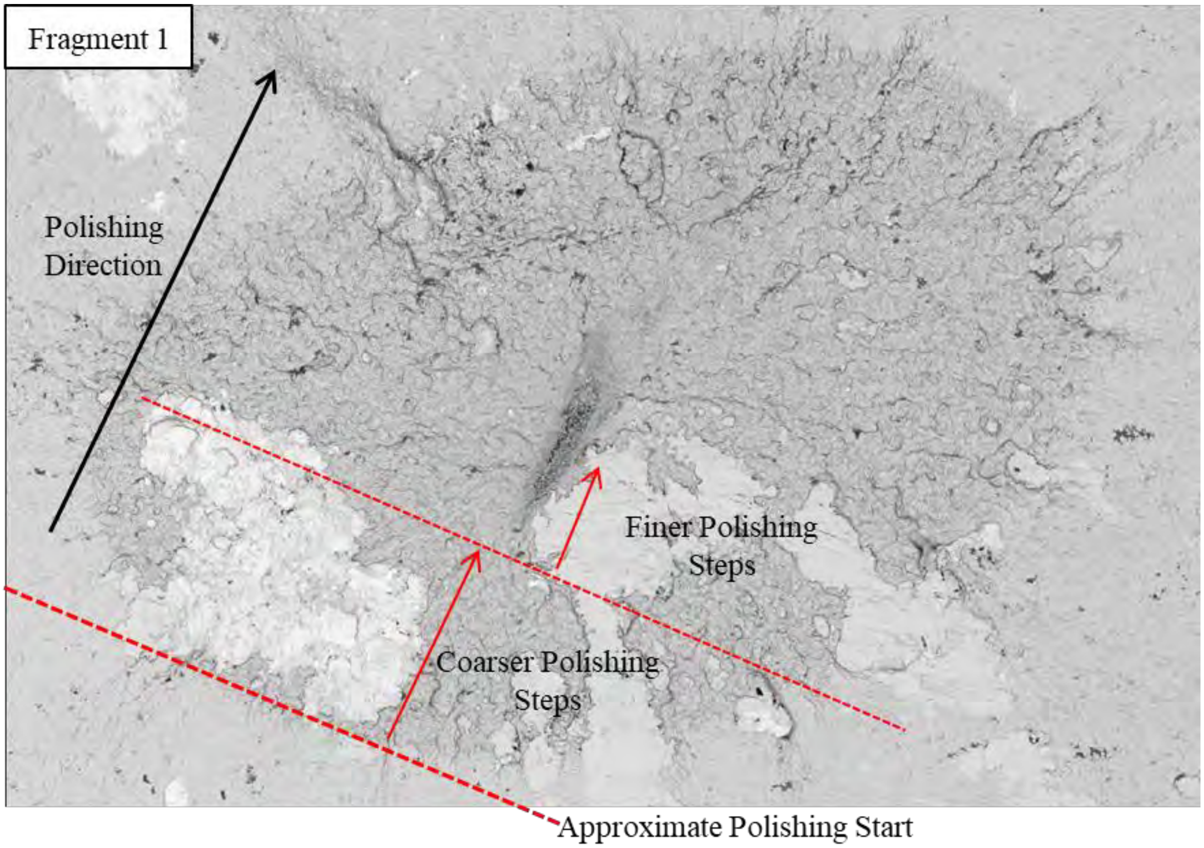

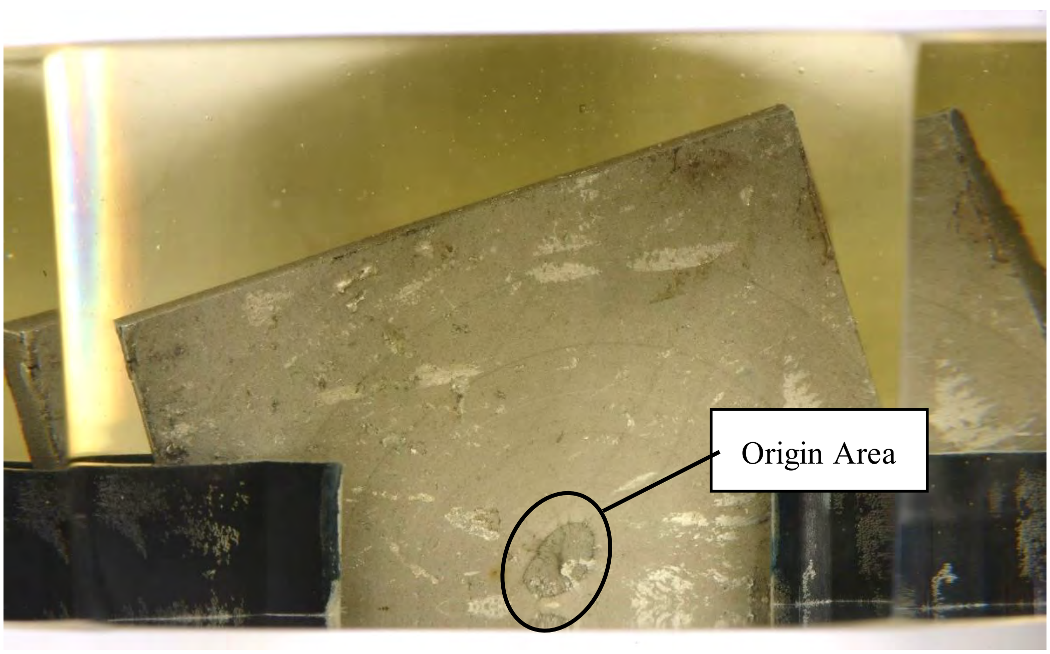

Figure 45: SEM image showing direction and orientation of serial polish sections through the Fragment 1 origin area (top) and image of metallographic section prepared in a clear epoxy mount(bottom).

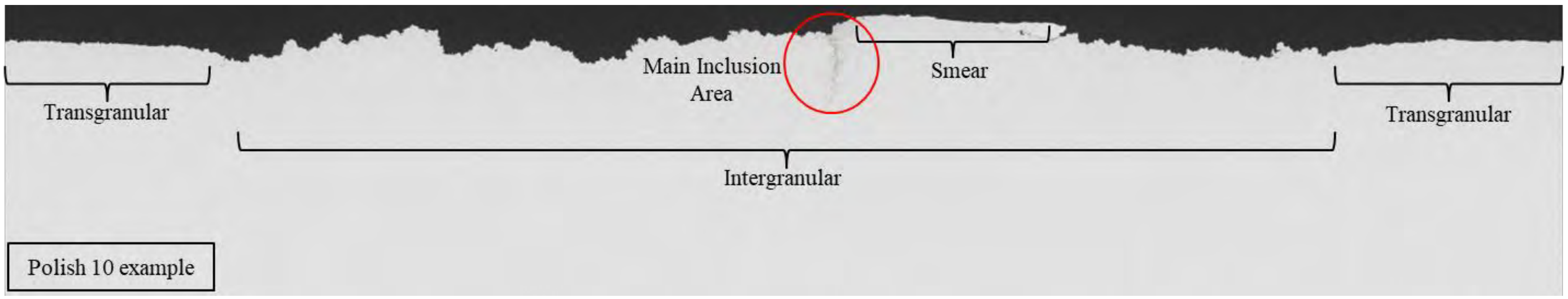

Figure 46: Photomicrograph showing the inclusion area, intergranular, and transgranular features observed within the cross section on Polish 10.

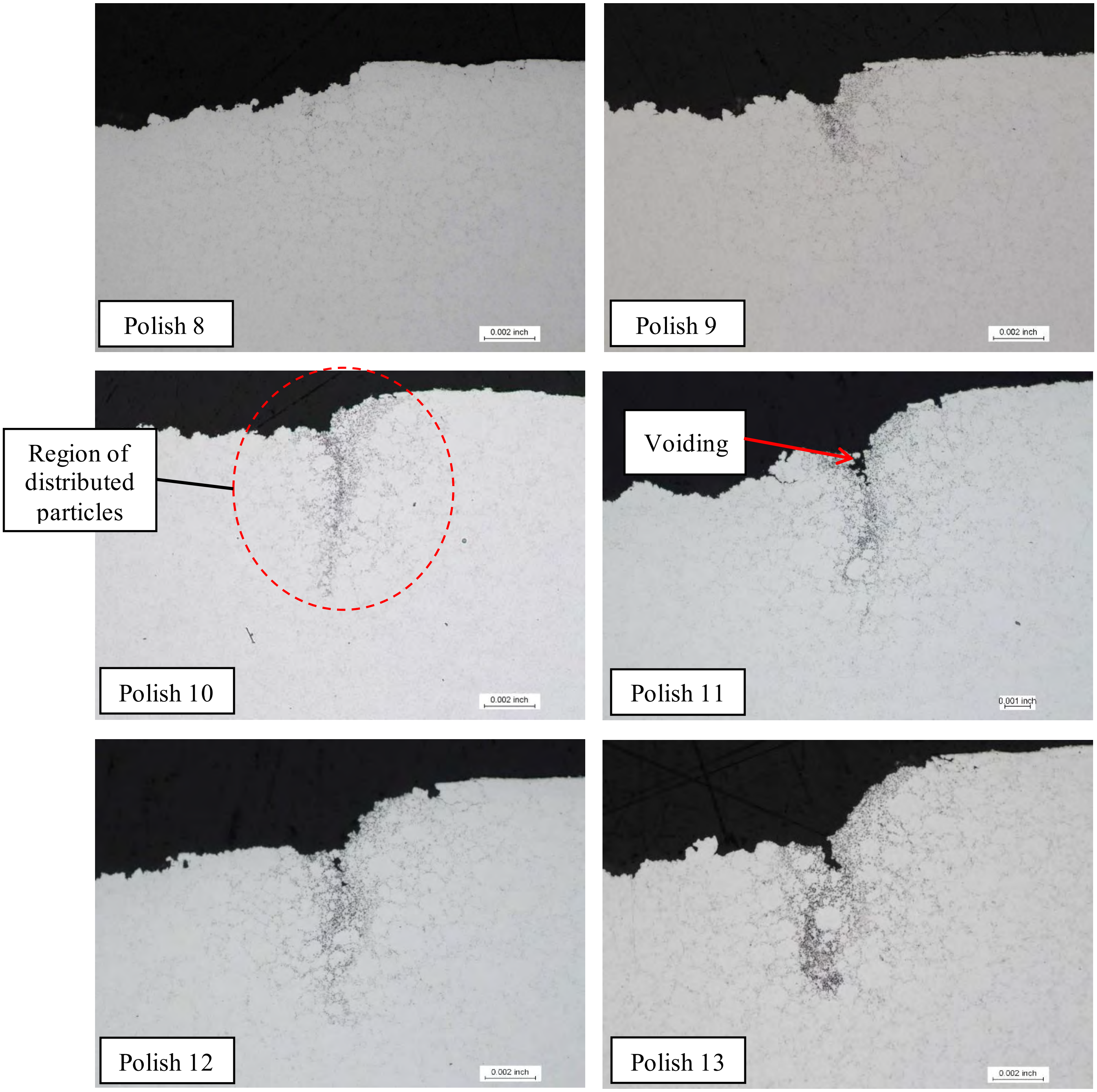

Figure 47: Serial polish steps 8-13 through the Fragment 1 fracture surface. The inclusion was visible as a region of distributed particles, or particle cloud (dark gray/black particles, above). Voiding was observed starting at Polish 11.

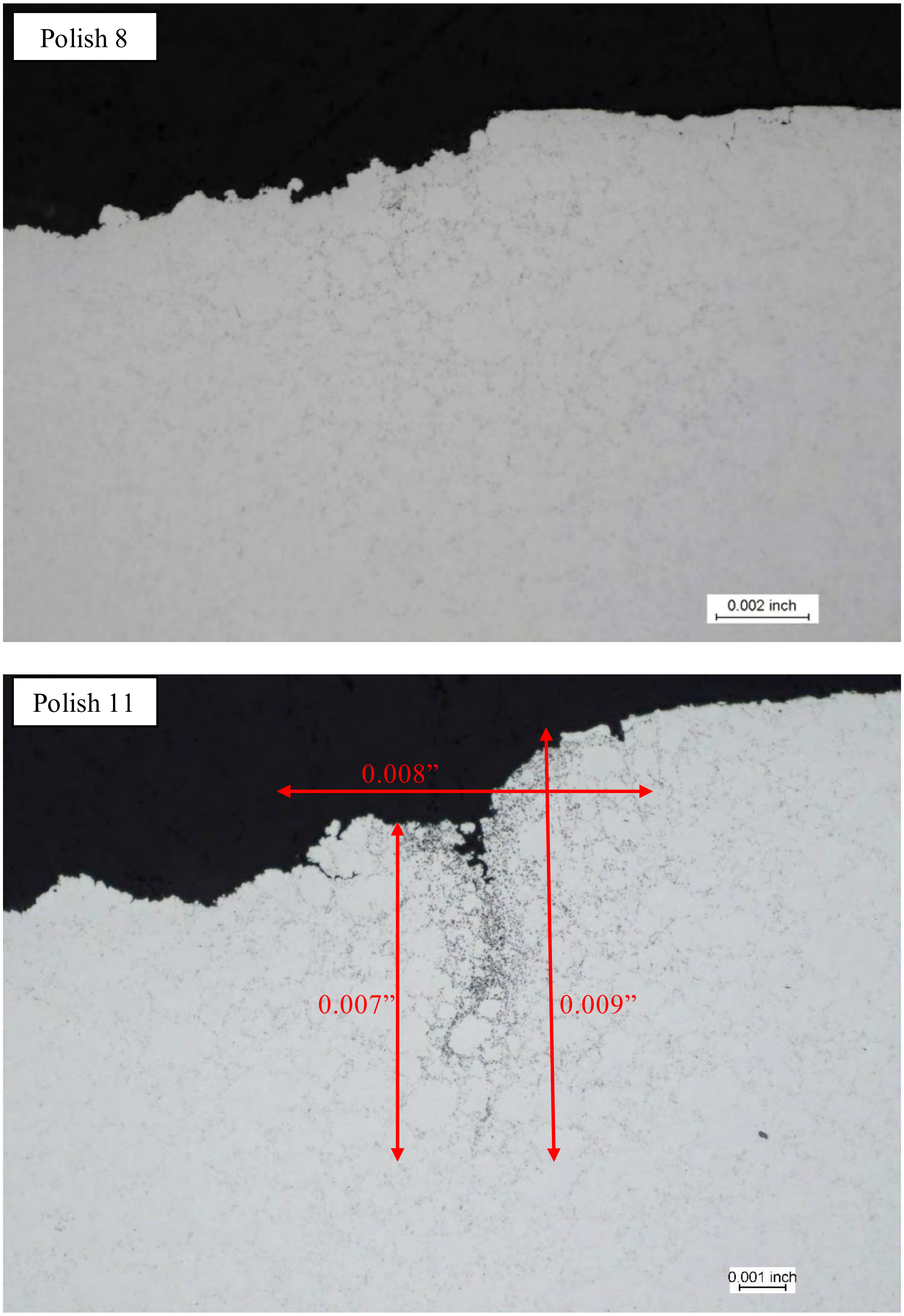

Figure 48: Polishes 8 (top) and 11 (bottom). The inclusion was first visible at Polish 8. Maximum size of the particle cloud at Polish 11 was 0.008” wide by 0.009” deep.

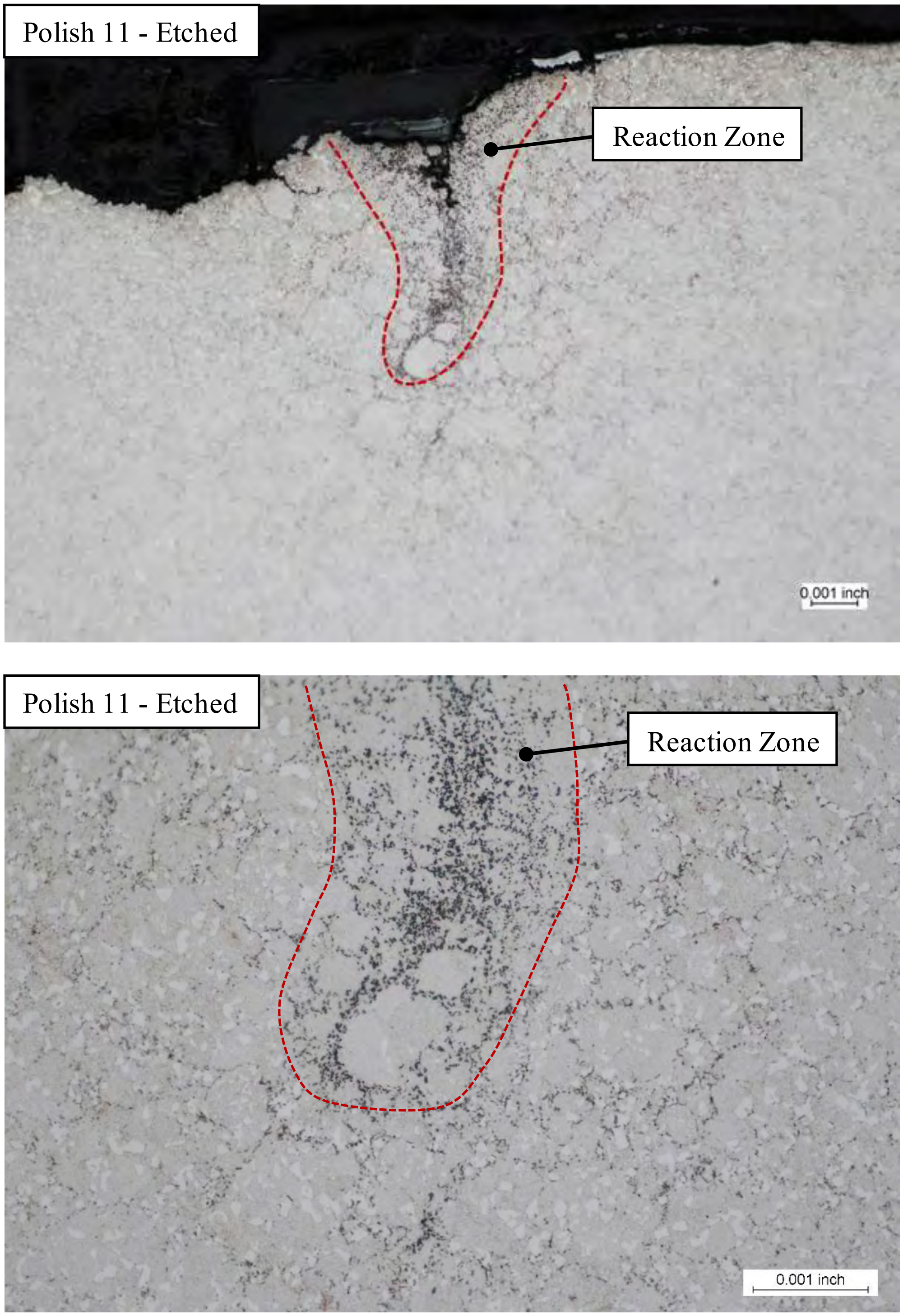

Figure 49: Photomicrographs of Polish 11 etched with a mixed acid etch to reveal the gamma prime phase. The reaction zone was denoted by the area that was denuded of primary gamma prime phase.

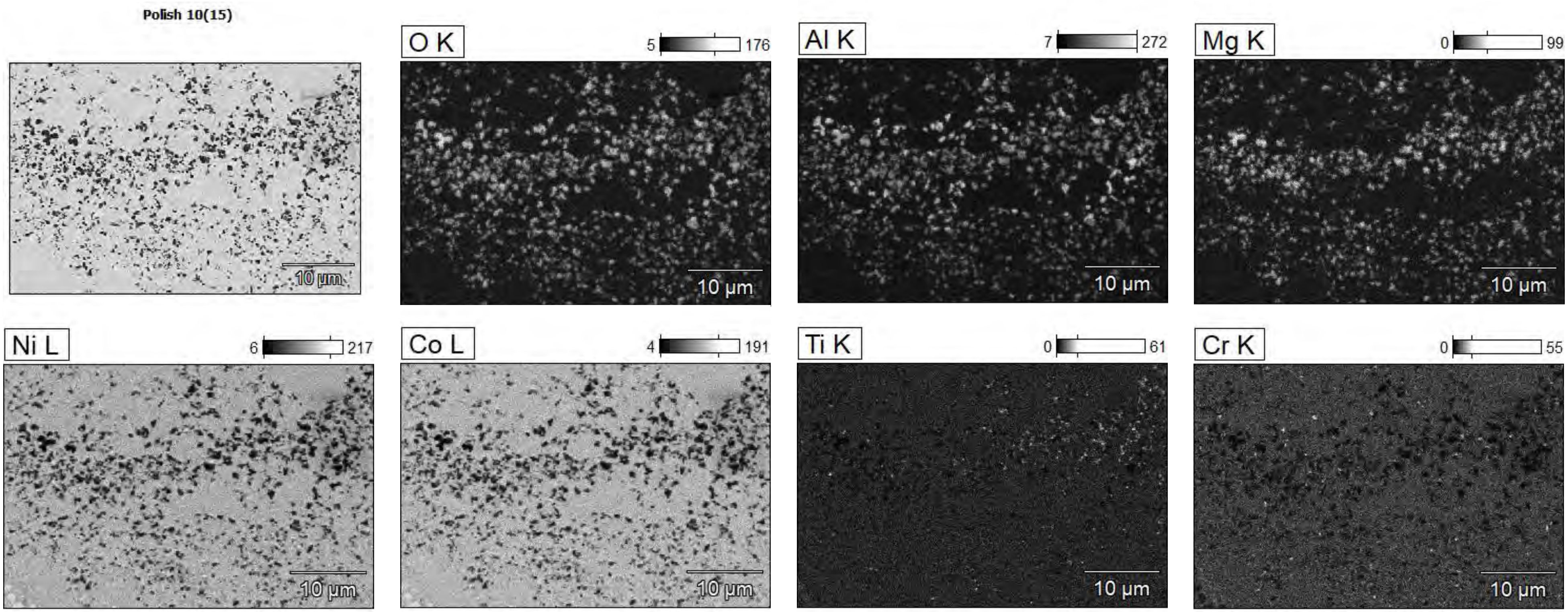

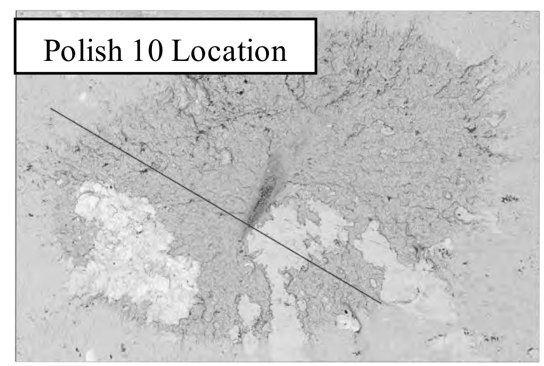

Figure 50: X-ray maps (EDS) taken at Polish 10 showing elements observed. Brighter color in maps indicates a higher concentration of the given element.

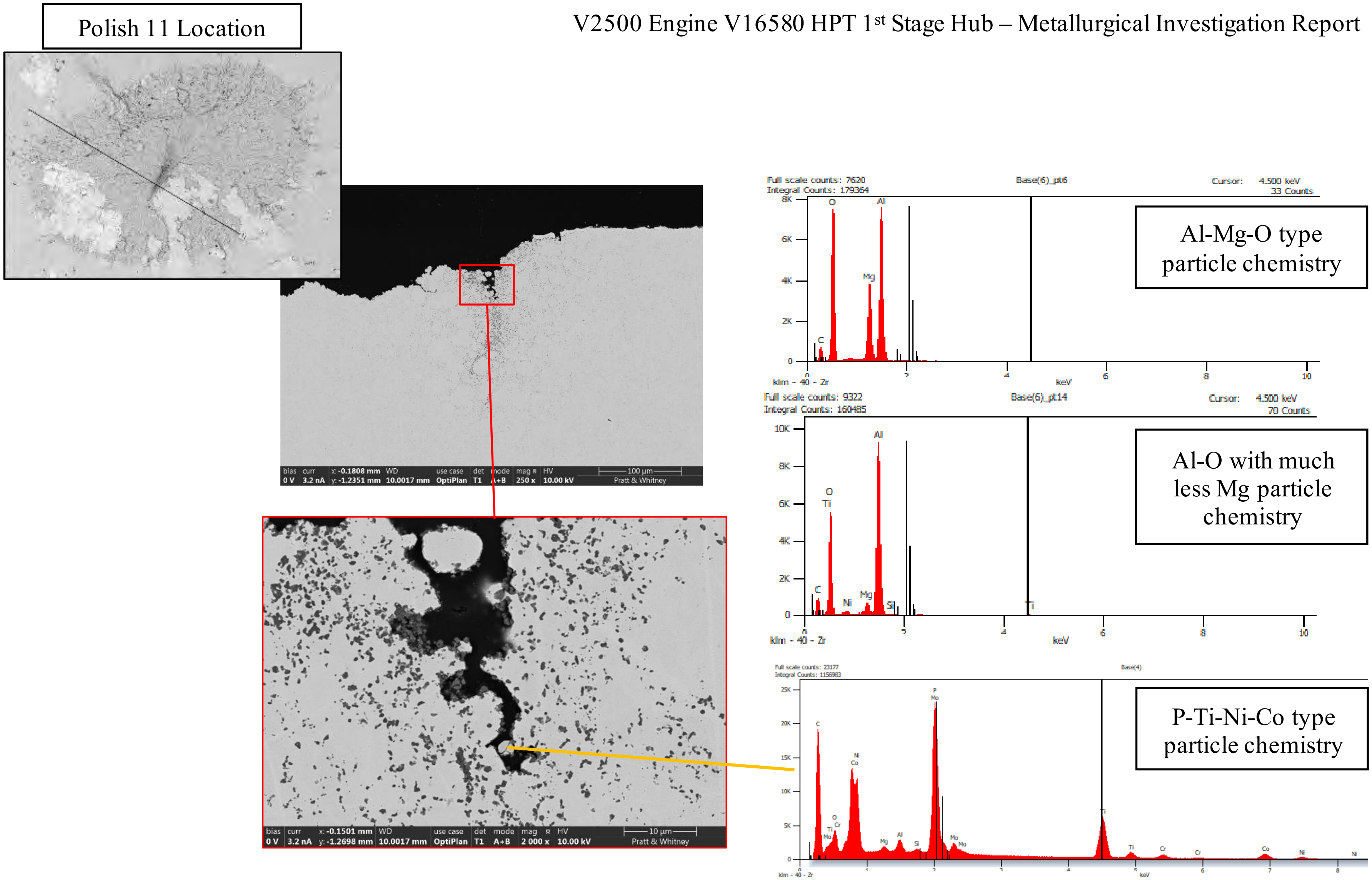

Figure 51: EDS spectra taken on particles observed at the Polish 11 location (location notated at upper left). The Al-Mg-O, Al-O, and P-Ti-Ni-Co type particles were all identified.

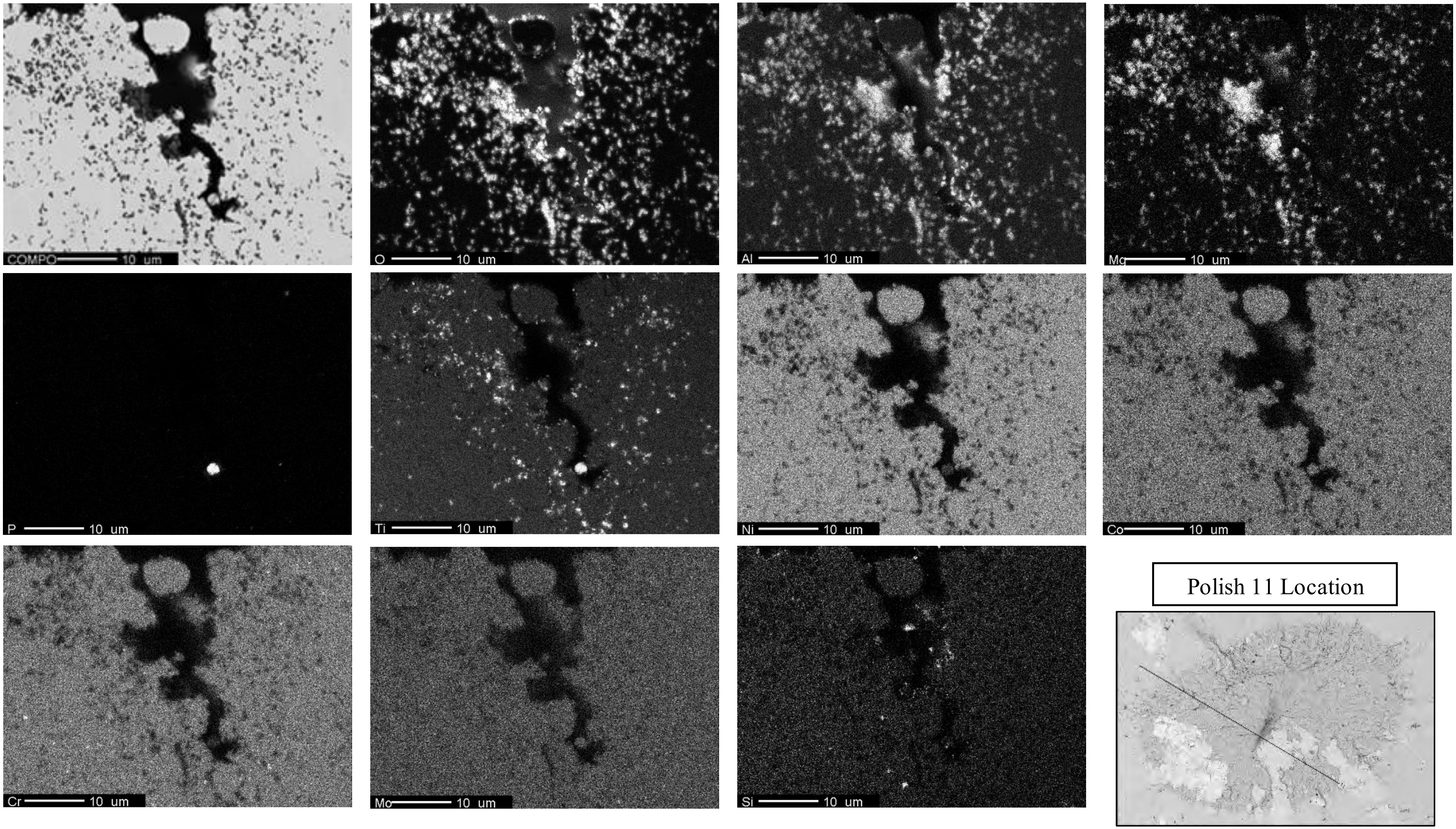

Figure 52: X-ray maps (EDS and WDS) taken at Polish 11 showing elements observed. Brighter color in maps indicates a higher concentration of the given element.

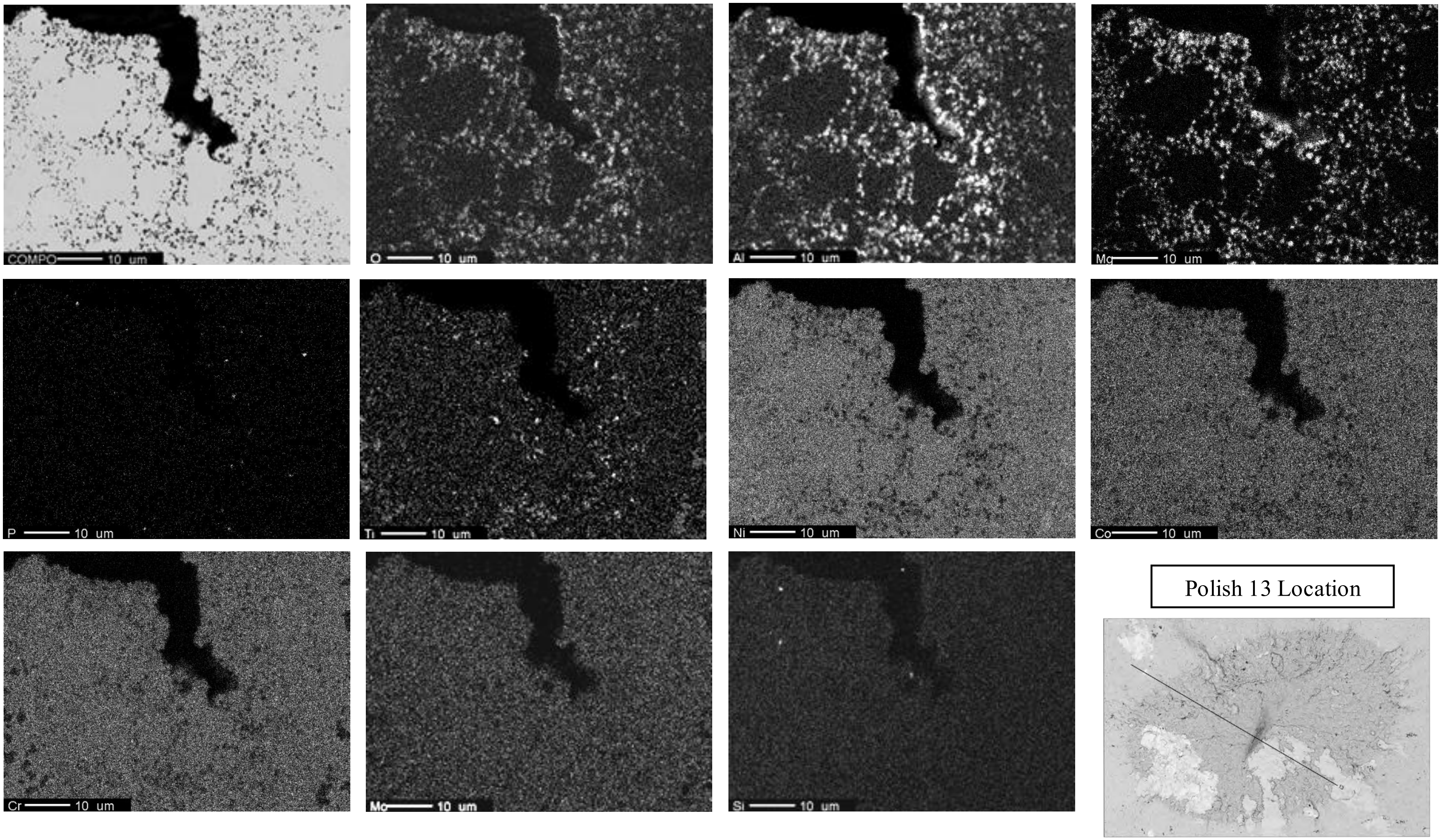

Figure 53: X-ray maps (EDS and WDS) taken at Polish 13 showing elements observed. Brighter color in maps indicates a higher concentration of the given element.

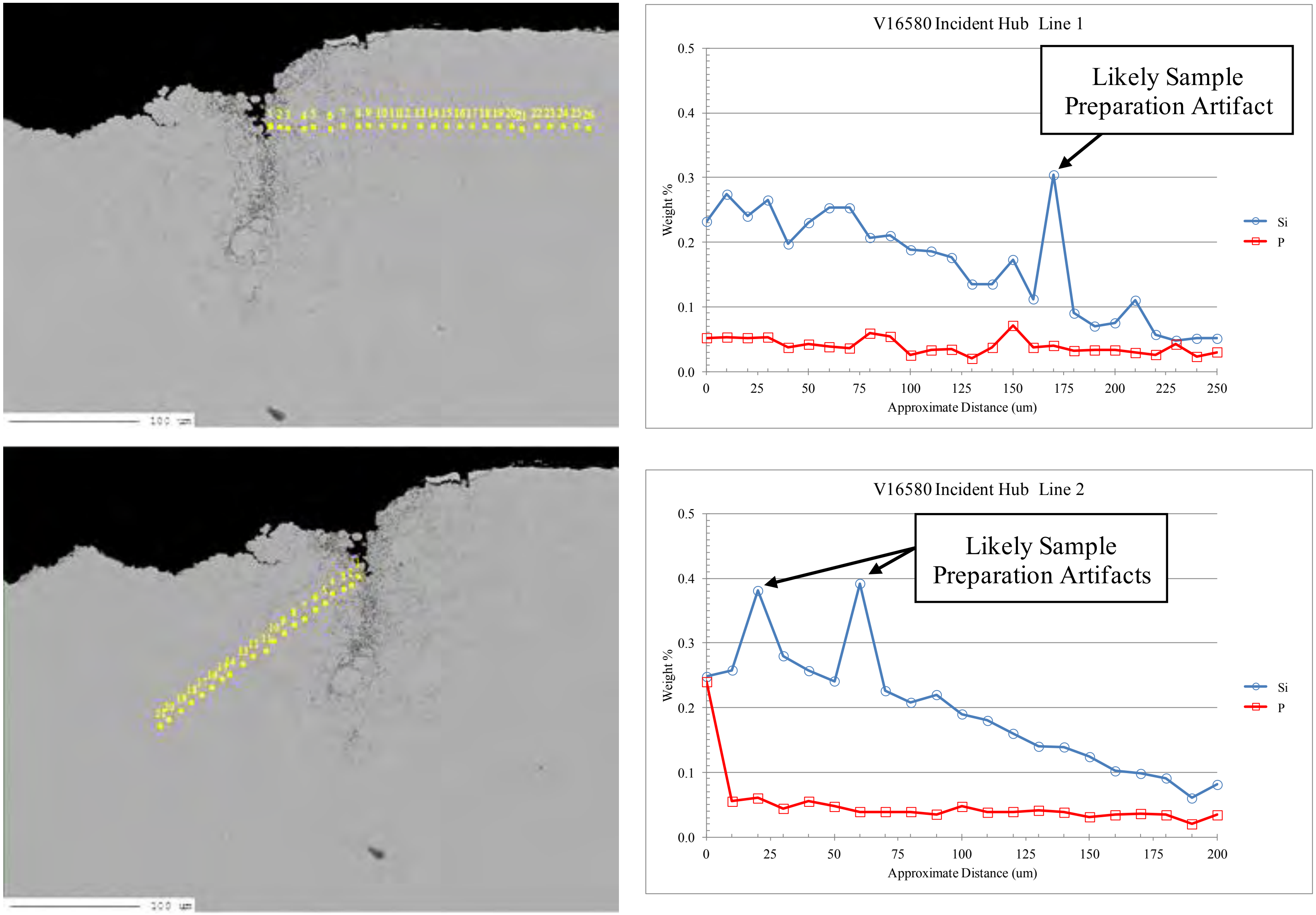

Figure 54: Electron microprobe line scans taken on Polish 11 moving away from the inclusion. Weight percent values of Si and P for each trace shown on right. It should be noted that while this data can be used to understand general trends, the absolute value of the weight percent measurement is uncertain due to a lack of calibration of the electron microprobe at the levels observed.

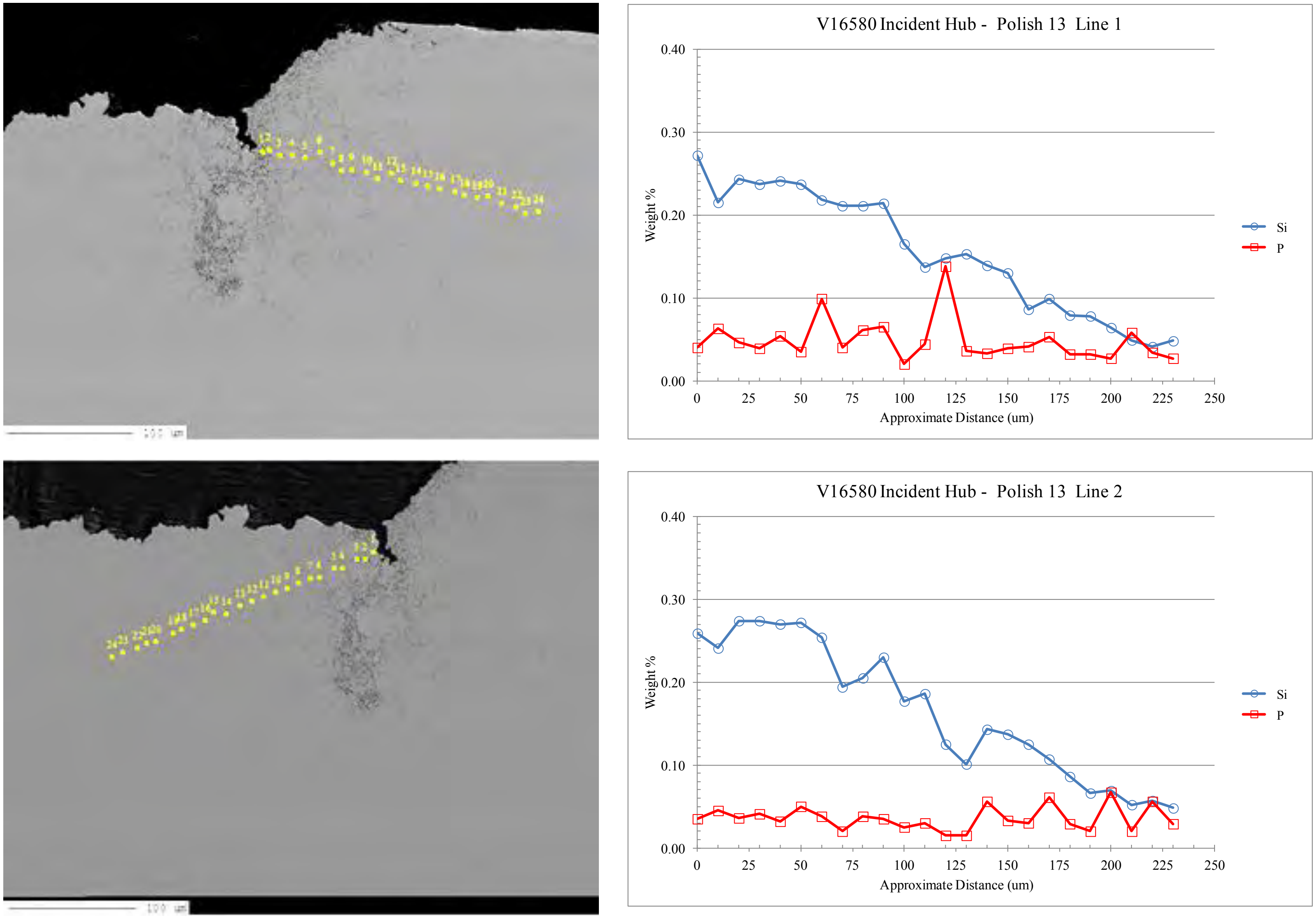

Figure 55: Electron microprobe line scans taken on Polish 13 moving away from the inclusion. Weight percent values of Si and P for each trace shown on right. It should be noted that while this data can be used to understand general trends, the absolute value of the weight percent measurement is uncertain due to a lack of calibration of the electron microprobe at the levels observed.

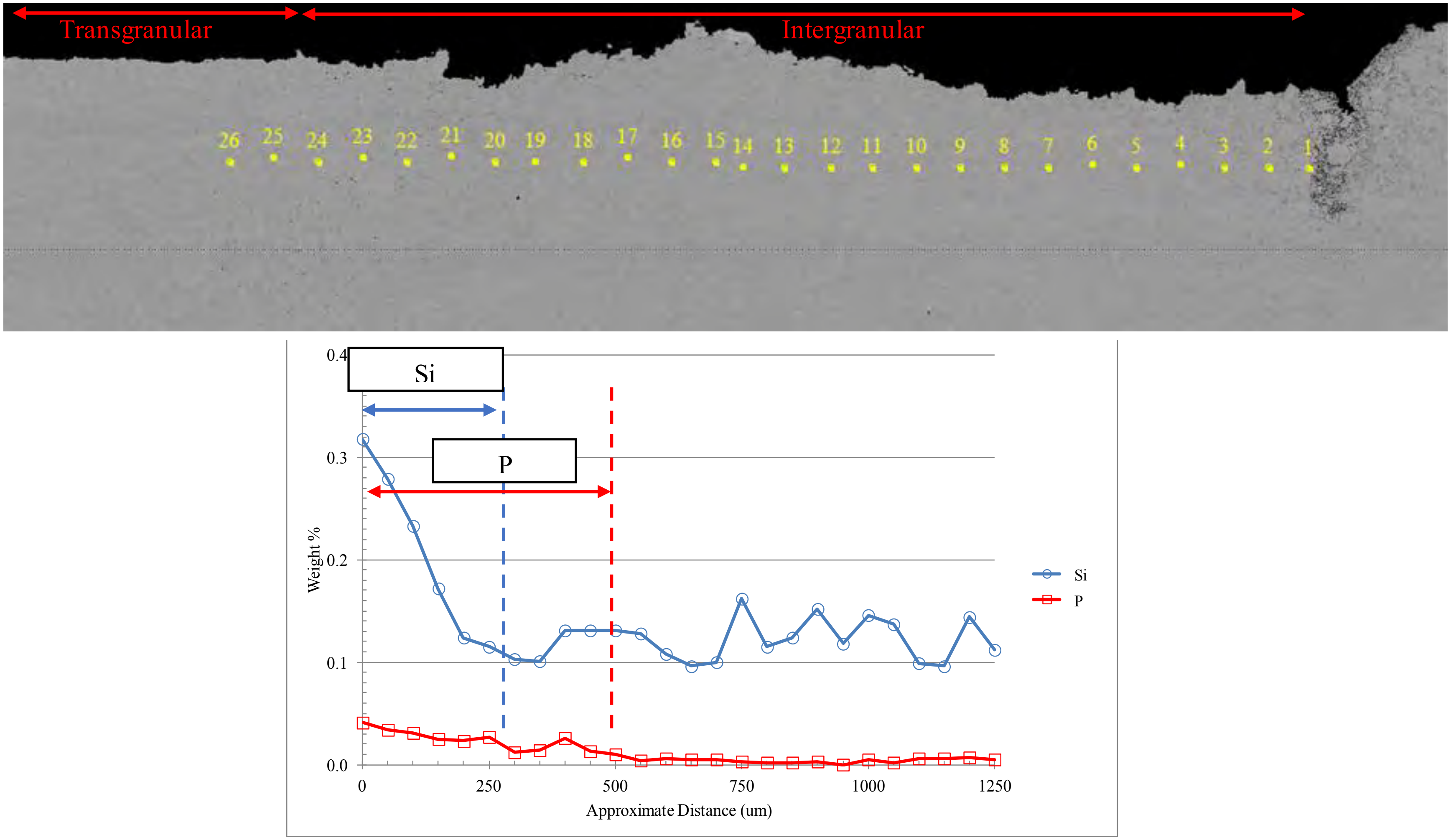

Figure 56: Electron microprobe line scans taken on Polish 13 moving away from the inclusion through the intergranular area and into the transgranular area. Weight percent values of Si and P for each trace shown at bottom. It should be noted that while this data can be used to understand general trends, the absolute value of the weight percent measurement is uncertain due to a lack of calibration of the electron microprobe at the levels observed.

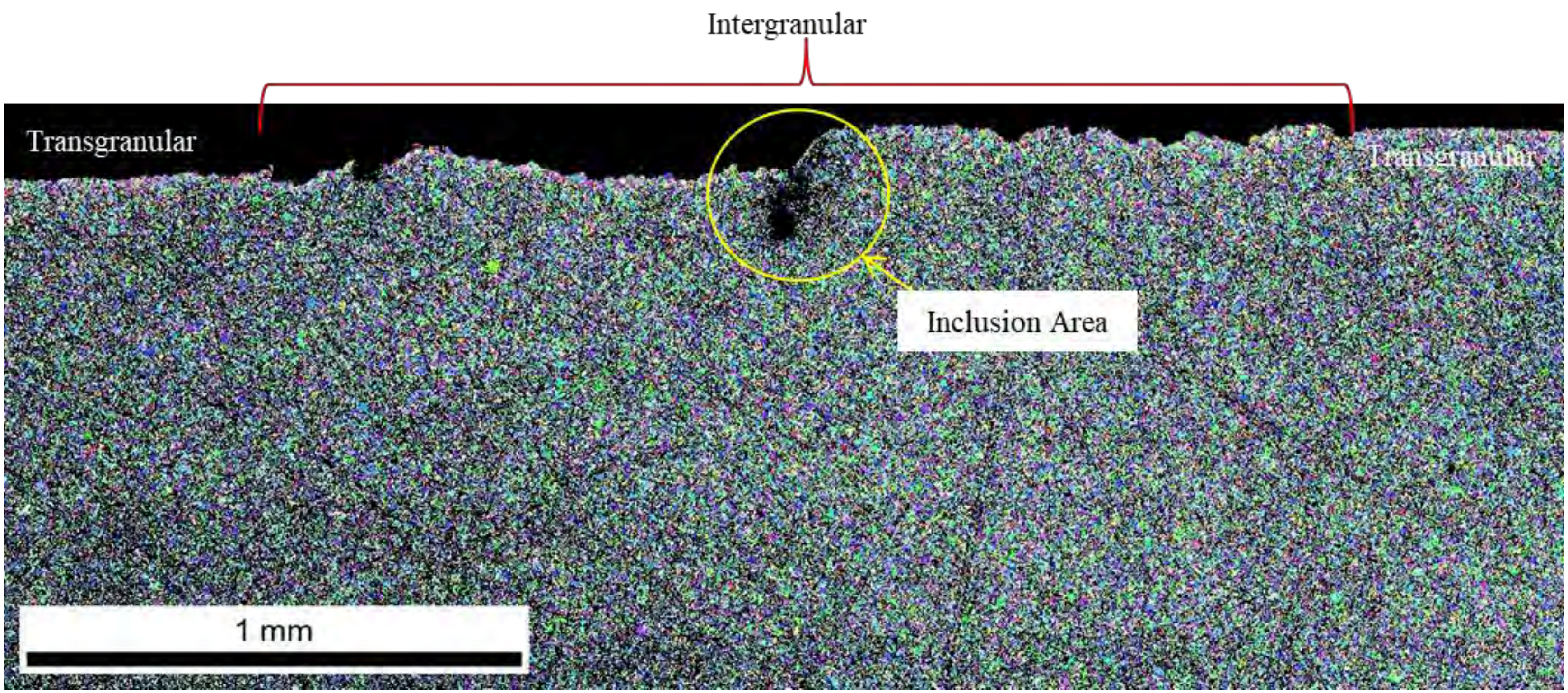

Figure 57: Inverse pole figure (IPF) produced by EBSD showing no discernable difference between the intergranular and transgranular areas.

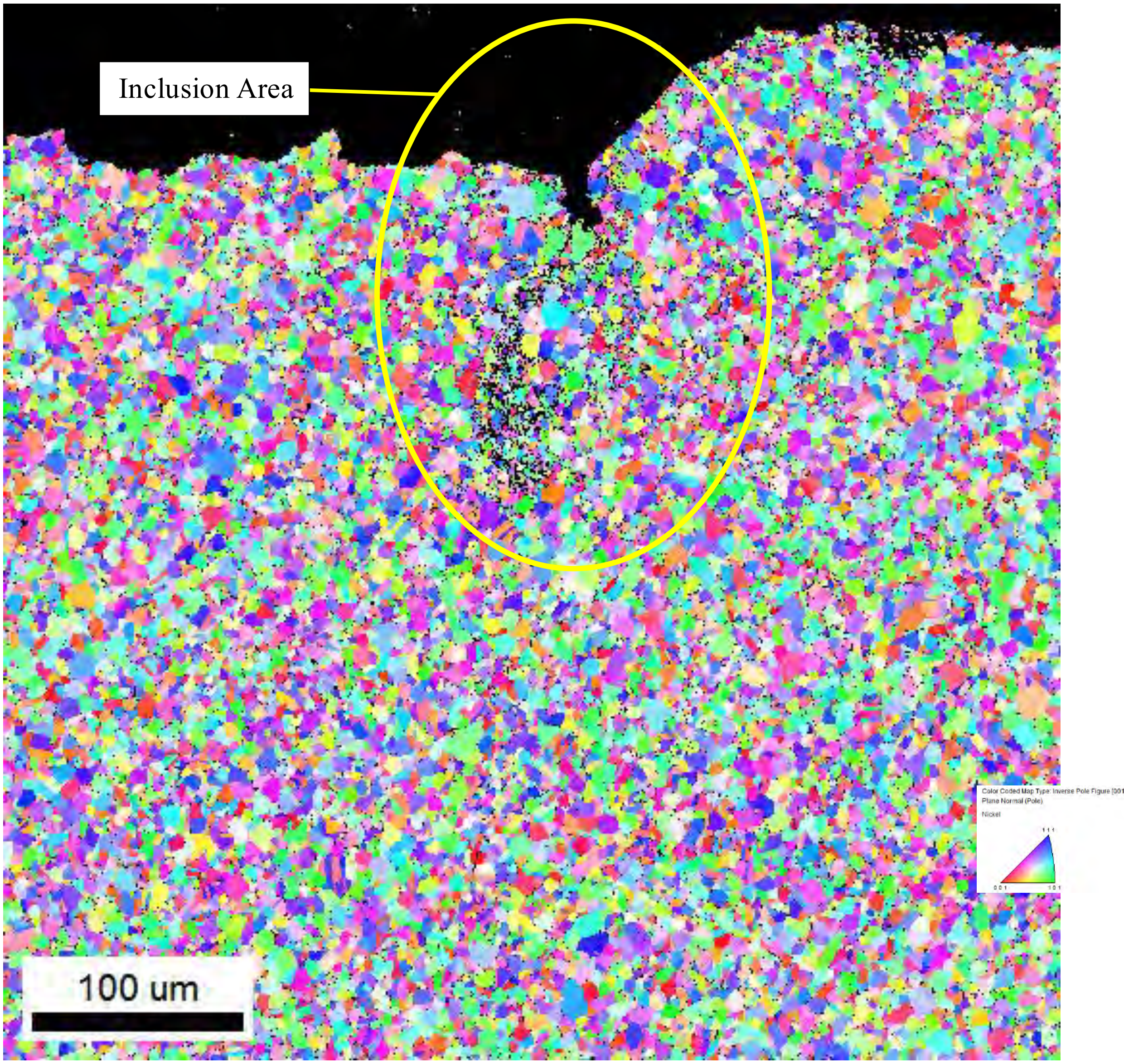

Figure 58: Inverse pole figure (IPF) produced by EBSD showing no discernable difference between the inclusion area and the surrounding intergranular area.

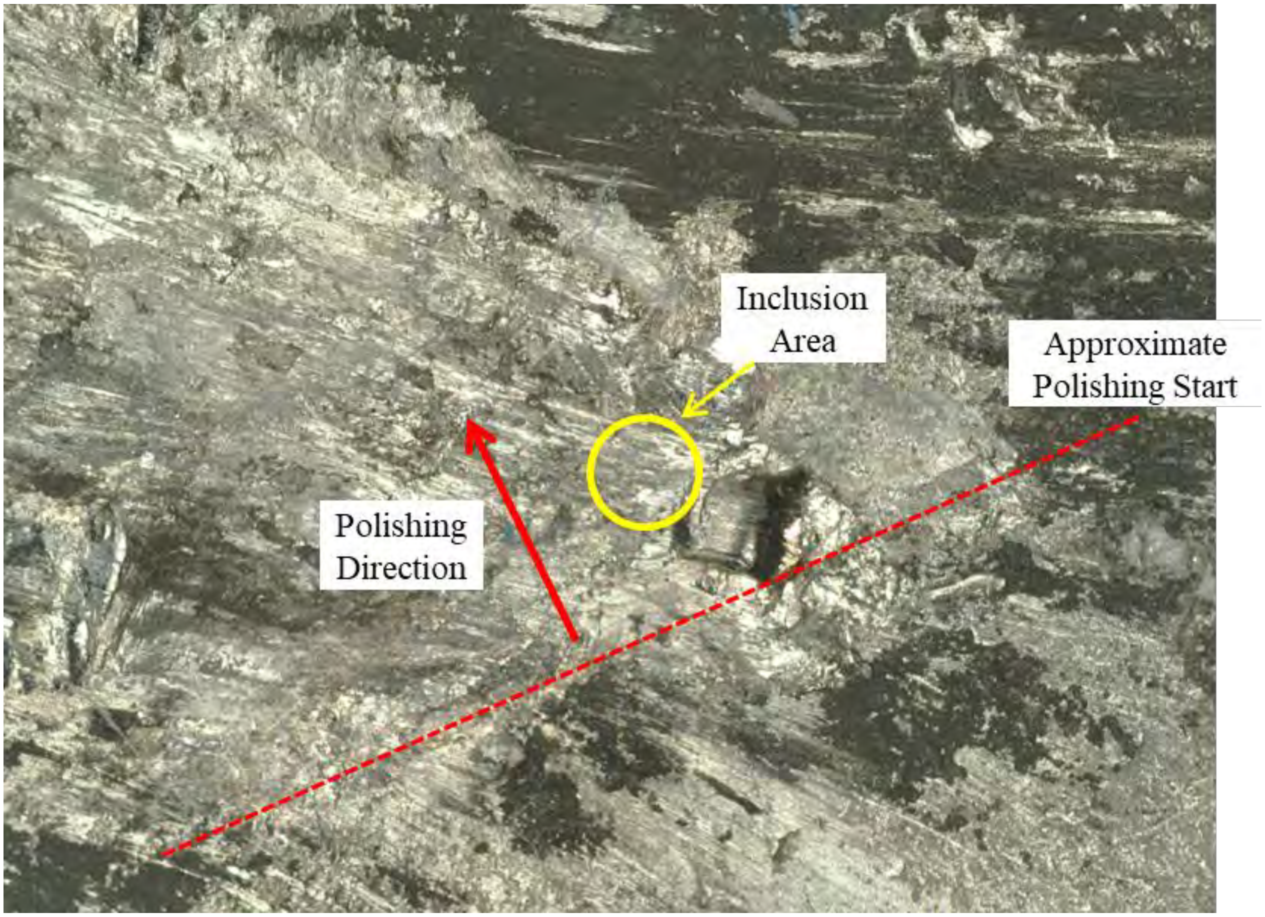

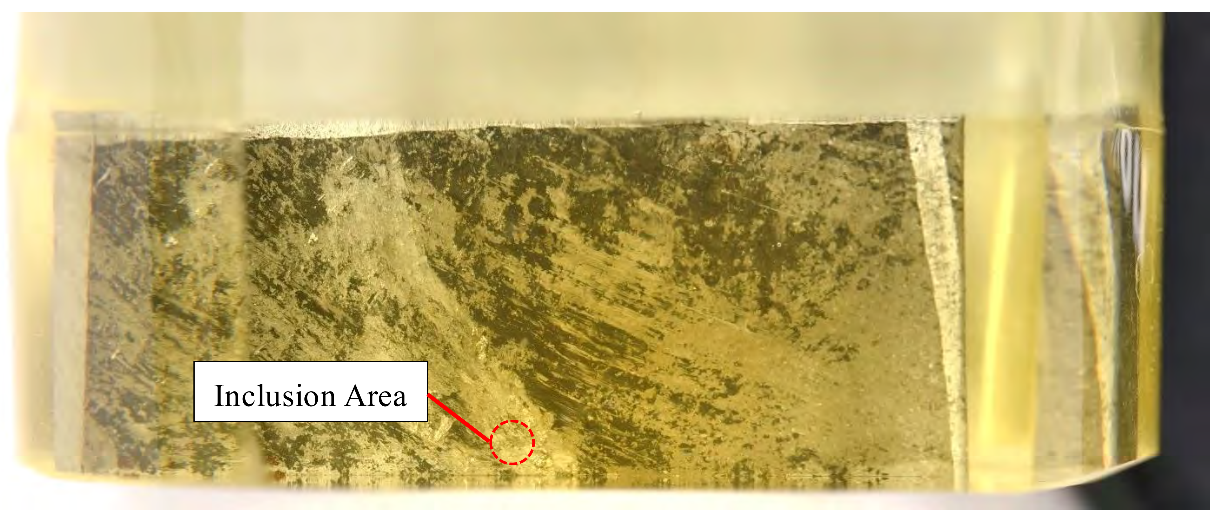

Figure 59: Binocular microscope image showing direction and orientation of serial polish sections through the Fragment 2 origin area (top) and image of metallographic section prepared in a clear epoxy mount(bottom).

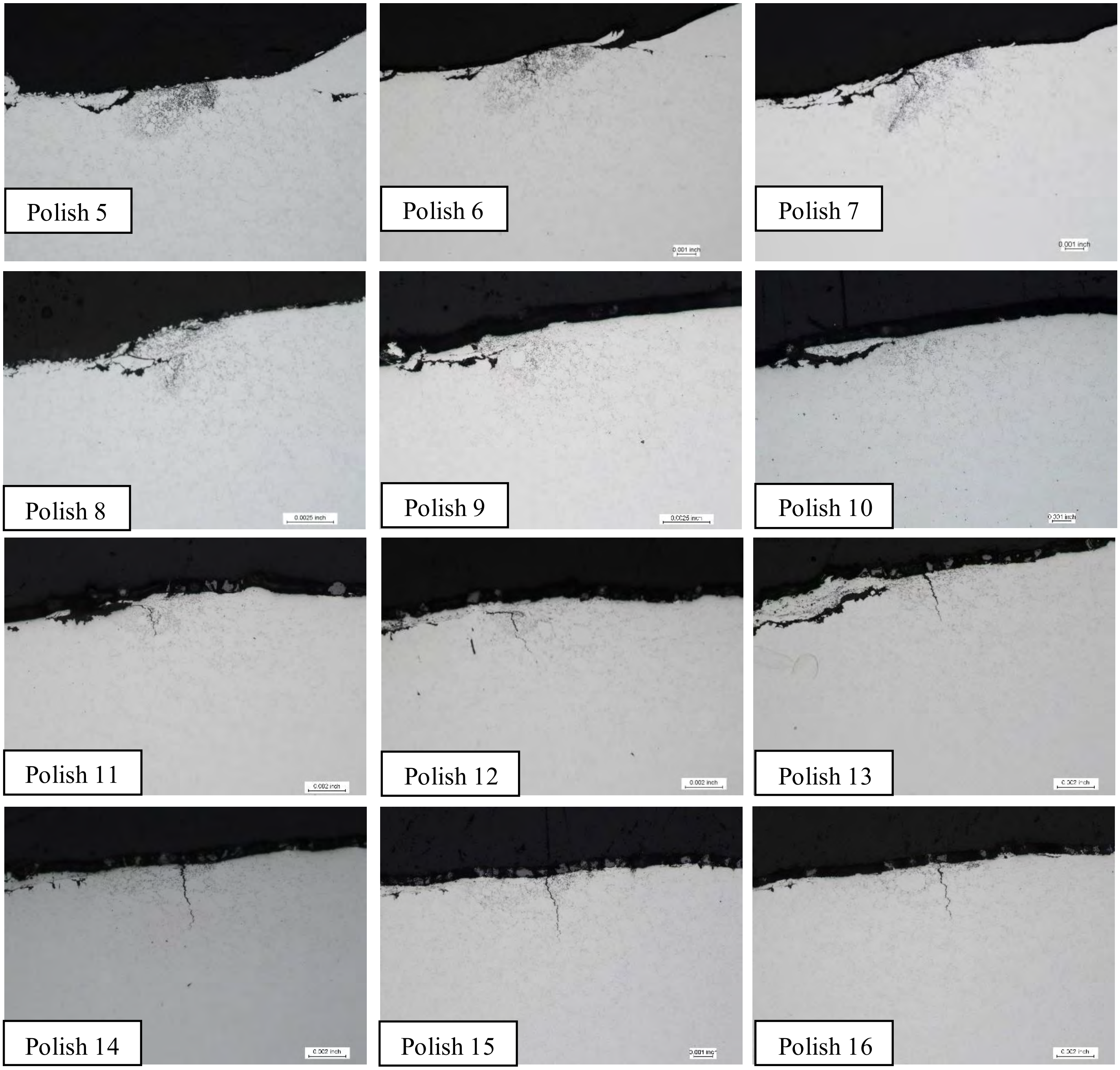

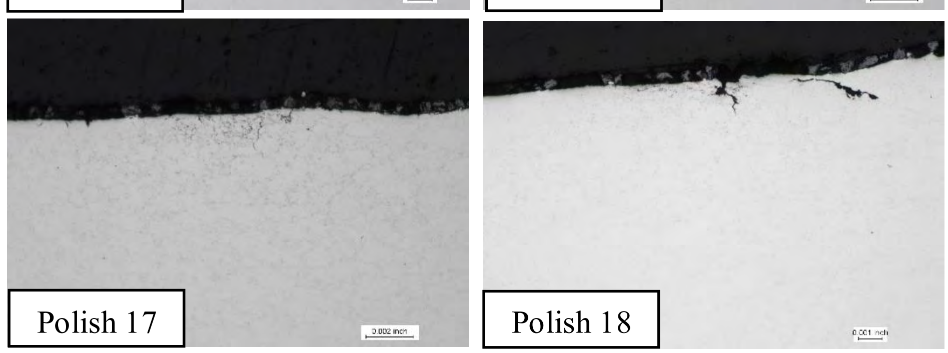

Figure 60: Serial polish steps 5-18 through the Fragment 2 fracture surface. The inclusion was visible as a region of distributed particles, or particle cloud (dark gray/black particles, above). It is unknown whether observed cracking occurred prior to or as a result of the event.

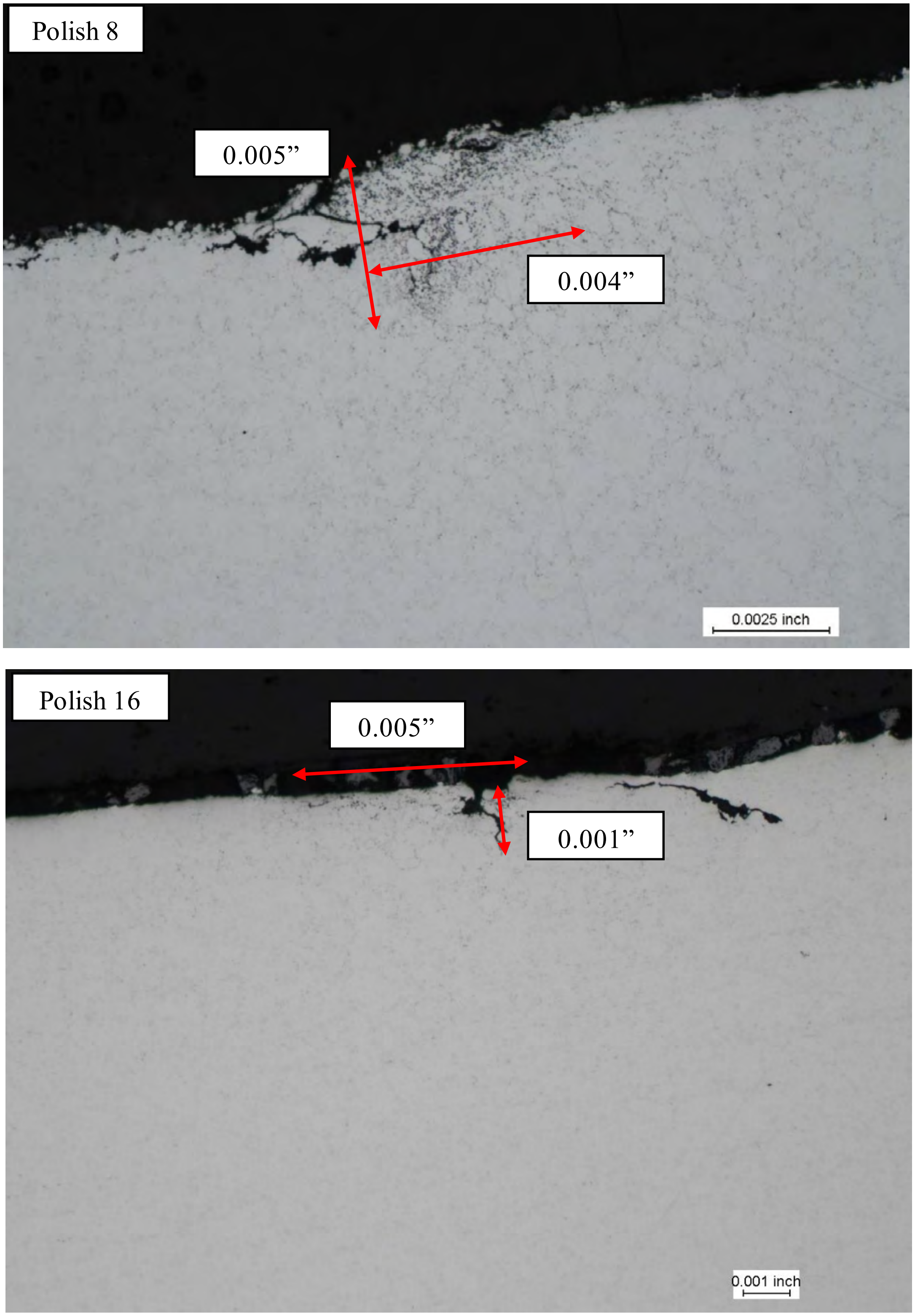

Figure 61: As-polished photomicrographs at Polishes 8 (top) and 18(bottom).

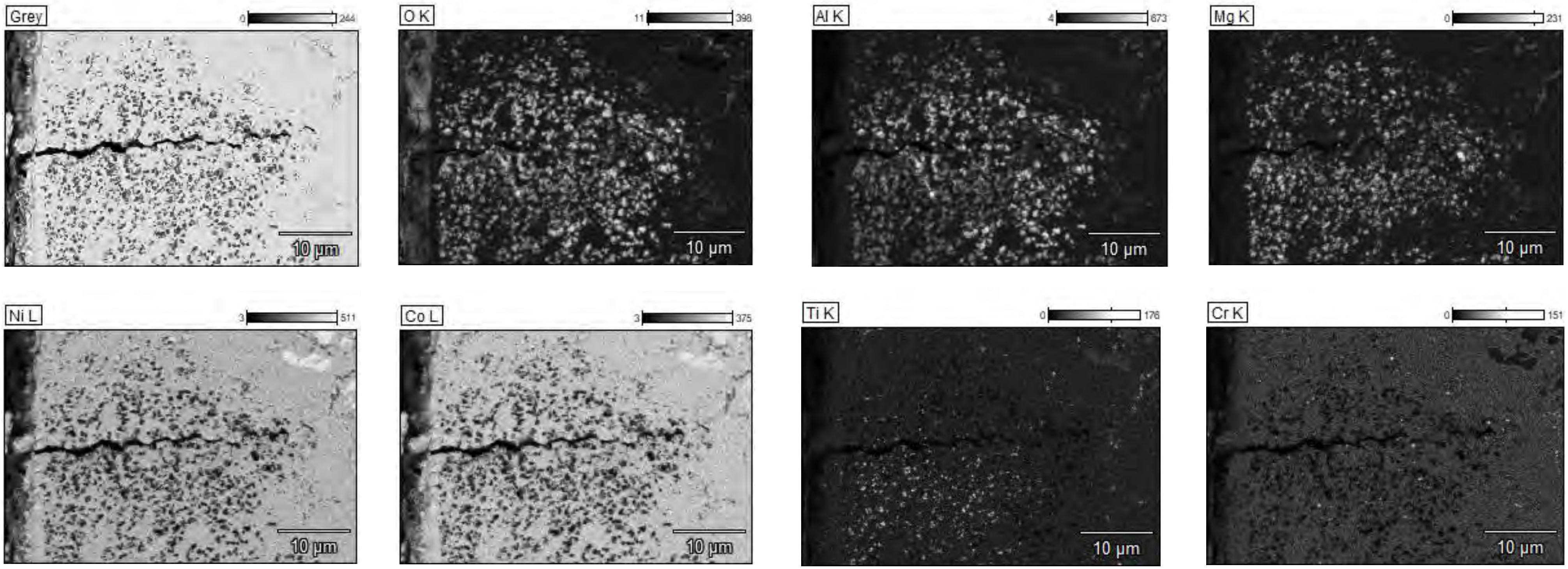

Figure 62: X-ray maps (EDS) taken at Polish 5 showing elements observed. Brighter color in maps indicates a higher concentration of the given element.

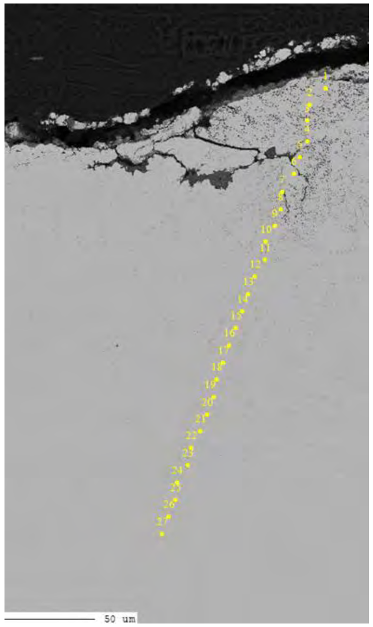

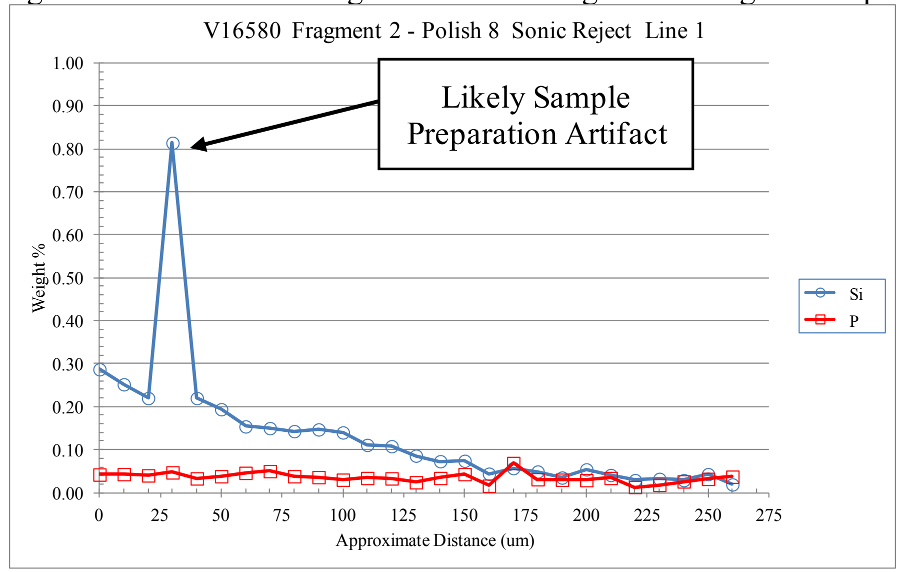

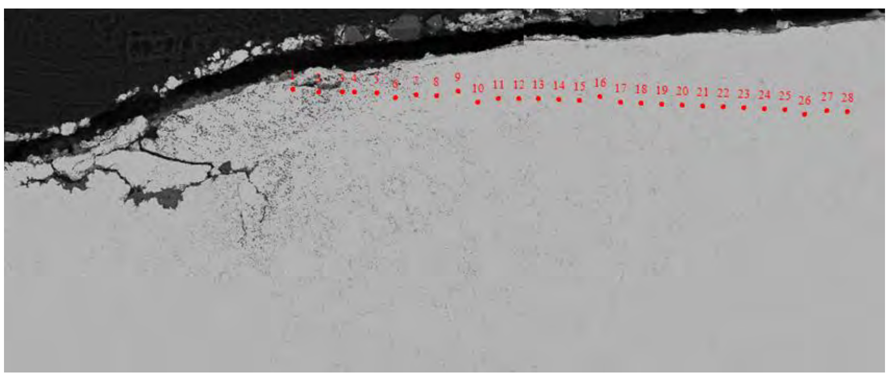

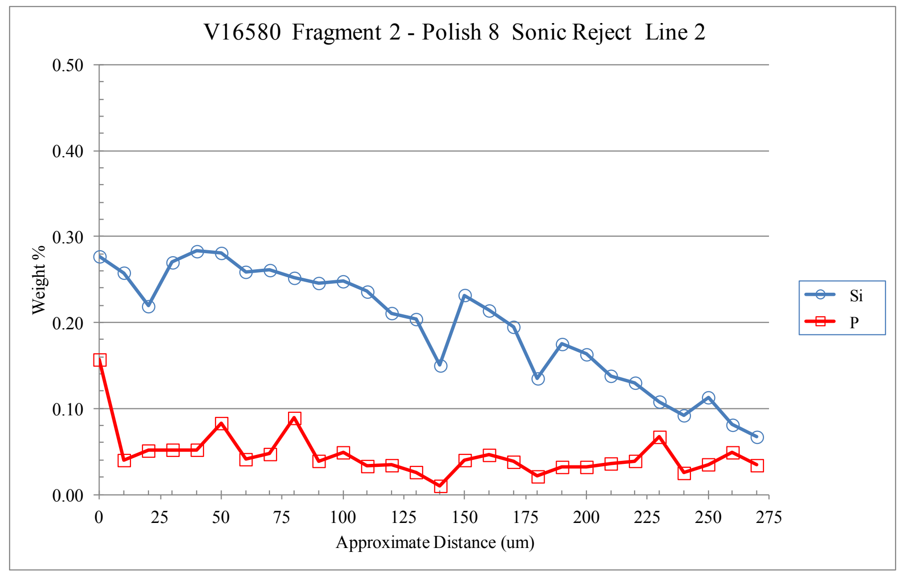

Figure 63: Electron microprobe line scans taken on Fragment 2 Polish 8 moving away from the inclusion. Weight percent values of Si and P for each trace shown on right. It should be noted that while this data can be used to understand general trends, the absolute value of the weight percent measurement is uncertain due to a lack of calibration of the electron microprobe at the levels ob served.